Distribution Agreement

In presenting this thesis or dissertation as a partial fulfillment of the requirements for an advanced degree from Emory University, I hereby grant to Emory University and its agents the non-exclusive license to archive, make accessible, and display my thesis or dissertation in whole or in part in all forms of media, now or hereafter known, including display on the world wide web. I understand that I may select some access restrictions as part of the online submission of this thesis or dissertation. I retain all ownership rights to the copyright of the thesis or dissertation. I also retain the right to use in future works (such as articles or books) all or part of this thesis or dissertation.

Signature:

_____ _____

Michael R. Santoro Date

An In Vivo Model to Study the Regulation of FMRP

By

Michael R. Santoro
Doctor of Philosophy

Graduate Division of Biological and Biomedical Science
Genetics and Molecular Biology

_____
Stephen Warren, Ph.D.
Advisor

_____
Gary Bassell, Ph.D.
Committee Member

_____
Tamara Caspary, Ph.D.
Committee Member

_____
William Kelly, Ph.D.
Committee Member

_____
David Weinshenker, Ph.D.
Committee Member

Accepted:

_____
Lisa A. Tedesco, Ph.D.
Dean of the James T. Laney School of Graduate Studies

_____
Date

An In Vivo Model to Study the Regulation of FMRP

By

Michael R. Santoro
B.S.E., Duke University, 1997

Advisor: Stephen Warren, Ph.D.

An abstract of
A dissertation submitted to the Faculty of the
James T. Laney School of Graduate Studies of Emory University
in partial fulfillment of the requirements for the degree of
Doctor of Philosophy
in Graduate Division of Biological and Biomedical Science
Genetics and Molecular Biology
2016

Abstract

An In Vivo Model to Study the Regulation of FMRP

By Michael R. Santoro

Fragile X syndrome (FXS) is the most common inherited form of intellectual disability. The syndrome results from the lack of fragile X mental retardation protein (FMRP), an mRNA-binding protein which plays a key role in learning and memory. FMRP's activity seems to be regulated by the phosphorylation of a key serine (Ser499 in the mouse). Previous work in cell culture and fruit flies suggests that when FMRP is phosphorylated at this residue it represses the translation of its target mRNAs and that dephosphorylation of the protein releases this repression, allowing the synthesis of new proteins. In this project I created a line of phosphomutant mice to further study the regulation of FMRP. Specifically, I mutated Ser499 to alanine, creating a constitutively unphoshporylated form of the protein. Surprisingly, these mice did not resemble either WT or KO mice in an assay of new protein synthesis. They were indistinguishable from WT mice in terms of susceptibility to audiogenic seizures, macroorchidism, and behavioral assays. These results suggest that the current view of FMRP regulation may be incomplete. The protein may be phosphorylated differently in vivo or alternative isoforms of FMRP may play a more important role than has previously been appreciated.

An In Vivo Model to Study the Regulation of FMRP

By

Michael R. Santoro
B.S.E., Duke University, 1997

Advisor: Stephen Warren, Ph.D.

A dissertation submitted to the Faculty of the
James T. Laney School of Graduate Studies of Emory University
in partial fulfillment of the requirements for the degree of
Doctor of Philosophy
in Graduate Division of Biological and Biomedical Science
Genetics and Molecular Biology
2016

Acknowledgements

In addition to my mentor and committee members, I would like to acknowledge the contributions to this project of the following members of the Emory community.

Current Warren Lab Members

Pankaj Chopra, Ph.D.
Georgette Gafford, Ph.D.
Helena Gong
Tamika Malone
Yaran Wen, Ph.D.

Previous Warren Lab Members

Reid Alisch, Ph.D.
Steven Bray, Ph.D.
Stephen Collins, Ph.D.
Anne Dodd
Morna Ikeda
Krayton Keith
Mika Kinoshita, M.D., Ph.D.
Brian Lynch
Julie Mowrey
Jennifer Mulle, Ph.D.
Leila Myrick, Ph.D.
Joshua Suhl, Ph.D.
Tao Wang, Ph.D.

Bassell Lab Members

Christina Gross, Ph.D.
Anwesha Banerjee, Ph.D.

Emory Mouse Behavioral Core Facility

Jason Schreoder, Ph.D.

Emory Mouse Transgenic and Targeting Core Facility

Helen Zhang

I would also like to thank the NIH for funding my training and research through the GMB Training Grant and the Fragile X Center Grant.

Table of Contents

Table of Figures

Table of Tables

Chapter 1
Introduction

Inherited intellectual disability (ID) comprises a broad, heterogeneous group of disorders, and with an incidence of 1 in 5,000 in males [1], fragile X syndrome (FXS) represents one of the most common forms of inherited ID. Since the cloning of the underlying gene in 1991 there has been tremendous progress in our understanding of the neurological deficits that contribute to FXS. As would be expected, research into FXS has revealed many of the pathways critical to learning and memory formation. Knowledge of these pathways has enabled the rational design of potential therapeutics for FXS. Additionally, it has opened new avenues of investigation into the molecular mechanisms behind other forms of ID and autism.

Identification of FXS as a Distinct Syndrome

In 1969, Lubs identified a family with four male members diagnosed with ID, each of whom had an unusual chromosomal gap on his X chromosome long arm [2]. This observation that had limited clinical utility until 1977, when Sutherland showed specific culture conditions were necessary to visualize the gap consistently [3]. These chromosomal gaps or constrictions in metaphase spreads were termed “fragile sites” due to their propensity to break under certain conditions [4]. It soon became clear that this cytogenetic marker was diagnostic for a distinct X-linked form of ID, designated fragile X syndrome, after the fragile site found in patients.

Individuals with FXS have mild to severe ID, often with autistic-like behaviors [5]. Other neurological symptoms include developmental delay and increased susceptibility to seizures [5]. Upon post-mortem examination, the neurons of FXS patients are found to have dense, immature dendritic spines [5]. The most prominent physical symptom is macroorchidism in males, which usually develops just before puberty [5]. More subtle physical symptoms can include a long, narrow face with prominent ears, joint laxity, and flat feet [5]. These point to a potential connective tissue disorder that has yet to be elucidated in any detail.

With the analysis of more FXS pedigrees, it became apparent that the syndrome did not follow a typical pattern of inheritance for an X-linked disease. Most prominently, pedigrees contained male obligate carriers with no symptoms of FXS [6, 7]. Furthermore, the grandchildren of these healthy male carriers developed FXS at much higher rates than did the siblings of the carriers [6]. This example of genetic anticipation was named the Sherman paradox and remained a mystery until the mutation underlying FXS was identified.

Identification of the *FMR1* Gene

The gene for FXS was cloned in 1991 and named fragile X mental retardation gene 1 (*FMR1*) [8]. *FMR1* is located at cytogenetic position Xq27.3, the exact location of the diagnostic fragile site [9]. In almost all cases, the causative mutation is the expansion of a CGG repeat located in the 5'-UTR of *FMR1*. Although this was a novel mutational mechanism at the time of its discovery, such trinucleotide repeat expansions have since been found in other disease genes. In *FMR1*, the length of the CGG repeat is polymorphic

in the healthy population, ranging from 6 to 54 repeats [10]. When the number of repeats exceeds 200, it is referred to as a full mutation allele and results in FXS [10]. At the molecular level, the large number of CGG repeats in the full mutation leads to hypermethylation both of the CGG repeats and the *FMR1* promoter, hypoacetylation of associated histones, and chromatin condensation; these epigentic changes result in transcriptional silencing of *FMR1* and subsequent loss of its protein product, fragile X mental retardation protein (FMRP) [11-14]. Alleles with an intermediate number of repeats, 55-200, are referred to as premutation alleles [10]. Premutation alleles do not cause an FXS phenotype, but are prone to large increases in repeat length during meiosis, especially female meiosis [10]. The observation that premutation alleles are more vulnerable to expansion during meiosis also helped resolve the Sherman paradox; we now understand that males with a premutation allele will transmit it intact to their healthy daughters [10]. The premutation alleles in the daughters often expand to full mutation alleles during oogenesis, resulting in the higher incidence of FXS seen in the next generation [10].

It is now standard of care to measure the *FMR1* CGG repeat size in all children presenting with developmental delay, intellectual disability, or autism [5]. Given the broad heterogeneity of such patients, only 1-3% of such children tested are typically found to have the full mutation, resulting in a diagnosis of FXS [15]. The full mutation is almost completely penetrant in males, but only 50% of females with a full mutation show FXS symptoms, likely due to random X inactivation. While most known FXS cases are caused by the expansion of the CGG repeat to a full mutation, a small number of deletions and missense mutations in the *FMR1* gene have also been reported [16-18].

Recent studies suggest that more comprehensive screening for such mutations may increase the diagnostic yield by 30% compared to screening for repeat length alone [17]. In particular, there remains an unexplained deficit of *FMR1* missense mutations, with only a small number reported thus far [17-19].

Animal Models of FXS

FMR1 is highly conserved across species [8], making the development of several animal models of FXS possible. The most widely used models have been generated in the mouse and fruit fly. The *FMR1* ortholog in the mouse, *Fmr1*, is located on the murine X chromosome, and its amino acid sequence has 97% homology to FMRP [20]. Unfortunately, there is no relevant animal model of the full CGG expansion, as mice engineered with an expanded number of repeats fail to recapitulate the epigenetic changes and transcriptional silencing seen in humans [21]. However, a targeted deletion of exon 5 created a knockout (KO) mouse lacking FMRP, the functional equivalent of the human full mutation [22]. These mice recapitulate many of the phenotypes seen in FXS patients, including disrupted learning and memory, increased susceptibility to seizures, and large testes[22] . They also show an abundance of dense, immature dendritic spines, as seen in FXS patients [23]. More recently, a mouse line was engineered with loxP sites flanking the promoter and exon 1 of *Fmr1*, allowing for conditional KO of the gene [24]. This will enable the creation of null alleles in specific cell types and at specific stages of development, providing new ways to explore FMRP's function in vivo.

D. melanogaster models of FXS have also been created by making null mutations in the fly ortholog of *FMR1, dFmr1*. These flies have abnormal neuronal architecture and

synaptic function [25-27], impairment of long-term memory [28], and reduced courtship interest (a model of behavioral abnormalities) [29]. These defects can be rescued by a transgene containing human *FMR1* [30]. This makes *D. melanogaster* a convenient system for modeling mutations in FMRP.

FMRP Expression and Functional Protein Domains

FMRP is widely expressed in mammalian tissues [31], but it is especially abundant in the brain and testes [31, 32], consistent with the predominant phenotypes (ID and macroorchidism) observed in patients with FXS. In the brain, FMRP is expressed primarily in neurons, where it is found in the cell body, dendrites, and synapses [31, 33, 34]. A small amount of FMRP can be detected in the nucleus. The timing of FMRP expression seems to begin early in development and continue throughout life [32]. Because of the focus on patients' cognitive deficits, the function of FMRP in nonneuronal cells has received little attention.

Multiple alternatively spliced isoforms of FMRP exist in humans [20, 35], mice [20], and fruit flies [36], with some evidence that individual isoforms may have important differences in expression and function. An example of this would be the long and short isoforms of the *D. melanogaster* dFMR1. The short dFMR1 lacks a glutamine/asparagine (QN)-rich protein interaction domain in the C-terminus of the protein; deleting the long isoform revealed that the short isoform, without the QN domain, is insufficient to properly form short- or long-term memories [36]. The corresponding C-terminal region in human FMRP mediates interaction with kinesin and dendritic transport [37], suggesting it is also important in humans.

Despite this, most research in FXS has used isoform 1 of the human or murine genes. Isoform 1 is the full-length form of the gene and has been designated as the canonical isoform. However, in Brackett et al. the authors showed that, at the mRNA level, isoform 7 is typically the most abundant isoform [38]. It is currently unclear what function individual isoforms might have in mice or humans.

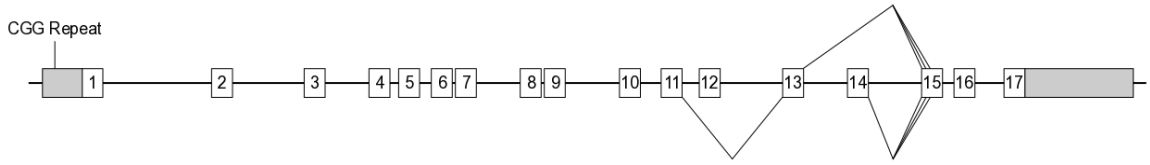

Figure 1. Alternative splicing of FMR1.
FMR1 contains 17 exons. The alternative splicing at the 3'-end of the gene results in 12 isoforms (all possible combinations of including/excluding exon 12, including/excluding exon 14, and using the three different splice acceptor sites in exon 15). The CGG repeat expansion in the 5'-UTR is prone to expansion, particularly during oogenesis. When it expands above 200 repeats, epigenetic changes result in the silencing of the gene. Boxes: exons; straight lines: introns; angled lines: alternative splicing; grey boxes: UTRs.

In mammals, the main isoform of FMRP is a 71-kDa protein composed of several conserved functional domains. FMRP has four RNA-binding motifs, including three K homology domains (KH0, KH1 and KH2) and the arginine-glycine-glycine (RGG) box [39]. FMRP binds RNAs in a sequence-specific manner mediated by these domains. In particular, the methylation status of the arginines in the RGG box seems to regulate FMRP's affinity for certain RNAs [40]. FMRP also contains nuclear localization and export signals (NLS and NES) [41], which facilitate its shuttling in and out of the nucleus [33]. A recent study identified a patient with developmental delay harboring a novel R138Q mutation in the NLS [17]. Although the functional significance of this mutation is unclear, it does point to the importance of the domain [42].

Though not fully appreciated until recently, FMRP also contains two tandem

Agenet domains at its N-terminus [43]. The Agenet domain is part of a proposed "Royal Family" of protein domains that also includes the Tudor, MBT, and Chromo domains [43]. Agenet domains have been shown to bind trimethylated lysine residues and are structurally similar to the UHFR1 protein, which is believed to interact with methylated histone H3K9 [44].

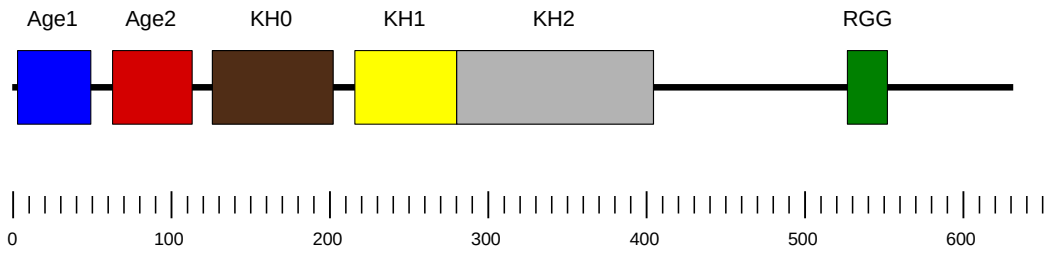

Figure 2. Major domains of FMRP.
The amino acid sequences of human and mouse forms of FMRP have 97% homology. The KH0, KH1, KH2, and RGG domains mediate RNA-binding. The Agenet domains are similar to other protein domains known to interact with histones and trimethylated peptides. FMRP also contains an NES and NLS.

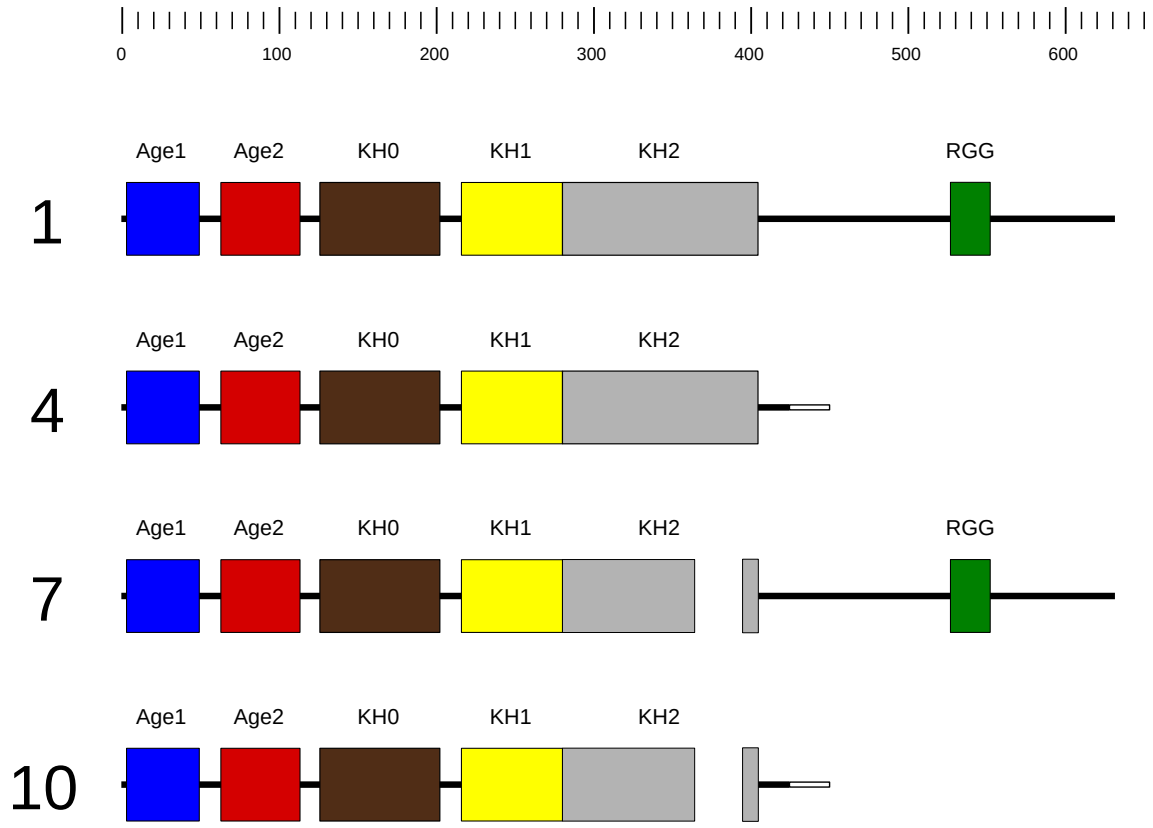

Figure 3. Isoforms of FMRP.
Shown are four of the 12 known isoforms of FMRP. The skipping of exon 12 results in an in-frame deletion of 21 amino acids in the KH2 domain, as seen in isoforms 7 and 10. The skipping of exon 14 results in a frameshift and truncated protein, as seen in isoforms 4 and 10. For each isoform shown, there are two more isoforms resulting from two alternative splice acceptor sites in exon 15.

FMRP is an mRNA-binding Protein

FMRP is a selective RNA-binding protein, binding to as much as 4% of the mRNA in the mammalian brain [45]. Microarray and yeast 3-hybrid assays have identified over 400 putative mRNAs that associate with FMRP [46-49], although only 14 of these have been validated by showing direct biochemical interaction.

Direct binding of FMRP with its target RNAs is mediated by the presence of RNA secondary structures, the best studied of which is called the G-quadruplex. A G-

quadruplex consists of two to four G-quartets/tetrads stacked on top of each other, with each G-quartet made of four guanines in a planar conformation interacting via cyclic hydrogen bonds [50]. FMRP's C-terminal RGG box recognizes the G-quadruplex in vitro [51], and several of FMRP's target mRNAs possess putative G-quadruplex structures. Biochemical assays confirmed that G-quadruplexes mediate the interaction of FMRP with *Fmr1*, *MAP1b*, and *Sema3F* mRNAs [52-54].

Other RNA secondary motifs have also been identified in FMRP targets. Multiple U-rich pentamers were found in both coding and 3'-UTR regions of some FMRP target mRNAs [55], and a study used UV crosslinking and mutagenesis assays to show FMRP binds to a U-rich region in the 5'-UTR of *hASH1* [56]. In addition, another secondary structure referred to as the "kissing complex" has been reported to bind FMRP's KH2 domain in vitro [57]. Finally, a recent study also showed that FMRP binds to superoxide dismutase 1 (*Sod1*) mRNA through a novel RNA structure termed Sod1 Stem Loops Interacting with FMRP (SoSLIP) [58]. SoSLIP consists of three stem-loop structures separated by short stretches of single-stranded RNA and acts as a translational activator [58]. SoSLIP interacts with FMRP's C-terminal region, which includes the RGG box, and competes for binding with the G-quadruplex structure [58].

The cognitive deficits suffered by FXS patients along with the dense, immature dendritic spines observed in the brains of both FXS patients and *Fmr1* KO mice indicated that FMRP plays a role in dendritic development and function. Indeed, many of the mRNAs identified as targets of FMRP have since been shown to localize to dendrites. In situ hybridization demonstrated the dendritic localization of *RGS5*, *GABA-Aδ*, *SAPAP3/4*, and *eEF1A* mRNAs [47, 59, 60]. *Map1b* mRNA was proven to be dendritically localized

through FISH [61]; it and *Arc/Arg3.1* mRNA both coprecipitate with FMRP in brain extracts [62]. In addition, *Arc/Arg3.1* and *CamKIIα* mRNAs have been reported to be present in dendrites [63]. Finally, *PSD-95* mRNA has been shown to directly associate with FMRP in dendrites both in vitro and in vivo [64, 65]. Together, these findings support a model in which FMRP binds and regulates a subset of dendritic mRNAs.

FMRP is a Translational Repressor

In subcellular fractionation experiments, FMRP was found to cosediment with polyribosomes in both neuronal and nonneuronal cells [66-68]. FMRP's association with polyribosomes supports the hypothesis that FMRP acts as a translational regulator of its mRNA targets. This association is disrupted by puromycin, which disrupts actively translating polyribosomes, indicating that FMRP is associated with actively translating polyribosomes [68]. In an FXS patient with an I304N missense mutation, FMRP's interaction with actively translating polyribosomes was abolished[66], showing this association is crucial to its normal function. In addition to interacting with polyribosomes, FMRP is also found in stress granules, which are believed to sequester mRNAs whose translation is being suppressed, in mRNP complexes [69]. Together, these observations implicate FMRP in dynamic translational regulation of its mRNA partners.

The majority of evidence is consistent with FMRP inhibiting translation of most of its target mRNAs. FMRP has been shown to reduce translation of various mRNAs in rabbit reticulocyte lysate, *Xenopus laevis* oocytes [70], and immortalized cells from an *Fmr1* KO mouse [71]. In the reticulocyte assay, removal of the FMRP binding site from *MBP* mRNA abolished FMRP's ability to repress its translation, confirming that FMRP

binding was necessary for translation regulation [72]. Biochemical and genetic assays also indicate that *D. melanogaster* dFmr1 represses translation of the *Map1B* ortholog *futsch* [26]. In vivo assays further demonstrated that the target proteins Map1B, Arc/Arg3.1, and CamKIIα are overexpressed in the brains of *Fmr1* KO mice, consistent with the loss of FMRP-mediated repression [62, 73]. To specifically interrogate FMRP's effect on translation at synapses, synaptoneurosomes (SNS) from *Fmr1* KO mice were examined and showed increased levels of Map1B, CamKIIα, and Arc/Arg3.1 proteins [62]. Subcellular fractionation of *Fmr1* KO SNS also revealed a shift of CamKIIα, PSD-95, and GluR1/2 mRNAs to actively translating polyribosomes, consistent with these mRNAs being de-repressed [64]. Surprisingly, FMRP seems to upregulate the translation of *Sod1* mRNA by strengthening SoSLIP's ability to activate translation [58] and to increase translation of *hASH1* through an unknown mechanism [56], signifying that FMRP may also activate translation of some transcripts.

Mechanisms of Translational Repression

One model of how FMRP regulates the translation of mRNAs proposes that it inhibits the initiation of translation. In cap-dependent translation, which is known to be important in neurons, initiation requires the eIF4A-eIF4G-eIF4E (eIF4F) complex to associate with the 5'-m^7 cap of the mRNA template. 4E binding proteins (4E-BP) interfere with the eIF4E-eIF4G interaction, thereby regulating the formation of the eIF4F complex. Recently, cytoplasmic FMRP-interacting protein (CYFIP1), a known protein-binding partner of FMRP, was discovered to be a 4E-BP [74]. Coimmunoprecipitation confirmed that both CYFIP1 and eIF4E are associated with FMRP in vivo; however, the

FMRP/CYFIP1 association is independent of eIF4E binding [74]. Interestingly, the formation of the FMRP/CYFIP1/eIF4E complex was increased by the presence of capped-*Arc* mRNA, a known FMRP target, but not capped-luciferase mRNA [74]. These data have led to a model in which FMRP recruits CYFIP1 to specific mRNAs, subsequently associates with eIF4E, and blocks recruitment of the translation initiation machinery.

An alternate model for how FMRP inhibits translation posits that FMRP causes ribosomes to stall during the elongation phase of translation. This model is supported by data showing that some FMRP cosediments with polyribosomes, even after treatment with puromycin, meaning these polyribosomes likely represent stalled ribosomes [68]. Ribosome run-off experiments in which cells were treated with sodium azide, a non-specific inhibitor of translation initiation that does not affect elongation, also revealed that a portion of FMRP was associated with stalled ribosomes [75]. Ribosome stalling has not been thoroughly characterized, but is presumed to be influenced by tRNA availability, subcellular localization, folding dynamics of the nascent protein, and RNA secondary structure [76].

Data also indicate that FMRP represses translation of its target mRNAs through the RNAi pathway. Both the *D. melanogaster* dFMR1 and mammalian FMRP associate with Argonaute 2 (AGO2) and Dicer, critical components of the RNA-induced silencing complex (RISC) [77-79], as well as associating with specific microRNAs (miRNAs) [80]. Experiments in *D. melanogaster* further demonstrated that AGO2 is necessary for dFmr1-dependent synaptic plasticity [80]. In vitro, FMRP can help assemble miRNAs on target RNAs, an activity directed by its KH domains [79]. In addition, a recent study

showed that FMRP selectively associates with several miRNAs in the mouse brain [81]. Overexpression of two of these miRNAs, miR-125b and miR-132, in cultured rat hippocampal neurons resulted in longer and thinner dendritic spines or stubby and mushroom spines, respectively [81]. Knockdown of FMRP in these cells rescued both phenotypes [81]. Taken together, the genetic and biochemical data support a mechanism in which FMRP binds to the 3'-UTR of target mRNAs, where it then mediates or stabilizes the binding of the complementary miRNA-RISC complex in order to block translation. Whether the miRNA-RISC/FMRP complex blocks translation initiation or elongation is unknown, and both mechanisms have been implicated for miRNAs in general [82].

mGluR Theory of Fragile X Syndrome

Deficits in synaptic plasticity are known to correlate with learning and memory impairment in the brain, so it was expected that such deficiencies might be at the core of FXS. One form of synaptic plasticity, group1 metabotropic glutamate receptor (mGluR)-dependent long-term depression (mGluR-LTD), is dependent on the local protein synthesis of postsynaptic, dendritically-localized mRNAs in response to synaptic stimulation. This local protein synthesis results in α-amino-3-hydroxy-5-methyl-isoxazoleproprionic acide receptor (AMPAR) internalization, a key step of mGluR-LTD. The mGluR theory of FXS proposes that FMRP acts in this pathway downstream of mGluRs and upstream of local protein synthesis. As such, the mGluR theory predicts that FMRP represses translation of its mRNA targets in the normal basal state, but upon mGluR activation, FMRP repression is released, allowing the burst of local protein

synthesis necessary for AMPAR internalization and LTD [83]. When FMRP is absent, such as happens in FXS, protein synthesis should be constitutively elevated, leading to overactive AMPAR internalization and exaggerated LTD, even in the absence of mGluR activation.

In support of this theory, mGluR-LTD is enhanced in the hippocampus of *Fmr1* KO mice and does not require new protein synthesis [84, 85]. In agreement with this, the level of several FMRP target mRNAs associated with actively translating polyribosomes is increased in response to DHPG, an mGluR agonist, in wild type (WT) mouse SNS, but not in *Fmr1* KO SNS [64]. Furthermore, metabolic labeling with [^{35}S] methionine shows that the DHPG-induced synthesis of PSD-95 and CamKIIα proteins seen in WT SNS is absent in *Fmr1* KO SNS [64]. Both the persistently enhanced mGluR-LTD as well as the inability to further increase protein synthesis in response to new synaptic stimuli are the likely culprits behind ID in FXS.

The mGluR theory also predicts that antagonizing the mGluR pathway may lead to a reduction of FXS phenotypes. The mGluR antagonist MPEP is indeed able to rescue behavioral and cognitive deficits in the fruit fly, zebrafish, and mouse models of FXS [86-89]. MPEP also rescues the altered dendritic spine morphology seen in *Fmr1* KO neurons and restores proper AMPAR internalization [90]. Furthermore, genetic reduction of mGluR5 in *Fmr1* KO mice rescues many of the disease-related phenotypes [91, 92]. Pharmacological rescue of FXS phenotypes has now opened many new avenues for potential therapeutic intervention in FXS and has spawned several clinical trials of drugs that target the mGluR pathway.

Phosphorylation Regulates FMRP-Mediated Translation Inhibition

In vivo, FMRP exists in both phosphorylated and unphosphorylated forms, although phosphorylated FMRP is the predominant form in dendritic granules [93]. FMRP contains a serine residue that is conserved from *Drosophila* to humans (human Ser500, murine Ser499, Drosophila Ser406) and is the primary phosphorylated residue in FMRP [75]. Phosphorylation is hierarchical, with phosphorylation of this key residue triggering phosphorylation of other nearby Serines [75]. The belief is that the phosphorylation status of this key serine controls the functionality of FMRP. Though phosphorylation of FMRP does not affect its ability to bind RNA, it does affect its association with polyribosomes and its ability to inhibit translation [75, 94].

Using constitutively phosphorylated and unphosphorylated mimics of murine FMRP containing the S499D and S499A mutations, respectively, Ceman et al. showed that only the S499D-FMRP is still associated with polyribosomes after sodium azide-induced polyribosome run-off [75]. This suggests that phosphorylated FMRP is associated with stalled ribosomes, whereas unphosphorylated FMRP allows translation to proceed. In Coffee et al., the authors showed that a phospho-mimic form of human FMRP rescued defects in synaptic architecture, protein levels, and learning in dfmr1 null flies. In contrast, a constitutively unphosphorylated form of the protein was unable to rescue any of the defects [30].

This is consistent with the observation by Mudashetty et al. that overexpression of S499D-FMRP, but not S499A-FMRP, could inhibit translation of a PSD-95_UTR construct [94]. Furthermore, they showed that S499D-FMRP shifted PSD-95_UTR into

mRNP fractions on sucrose gradients [94], arguing that the phosphorylation of FMRP suppresses the translation initiation of PSD-95. In another experiment, the same group showed dephosphorylation of FMRP following mGluR activation coincides closely with the release of translation inhibition of FMRP target mRNAs, such as PSD-95 [93]. Interestingly, Dicer associates with unphosphorylated but not phosphorylated FMRP [95], indicating that phosphorylation of FMRP may also regulate the RNAi pathway by blocking the processing of pre-miRNAs by Dicer. These data support a model in which phosphorylated FMRP inhibits translation of its target mRNAs, while unphosphorylated FMRP allows translation to proceed.

All the previous work examining the effects of phosphorylation of FMRP has relied on overexpressing the protein in mammalian cell culture or expressing a human transgene in fruit flies. While it all supports the conclusion that FMRP is regulated by the phosphorylation of the key serine, we wished to confirm this in a more physiologically representative system. To that end, we created knockin mouse models to study the effects of phosphorylation in vivo.

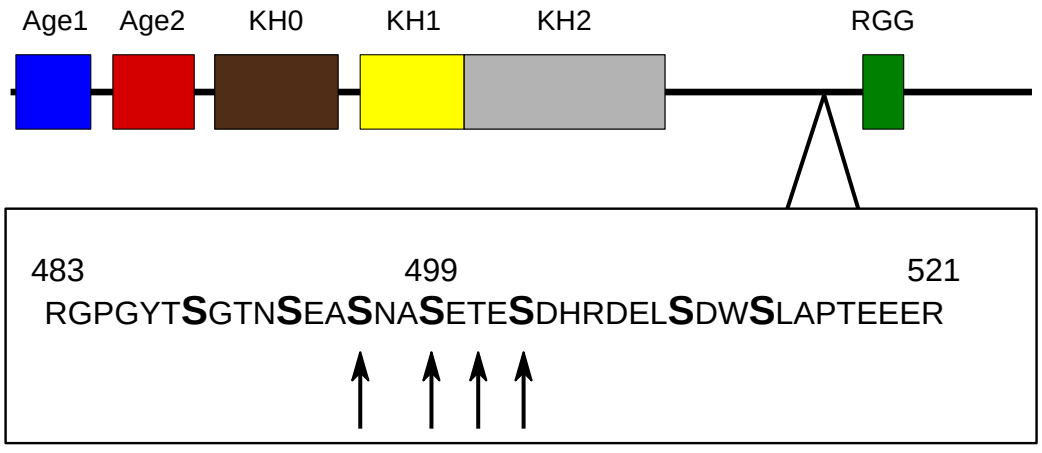

Figure 4. Phosphorylation of FMRP.
Arrows denote the four possible sites of phosphorylation as identified by mass spectrometry.

Ser499 (Ser500 in humans, Ser406 in flies) is the primary phosphorylated serine in FMRP. Phosphorylation of Ser499 casues one or more of these sites to be phosphorylated in a hierarchical fashion. Serines are in bold. Numbers refer to amino acid position in mouse.

Chapter 2
Phosphomutant FMRP

In order to study the effects of phosphorylation of FMRP we created two knockin mouse models, mutating serine residue 499 to either alanine or aspartic acid. The R group on alanine does not contain a hydroxyl group and therefore cannot be phosphorylated. In contrast, the charge and structure of aspartic acid is similar to that on a phosphorylated serine. A protein with the serine mutated to aspartic acid often acts like a constitutively phosphorylated protein. These mutations parallel the work previously done using cell culture and fruit flies [30, 75]. However, our models would allow us to study the effects of these mutations in the context of a WT promoter and regulatory elements.

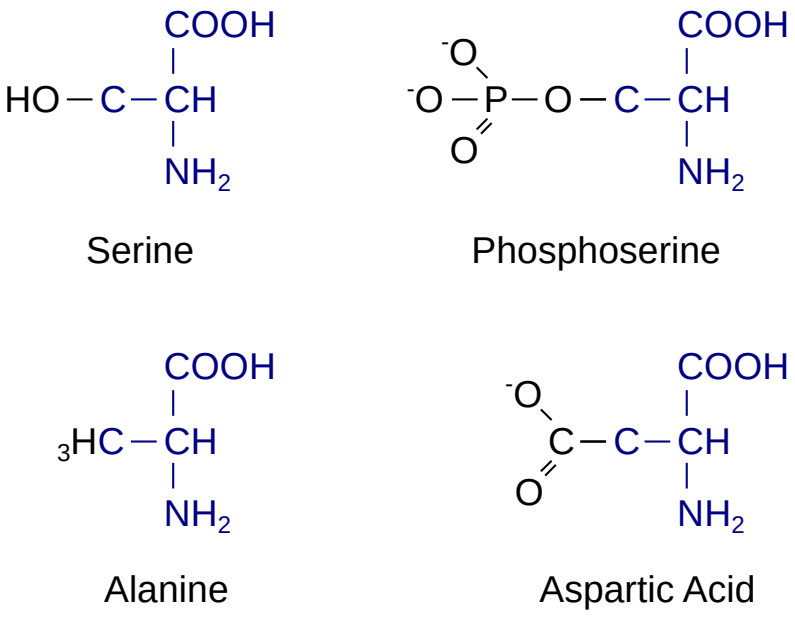

Figure 5. Amino acid structure.

The role of phosphorylated serine can be studied by mutating the serine residue to either alanine or aspartic acid. Serine contains a hydroxyl group that acts as a substrate for phosphorylation by kinases. The lack of a hydroxyl group on alanine prevents its phosphorylation. The charge and structure of aspartic acid mimic those of phosphoserine.

The codon for Ser499 is in exon 15 of the *Fmr1* gene and the alternative splicing of this exon presented a problem. Exon 15 contains two alternative splice acceptor sites, both of which are located 3' of the codon for Ser499. This results in isoforms of FMRP that lack the Ser499 residue. We wanted to focus our study on the effects of phosphorylation at Ser499, and therefore decided to remove these two alternative splice acceptor sites. However, this meant that in order to isolate the effects of the Ser499 mutations we needed to also create a control line of mice. This control line (referred to as SA2) would have both alternative splice acceptor sites removed but still contain the WT Ser499. The other two lines would also have the alternative splice acceptor sites removed but have Ser499 mutated to alanine or aspartic acid (referred to as Ser499Ala and Ser499Asp, respectively).

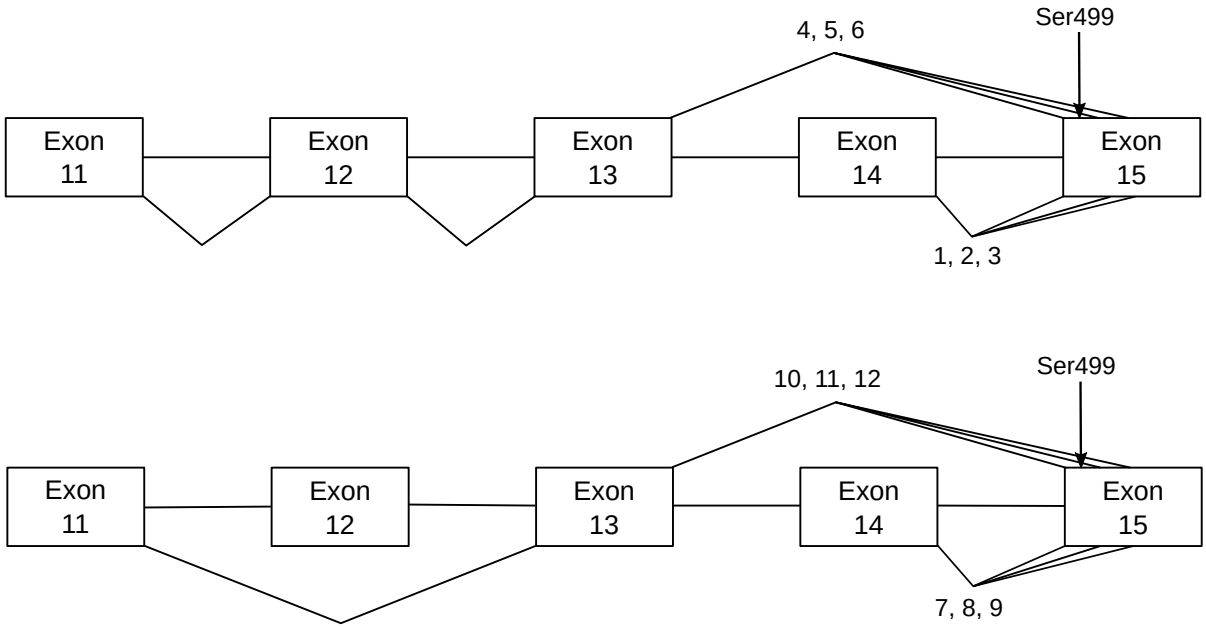

Figure 6. Alternative splicing of *Fmr1*.
The C-terminal region of the *Fmr1* gene is subject to alternative splicing. The skipping of exon 12 results in an in-frame deletion of 21 amino acids. The skipping of exon 14 results in a frameshift and a truncated protein. There are two alternative splice acceptor sites in exon 15. The use of either alternative splice acceptor site results in an in-frame deletion and the absence of Ser499. mRNA from all 12 possible isoforms can be detected in mice.

Creation of Mice

In order to construct the required targeting vectors, I followed the protocol described in Wu et al. [96]. This protocol uses recombineering, as opposed to traditional cloning techniques, to create the targeting vectors and the Capecchi lab has made available several plasmids which make the process easier. First, I cloned the desired section of genomic DNA using red-recombination. I then introduced the desired mutations in exon 15 using site directed mutagenesis. Finally, I cloned a neomycin resistance cassette, flanked by FRT sites, into intron 15.

I chose to have my targeting vector span from intron 12 to intron 16 of the murine

Fmr1 gene. I cloned this region of genomic DNA from the bacterial artificial chromosome (BAC) RP23-397L15. This BAC was derived from a five-week old C57Bl/6J female mouse and contains a 195 kb insert which includes the entire *Fmr1* gene. I used red-recombination to clone the desired section of the *Fmr1* gene into the plasmid pStart-K, a low copy plasmid designed by the Capecchi lab for this purpose. To this end, I designed primers to amplify the pStart-K backbone. The forward primer (pStart_Fmr1_5') contained 50 nucleotides homologous to intron 12 of *Fmr1* followed by 24 nucleotides homologous to pStart-K. Similarly, the reverse primer (pStart_Fmr1_3') contained 50 nucleotides homologous to intron 16 of *Fmr1* followed by 25 nucleotides homologous to pStart-K.

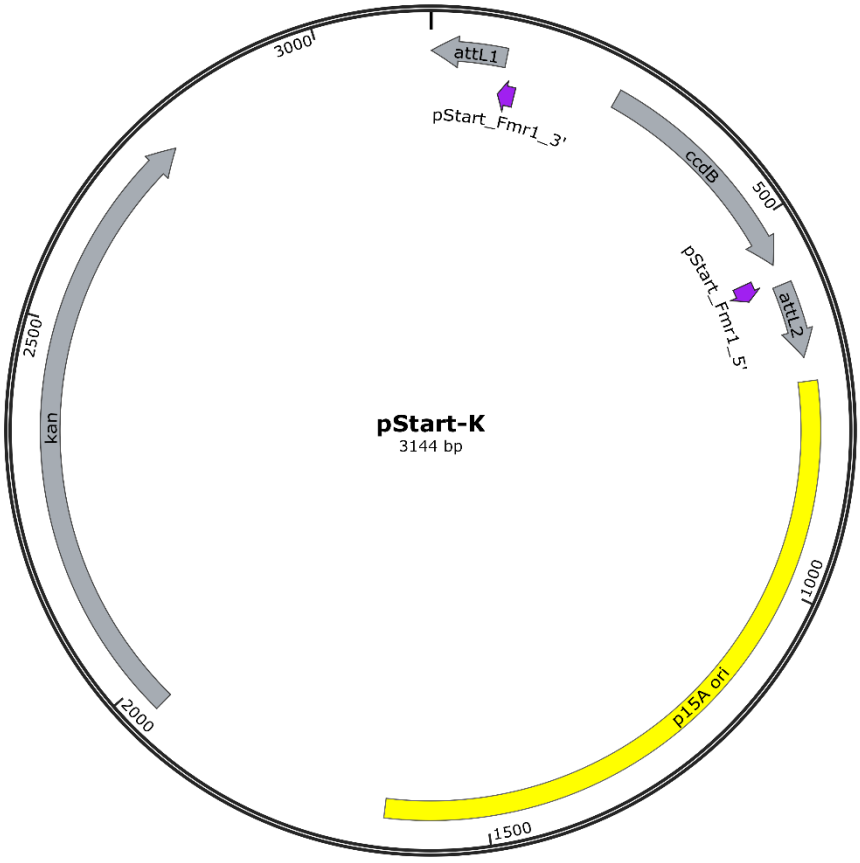

Figure 7. Plasmid pStart-K.

Plasmid pStart-K is a low copy plasmid provided by the Capecchi lab to help clone genomic DNA using the red-recombination system. The origin of replication and kanamycin resistance gene were amplified by PCR and used as a vector to clone the desired genomic DNA.

I used these primers and plasmid pStart-K to produce a linear fragment of DNA that contains the replication of origin and kanamycin resistance gene from pStart-K flanked by sequences homologous to *Fmr1* introns 12 and 16. I combined this DNA fragment, BAC RP23-397L15, and the components of the red-recombination system to create a low copy plasmid, with a kanamycin resistance gene, that contains 7.5 kb of genomic DNA spanning intron 12 to intron 16 of *Fmr1* (referred to as pStart-Fmr1-Ex15).

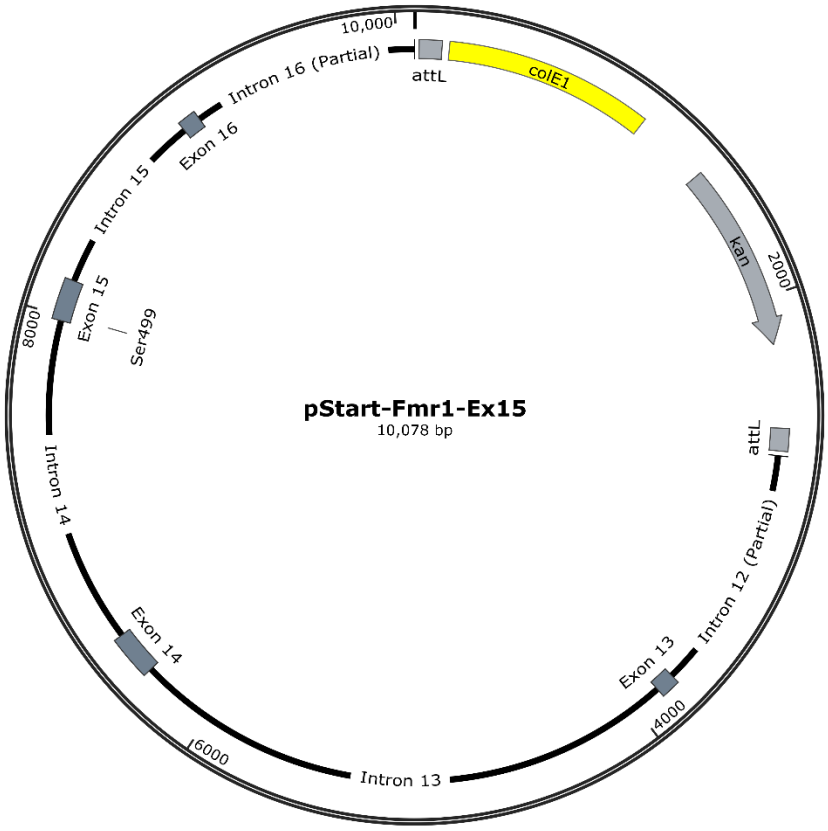

Figure 8. Plasmid pStart-Fmr1-Ex15.
Plasmid pStart-Fmr1-Ex15 is the basis for all the targeting vectors I created for this project. It contains the origin of replication and kanamycin resistance gene from plasmid pStart-K. It also

contains 7.5 kb of genomic DNA spanning from intron 12 to intron 16 of the murine *Fmr1* gene.

In order to destroy the two alternative splice acceptor sites in exon 15, I relied on the fact that splice acceptor sites invariably end in an "AG" dinucleotide. Mutating either of these nucleotides results in the destruction of the splice acceptor site. In both alternative splice acceptor sites, the A of the "AG" sequence is in the wobble position of a codon. This allowed me to introduce mutations to remove the splice acceptor sites without changing the amino acid sequence of the final protein. Specifically, I mutated the first site from "AG" to "TG," preserving the threonine residue at position 501. Similarly, I mutated the second site from "AG" to "GG," which keeps the lysine residue at position 514. Starting with pStart-Fmr1-Ex15, I sequentially introduced these two mutations using site directed mutagenesis to produce plasmid pStart-Fmr1-SA2.

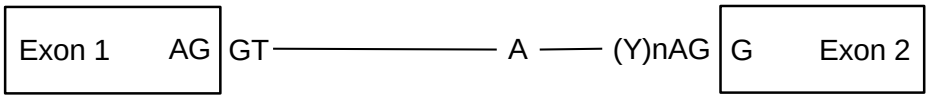

Figure 9. Splicing consensus sequence.
Most intronic sequences are not well conserved, but certain signals important to the spliceosome are nearly invariant. The 5'-end of the intron begins with a GT. The 3'-end of the intron ends with an AG; it is this invariant AG which I relied on to remove the alternative splice acceptor sites in exon 15. Upstream of the AG dinucleotide is a polypyrimidine tract (cytosine and thymidine nucleotides). Further upstream of that is the adenine nucleotide involved in lariat formation.

First Alternative Splice Acceptor Site

Residue	Glu500	Thr501	Glu502	Ser503
Codon	GAA	AC**A**	**G**AA	TCT
Alternative Codons		ACC ACG ACT	GAG	

Second Alternative Splice Acceptor Site

Residue	Ser513	Leu514	Ala515	Pro516
Codon	TCA	TT**A**	**G**CT	CCA
Alternative Codons		TTG CTA CTC CTG CTT	GCC GCA GCG	

Figure 10. Possible ways to remove alternative splice acceptor sites.
The AG sequence for the first alternative splice acceptor site consists of the third nucleotide in residue Thr501 and the first nucleotide residue Glu502. The A could be changed to any other nucleotide without affecting the threonine at residue 501. The G could not be altered without changing Glu502 to a different amino acid. Similarly, the AG sequence for the second alternative splice acceptor site consists of the third nucleotide in residue Leu514 and the first nucleotide in residue Ala515. The A could be changed to a G without affecting the leucine at residue 514. The G could not be altered without changing Ala515 to a different amino acid. Residue numbers refer to the mouse protein.

I also used site directed mutagenesis to change residue 499 from serine to either alanine or aspartic acid. The codon for Ser499 is "TCT." I altered this to "GCT" for alanine and "GAC" for aspartic acid. I chose these codons because the same mutations were made in the *Fmr1* cDNA used in earlier cell culture-based experiments studying the phosphorylation of Ser499 [75]. I mutated the Ser499 in pStart-Fmr1-SA2 to either alanine or aspartic acid, to create pStart-Fmr1-S499A and pStart-Fmr1-S499D respectively.

Having created three plasmids with the mutations I wanted to introduce into mice,

I next added a selectable marker to the plasmids. I chose plasmid FnF11 as the DNA donor for this. FnF11 carries a neomycin resistance gene driven by a PolIII promoter, allowing for selection of this DNA in embryonic stem cells treated with neomycin. This cassette is flanked by two FRT sites, so the cassette can be removed post integration. Furthermore, the cassette also carries the FLPe gene driven by the testis specific Prm1 promoter. This is designed to make the whole cassette self-excise when the DNA passes through the male germline, thereby removing the need to breed founder mice to FLP-expressing mice.

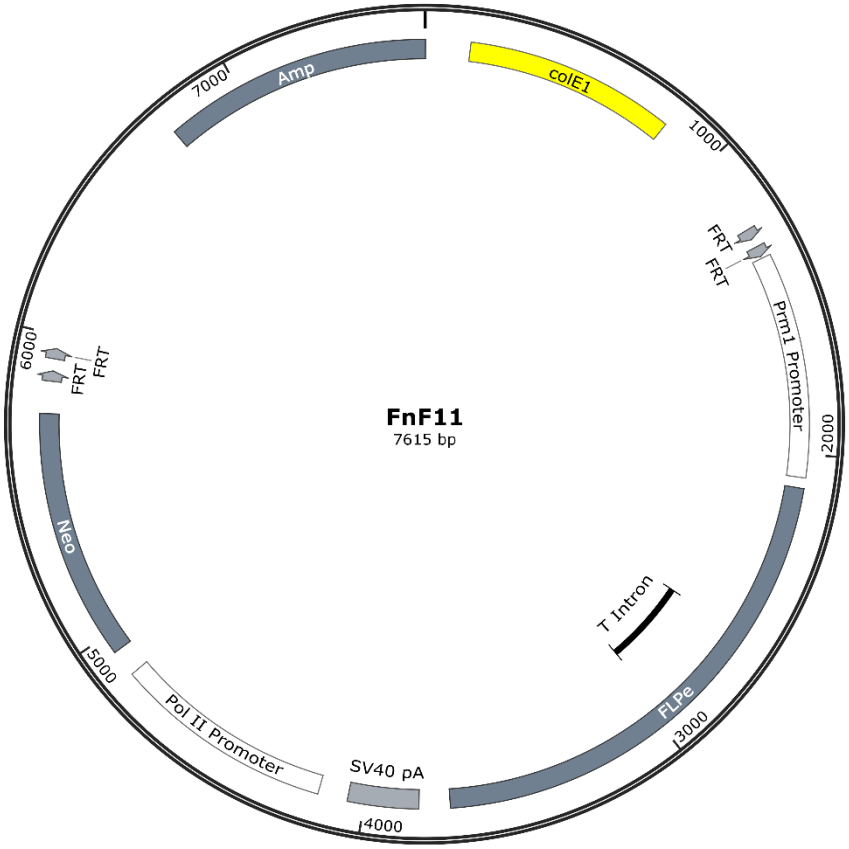

Figure 11. Plasmid FnF11.
This plasmid was made available by the Capecchi lab. It contains a neomycin resistance cassette flanked by FRT sites. The FLPe gene driven by the testis-specific Prm1 promoter is intended to allow the cassette to self-excise when passed through the male germline.

The above cassette consists of 4.7 kb of DNA. Traditionally this would be cloned using restriction enzymes but I used in vitro recombination technology. This allowed me wide choice in where to place the cassette. I placed it in intron 15, less than 900 bp from the mutations in exon 15. Since a single FRT site would be left behind after excision of the cassette, I chose a specific location that does not show strong conservation between species. This was intended to minimize the risk that the remaining FRT site would have any physiological effects. I introduced this cassette into pStart-Fmr1-SA2, pStart-Fmr1-S499A, and pStart-Fmr1-S499D to create pStart-SA2-Neo, pStart-S499A-Neo, and pStart-S499D-Neo, respectively.

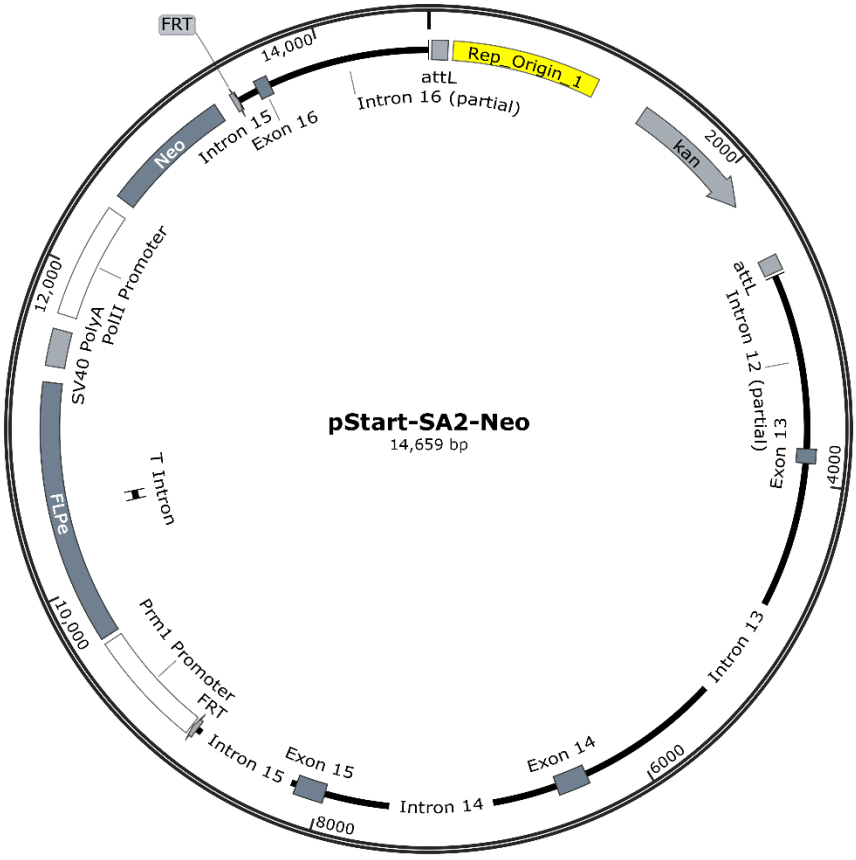

Figure 12. Plasmid pStart-SA2-Neo.
Plasmid pStart-SA2-Neo contains the mutations that destroy the two alternative splice acceptor sites in exon 15. It also contains the neomycin cassette from plasmid FnF11. Plasmids pStart-

S499A-Neo and pStart-S499D-Neo are identical to plasmid pStart-SA2-Neo except for the engineered missense mutations in exon 15.

The Emory mouse transgenic and gene targeting core linearized the three plasmids and electroporated them into embryonic stem cells (ESC) derived from strain 129 mice using standard protocols. Cells were grown in the presence of neomycin to select for cells that had incorporated the exogenous DNA. DNA was extracted from the cells in 96-well plate format and I screened the samples by Southern blot to identify clones that had incorporated the DNA through homologous recombination.

The screening strategy relied on a ScaI/BglI double digestion. ScaI cuts in intron 9 and exon 17 of the *Fmr1* gene; there is no other ScaI cut site nor a BglI cut site in the intervening DNA sequences. Both ScaI sites are outside the region of homology to my targeting vectors. The neomycin cassette contains a single BglI cut site but no ScaI sites. Therefore, digesting WT DNA with ScaI/BglI produces a 14 kb fragment in this region. Digesting DNA that has successfully recombined with the targeting vector produces two fragments from this region – a 12.4 kb 5'-fragment and a 6.1 kb 3'-fragment. For my screening strategy, I designed two probes which lay outside the regions homologous to my targeting vectors, one each for the 5' and 3' arms of the targeted region. These are designated probe M5 and probe M2, respectively.

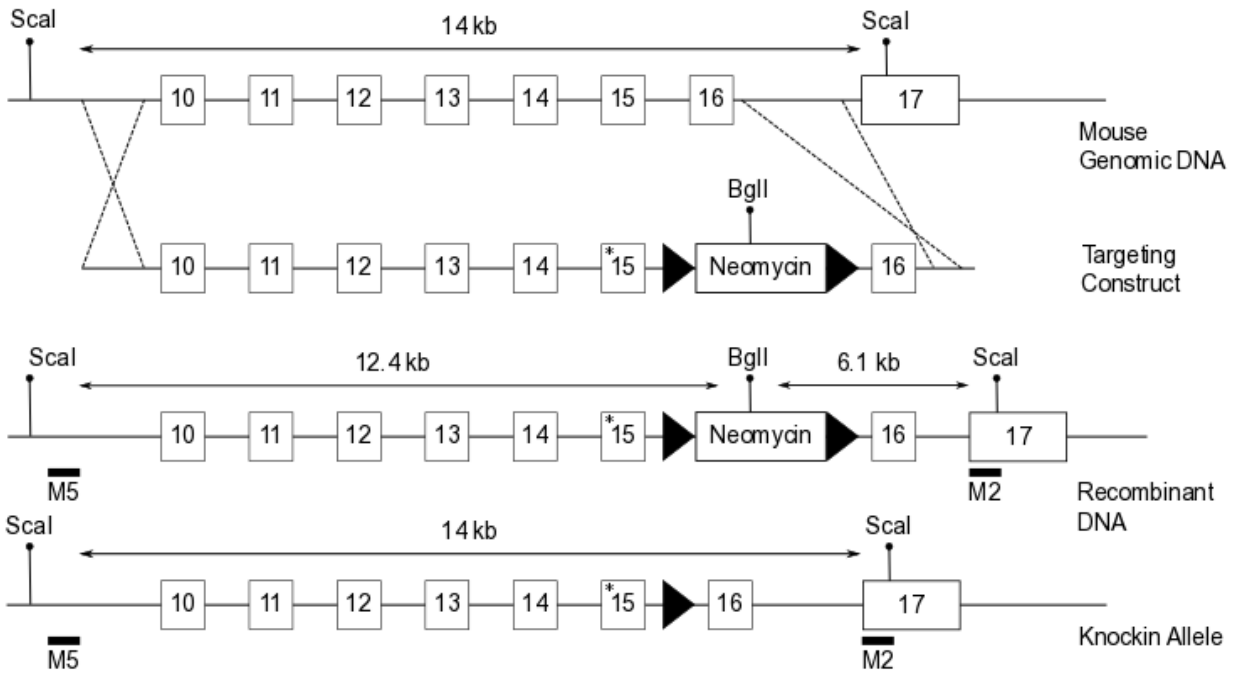

Figure 13. Recombination of the targeting vectors.
The neomycin cassette in the recombinant DNA contains a BglI restriction enzyme site which is used to detect the presence or absence of the cassette in a Southern blot. Breeding recombinant mice to FLPe expressing mice results in the removal of the neomycin cassette in offspring; a single FRT site remains in the genomic DNA. FRT sites are denoted by solid black triangles. Engineered mutations in exon 15 are denoted by an asterisk. Probes M2 and M5 for Southern blotting are denoted by black bars.

I screened potential recombinant clones by probing Southern blots for the 6.1 kb 3'-fragment. I screened 239 potential SA2 clones, 360 potential Ser499Ala clones, and 569 potential Ser499Asp clones. I identified two recombinant clones for the SA2 line (A3 and C2), one recombinant clone for the Ser499Ala line (2F1), but no recombinant clones for the Ser499Asp line. This represents a targeting efficiency of 0.84% for the SA2 construct and 0.28% for the Ser499Ala construct. For each potential recombinant clone, the targeting core cultured additional cells and provided me DNA from half those cells. I performed additional Southern blots on those samples to confirm the DNA had successfully recombined into the endogenous *Fmr1* locus. The targeting core injected those clones into blastocysts to produce chimeras, and I bred the chimeras to WT

C57BL/6J mice from the Warren lab mouse colony. All SA2 mice were derived from clone C2.

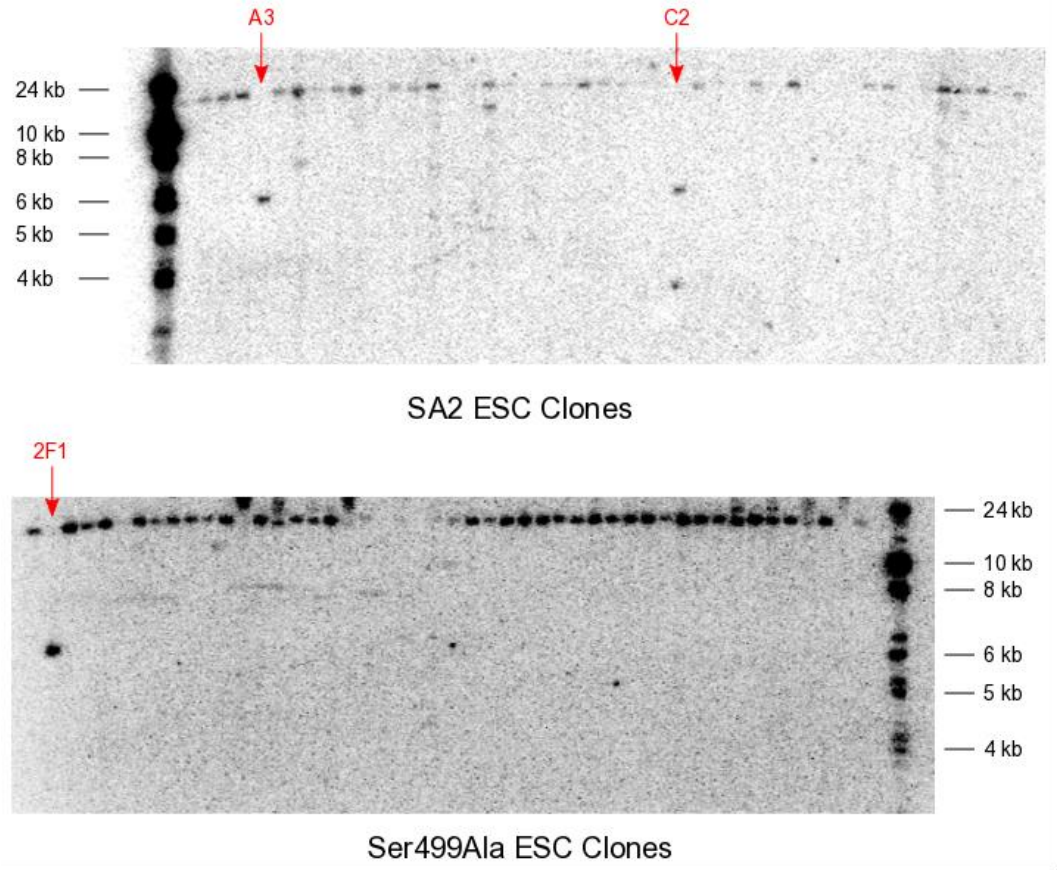

Figure 14. Screening ESC clones.
Putative ESC clones were screened by Southern blot using probe M2. The majority of clones contained WT DNA sequence, as indicated by the 14 kb bands seen in most lanes. The two recombinant SA2 clones and one recombinant Ser499Ala clone that were identified are indicated by red arrows. These clones contain a recombinant 6.1 kb band. Since *Fmr1* is an X-linked gene and the ES cells are male, recombinant clones contain only one allele and therefore do not have the 14 kb band. I never identified a recombinant Ser499Asp clone.

The neomycin cassette contained in the recombinant DNA was intended to be self-excising when it passed through the male germline. Therefore, any litters sired by male mice containing the recombinant DNA should have contained pups in which the neomycin cassette had been removed from the recombinant DNA, leaving behind a single FRT site. However, despite screening over 150 offspring from these matings by PCR I

was unable to detect any in which the neomycin cassette had been removed. Therefore, I bred my recombinant mice to Cre-FLPe mice. Resulting offspring should express FLPe recombinase in all cells. As expected, these crossings produced recombinant mice in which the neomycin cassette had been removed. The removal of the cassette was confirmed by both PCR and Southern blotting and the presence of the desired mutations in exon 15 was confirmed by amplifying the region by PCR and digesting the PCR product with restriction enzymes.

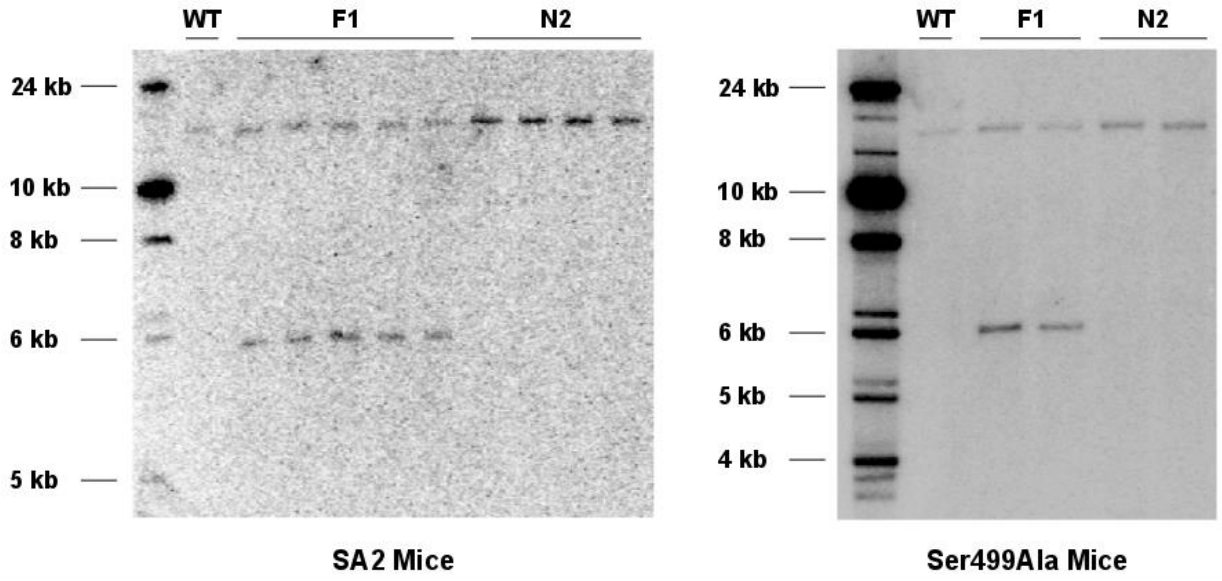

Figure 15. Removal of neomycin cassette.
Founder mice (F1) contain the neomycin cassette in intron 15 of the *Fmr1* gene. This results in the presence of a 6.1 kb band in the above Southern blots probed with probe M2. The offspring of the founder mice and FLPe expressing mice (N2) have had the neomycin cassette removed as shown by the 14 kb band. Note that this Southern blot strategy cannot distinguish between WT DNA and recombinant DNA that has had the neomycin cassette removed.

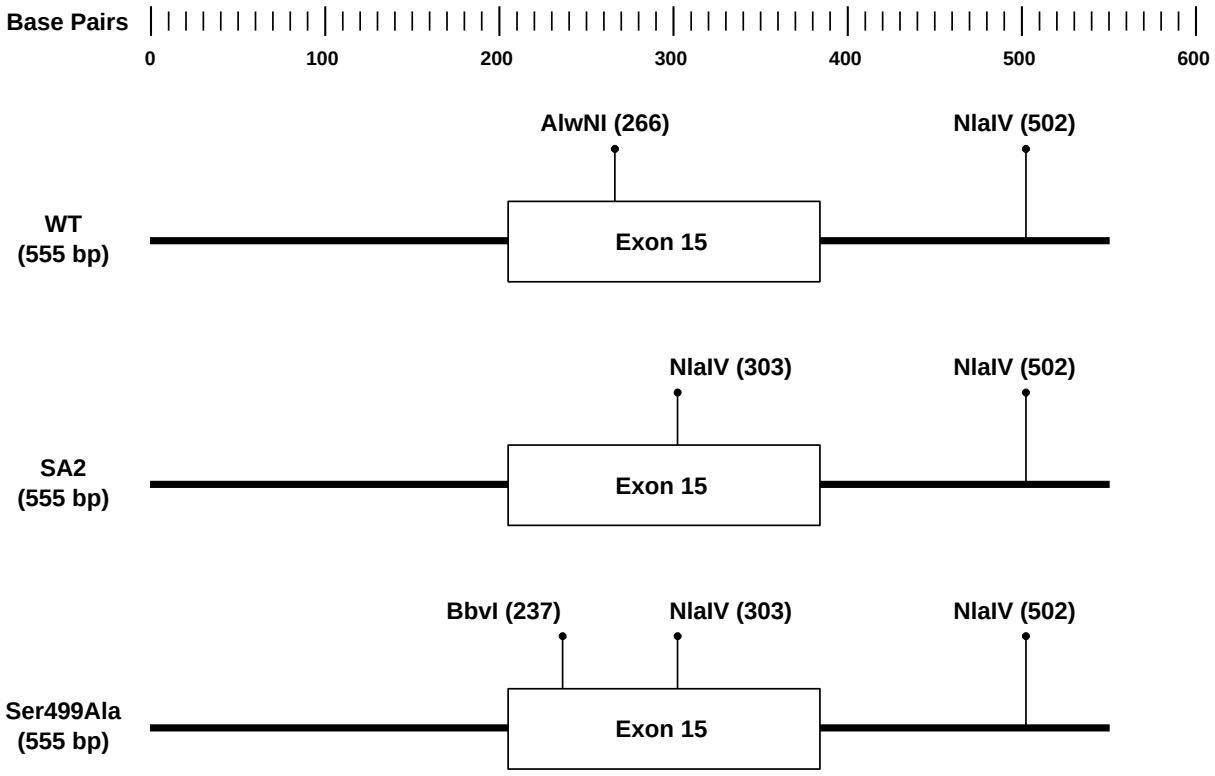

Figure 16. PCR/digestion strategy to genotype mice.
The removal of the first alternative splice acceptor site removes the AlwNI restriction digest site at position 266. The removal of the second alternative splice acceptor site creates the NlaIV restriction digest site at position 303. The Ser499Ala mutation creates the BbvI restriction digest site at position 237. I amplified the DNA in this region from WT, SA2, and Ser499Ala mice and used the presence or absence of these sites to verify the mice carried the desired mutations.

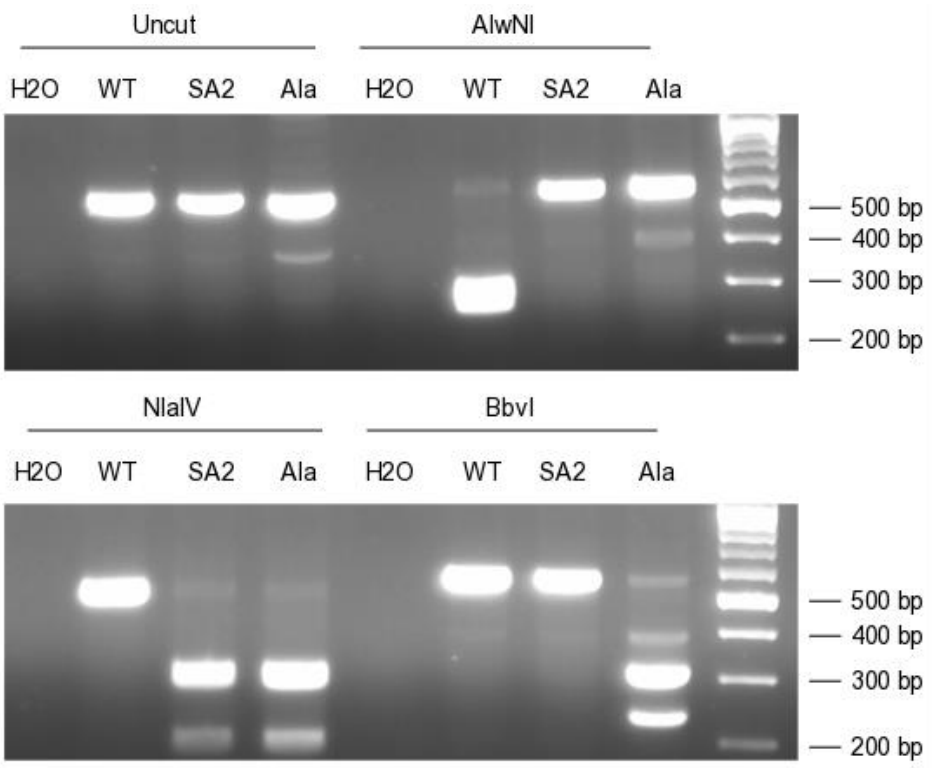

Figure 17. Verifying mutations in mice.
The region around exon 15 was amplified by PCR using water, WT DNA, SA2 DNA, and Ser499Ala DNA as templates. The products were either left intact (upper panel, left), digested by AlwNI (upper panel, right), digested by NlaIV (lower panel, left), or digested by BbvI (lower panel, right). All digests produced the expected results.

Genotyping the phosphomutant mice using the above method is not practical for routine genotyping. In particular, despite several attempts at optimization I was never able to develop a protocol that generated a large amount of PCR product. So genotyping requires performing 5-10 PCR reactions per sample, pooling and purifying the products, and finally digesting the products. Therefore, for routine genotyping I relied on a PCR protocol that detected the presence of the FRT site left behind in intron 15 after excision of the neomycin cassette. This site is less than 900 bp away from the relevant mutations in exon 15. It is unlikely that recombination will separate these two pieces of DNA.

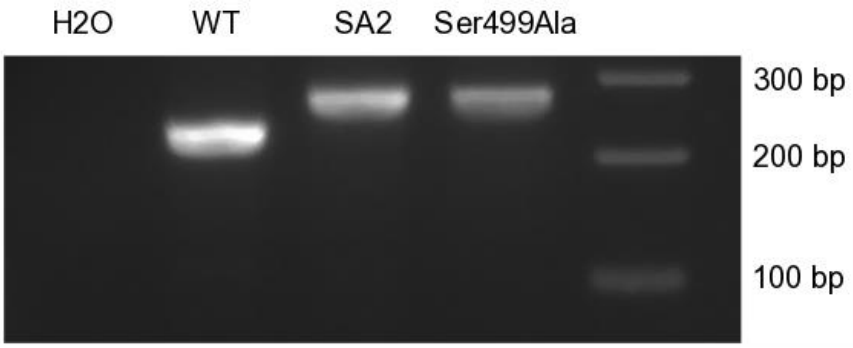

Figure 18. PCR for routine genotyping of mice.
The PCR typically used to genotype phosphomutant mice detects the presence of the FRT scar left behind after excision of the neomycin cassette. The WT PCR product is 235 bp. The SA2 and Ser499Ala PCR products are 275 bp. This genotyping method cannot distinguish between SA2 and Ser499Ala mice.

Phenotype of Mice

Since I introduced mutations to remove the two alternative splice acceptor sites in exon 15, I first verified the knockin mice were in fact not using these alternative splice acceptor sites. I reverse transcribed *Fmr1* mRNA and amplified the C-terminal region by PCR. I did not detect any isoforms which used the alternative splice acceptor sites. However, both the SA2 and Ser499Ala mice expressed novel isoforms. In all cases, the new isoforms were slightly smaller than isoforms that exist in the WT mice. I purified these novel PCR products from an agarose gel and sequenced them. This revealed that deletion of the two alternative splice acceptor sites resulted in the use of two cryptic splice acceptor sites in exon 15. The use of the first cryptic splice acceptor site results in a frameshift and premature stop codon. However, the use of the second cryptic splice acceptor site results in the deletion of 84 base pairs as compared to isoform 1. This in-frame deletion results in a protein missing 28 amino acids as compared protein isoform 1. However, this represents a deletion of only three extra amino acids compared to isoforms

using the second alternative splice acceptor site (i.e. isoforms 3, 6, 9, and 12).

To make discussion of the isoforms easier, I will refer to isoforms that use the first cryptic splice acceptor site with the name of the most similar WT isoform that uses the first alternative splice acceptor site. For example, I will refer to the isoform in SA2 and Ser499Ala mice that includes exons 12 and 14 but uses the first cryptic splice acceptor site as isoform 2. Similarly, I will refer to isoforms that use the second cryptic splice acceptor site with the name of the most similar WT isoform that uses the second alternative splice acceptor.

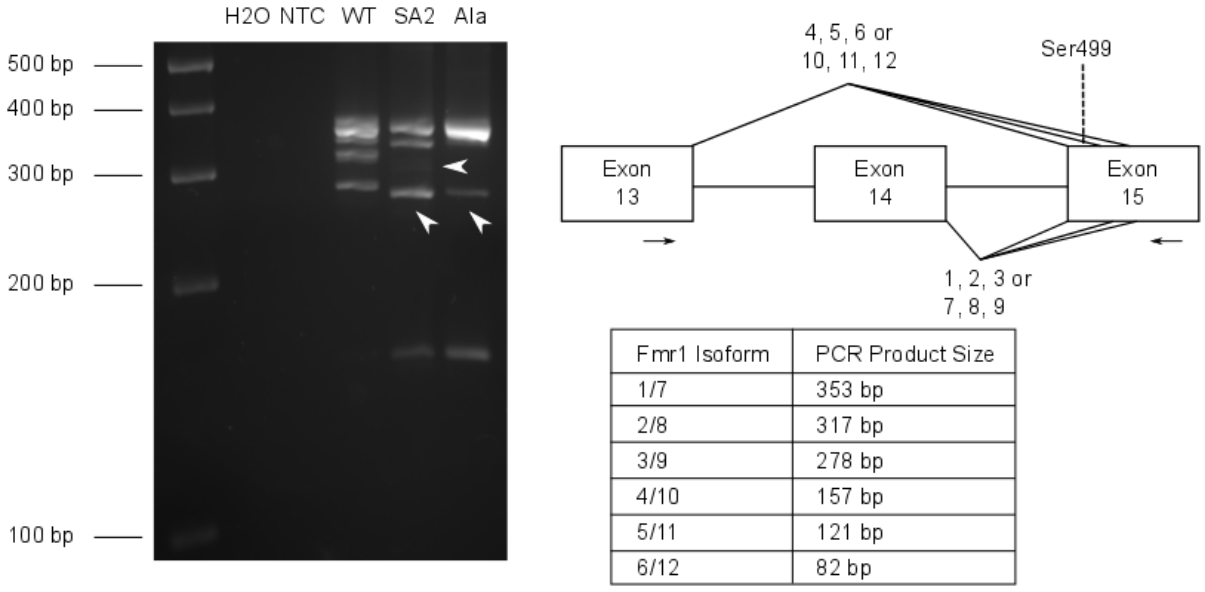

Fmr1 Isoform	PCR Product Size
1/7	353 bp
2/8	317 bp
3/9	278 bp
4/10	157 bp
5/11	121 bp
6/12	82 bp

Figure 19. Identification of cryptic spice acceptor sites.
I amplified the region spanning exon 13 to exon 15 of *Fmr1* cDNA by PCR (right panel, top). Note that this PCR cannot distinuguish between isoforms that only differ by the inclusion or exclusion of exon 12. SA2 and Ser499Ala mice did not use either alternative splice acceptor sites, as shown by the lack of bands at 317 bp and 278 bp (left panel). However, both mutant mice have novel bands which were slightly smaller than WT isoforms (white arrowheads, left panel).

In order to determine what effect the use of the cryptic splice acceptor sites had on isoform abundance, I measured the levels of all 12 isoforms by qPCR. I extracted mRNA from cortices from adult male mice, reverse transcribed the mRNA to cDNA, and

measured the isoform levels by qPCR. I normalized the isoform levels to the housekeeping gene *MuP0*. I combined data for isoforms that differ only in the inclusion or exclusion of exon 12 (i.e. isoforms 1 and 7). As expected, in SA2 and Ser499Ala mice the isoforms with a frameshift mutation were detected at substantially lower levels than the corresponding isoforms in WT mice (isoforms 2/8 $p < 0.0001$ for both SA2 and Ser499Ala; isoforms 5/11 $p < 0.05$ for both SA2 and Ser499Ala). Unexpectedly, isoforms 3 and 9 were present at lower levels in Ser499Ala mice as compared to SA2 mice ($p < 0.05$). Similarly, isoforms 5 and 11 were present at lower levels in Ser499Ala mice as compared to SA2 mice ($p < 0.01$). Although not statistically significant, there was a trend of higher levels of isoforms 1 and 7 and isoforms 4 and 10 in Ser499Ala mice as compared to SA2 mice.

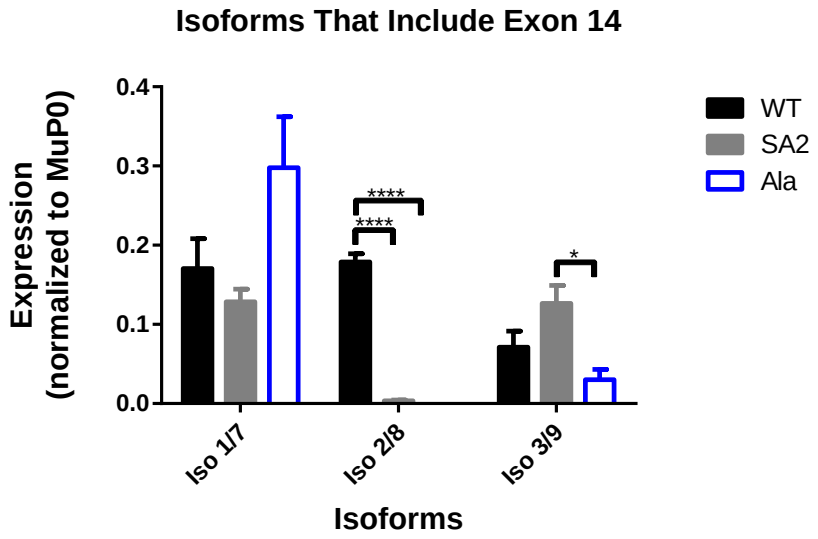

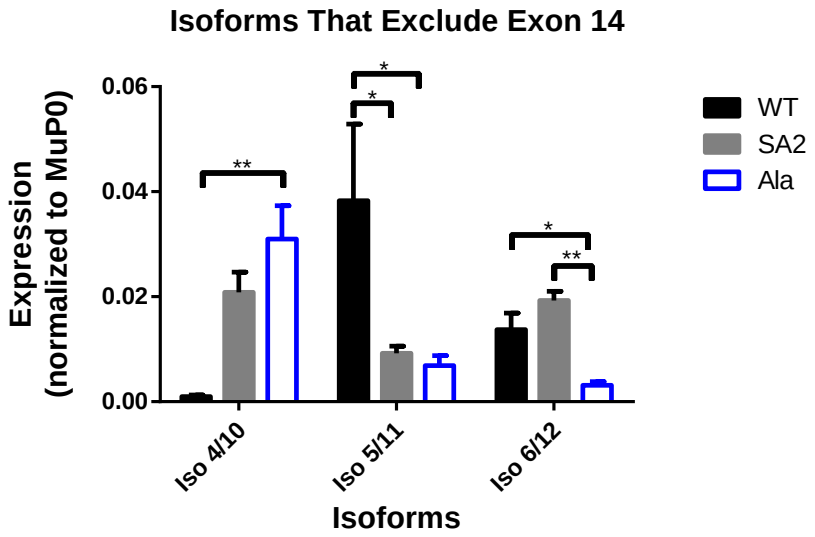

Figure 20. Distribution of isoforms in mouse cerebral cortex.
I extracted cortical mRNA from adult male mice, reverse transcribed it into cDNA, and measured the levels of all 12 isoforms by qPCR. Levels were normalized to the levels of MuPO mRNA. The values for isoforms that differ only in the inclusion or exclusion of exon 12 (i.e. isoforms 1 and 7) were combined. Isoforms that used the first cryptic splice acceptor site, which introduces a premature stop codon, were reduced in SA2 and Ser499Ala mice (isoforms 2/8 $p < 0.0001$ for both SA2 and Ser499Ala; isoforms 5/11 $p < 0.05$ for both SA2 and Ser499Ala). Isoforms 1 and 7, which include residue 499, show a trend towards higher levels in Ser499Ala mice as compared to SA2 mice. Isoforms that use the second cryptic splice acceptor site were reduced in Ser499Ala mice as compared to SA2 mice (isoforms 3/9 $p < 0.05$; isoforms 6/12 $p < 0.01$). Each group of three genotypes was analyzed by one-way ANOVA, with multiple tests comparing each mean to the other two means in the group.

I measured FMRP levels in cortices from adult male mice using Western blot analysis. I also examined if the mice expressed phospho-FMRP using an antibody specific for FMRP phosphorylated at Ser499. All samples were treated in parallel with lambda phosphatase to verify that the antibody used to detect pFMRP was specific to the phosphorylated form of the protein. Both SA2 and Ser499Ala expressed FMRP in the cerebral cortex. As expected, phospho-FMRP was present in SA2 mice but was undetectable in Ser499Ala mice.

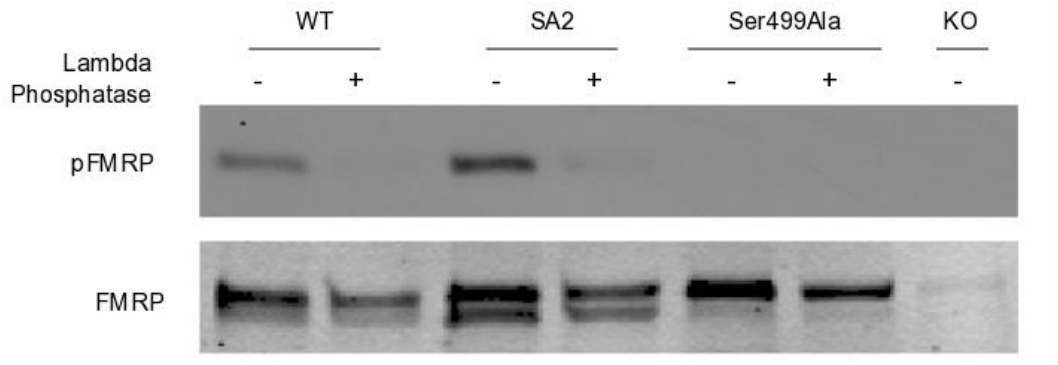

Figure 21. pFMRP/FMRP expression.
Western blot of cortical lysate from adult male mice. SA2 mice, but not Ser499Ala mice, express FMRP phosphorylated at Ser499. Both lines of mice express FMRP. The absence of pFMRP bands in WT and SA2 lysate treated with phosphatase shows that the antibody used is specific to phospho-FMRP.

We measured total protein synthesis in SNS from WT, KO, SA2, and Ser499Ala mice, both at basal levels and after 5 minutes of simulation with 100 μM (S)-3,5-Dihydroxyphenylglycine (DHPG). WT mice showed the expected increase in total protein synthesis after stimulation ($p < 0.0001$). As has been reported previously, protein synthesis levels in KO mice decreased upon stimulation with DHPG ($p < 0.0001$). KO mice typically have higher basal levels of protein synthesis, similar to levels seen in WT mice with stimulation. In our experiment, basal levels of protein synthesis were higher in KO mice than WT mice, but this difference was not statistically significant.

As predicted, SA2 mice showed increased levels of protein synthesis upon stimulation with DHPG ($p < 0.001$), similar to the WT phenotype. Unexpectedly, Ser499Ala mice did not show a phenotype similar to KO mice. In fact, protein synthesis levels in Ser499Ala mice did not significantly change in either direction upon stimulation with DHPG, meaning Ser499Ala mice responded differently than either WT or KO mice. Basal protein synthesis levels in Ser499Ala mice were slightly higher than basal levels in WT mice, but this was not statistically significant.

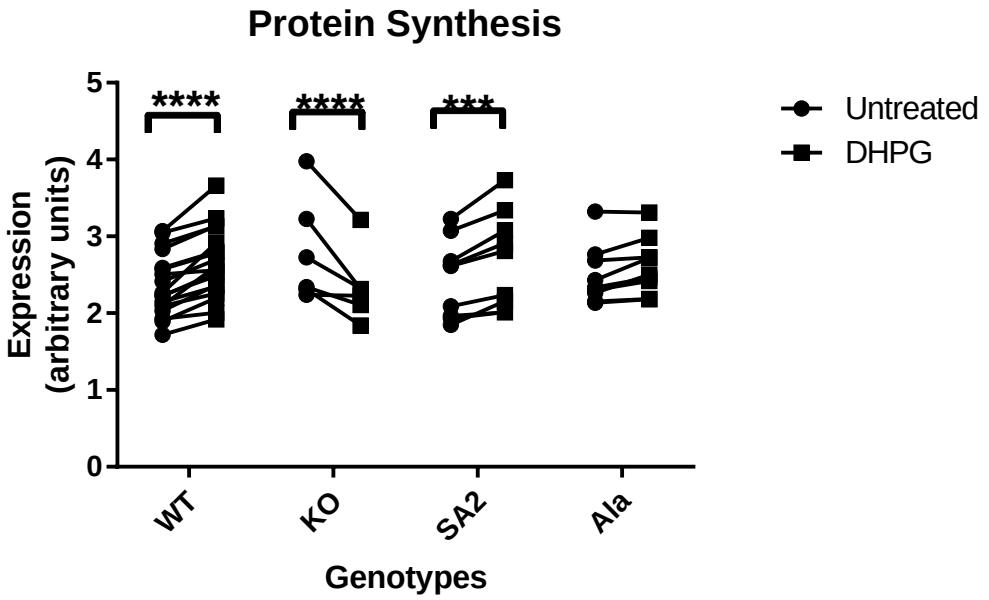

Figure 22. New protein synthesis.
Protein synthesis was measured in SNS from WT, KO, SA2, and Ser499Ala mice using radioactive labeling. As expected, levels of protein synthesis increased in SNS from WT mice when stimulated with DHPG ($p < 0.0001$). In addition, levels of protein synthesis decreased in SNS from KO mice when stimulated with DHPG ($p < 0.0001$). SNS from SA2 mice recapitulated the increase seen in WT mice when stimulated by DHPG ($p < 0.001$). Unexpectedly, SNS from Ser499Ala mice did not show a significant change in protein synthesis when stimulated with DHPG. Data was analyzed by two-way ANOVA, matching treated and untreated samples. This experiment was performed by Christina Gross, Ph.D.

We tested P21 WT, KO, SA2, and Ser499Ala male mice for susceptibility to audiogenic seizures. 30.8% of KO mice experienced audiogenic seizures when subjected to a loud alarm, substantially more than the 2.8% of wild type mice that experienced audiogenic seizures ($p < 0.0029$). This is consistent with previous reports in the literature[88]. In contrast, neither SA2 nor Ser499Ala mice showed any difference from WT mice.

Genotype	Mice displaying seizures	Differs from WT
WT	1/36 (2.8%)	-
KO	8/26 (30.8%)	Yes ($p < 0.0029$)
SA2	1/21 (4.8%)	No
Ser499Ala	1/20 (5.0%)	No

Table 1. Audiogenic seizures.
Mice were exposed to a personal alarm for 1 minute and monitored for seizures. As expected, WT mice were resistant to audiogenic seizures, with only 2.8% of WT mice experiencing seizures. Consistent with previous reports, KO mice experienced substantially higher frequency of seizures than WT mice (30.8% of KO mice, $p < 0.0029$). SA2 and Ser499Ala mice experienced frequencies of seizures indistinguishable from WT mice (4.8% and 5.0%, respectively). P-values for each WT/mutant comparison were calculated using a contingency table. This experiment was performed by Jason Schroeder, Ph.D. at the Emory Mouse Behavioral Core.

We tested adult male mice in a standard marble burying assay to asses their repetitive behavior. In this assay, mice are placed in a clean cage with standard bedding and 20 marbles. After 10 minutes they are removed and the number of marbles buried is counted. Previous reports indicate that *Fmr1* KO mice bury a greater number of marbles than WT mice[97], indicating they are more prone to repetitive behavior. In our assay *Fmr1* KO mice did bury a larger number of marbles than WT mice. This result is not statistically significant, but this experiment is still ongoing. I expect that at its completion there will be a statistically significant difference between WT and KO mice. SA2 and Ser499Ala seem to be indistinguishable from WT mice.

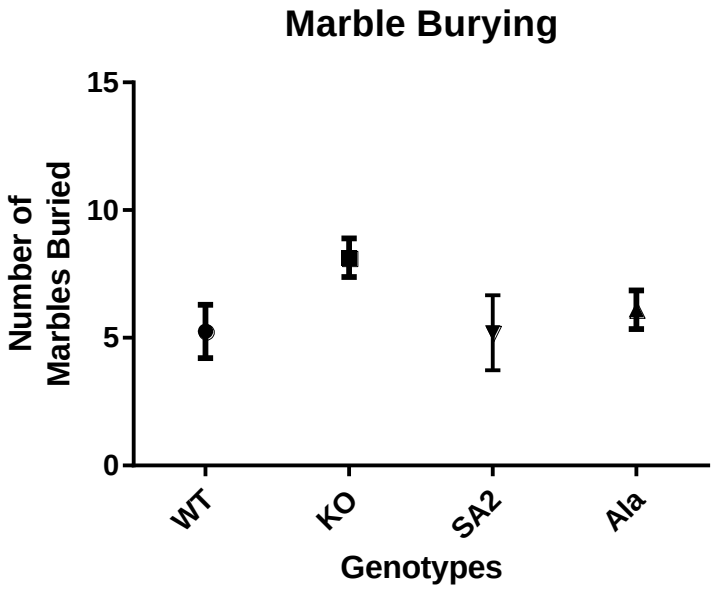

Figure 23. Marble burying.
Mice were placed in a clean cage with marbles for 10 minutes. The number of marbles buried more than 50% percent were counted. *Fmr1* KO (n = 15) mice bury more marbles than WT (n = 16) mice (not statistically significant, experiment still in progress). SA2 (n = 5) and Ser499Ala (n = 19) mice show no difference compared to WT. Error bars represent SEM. This experiment was performed by Anwesha Banerjee, Ph.D.

Both human FXS patients and *Fmr1* KO mice display macroorchidism[22, 98, 99]. We measured testis size in adult male mice. We normalized testis mass to body mass to control for any differences in mouse size. As expected, *Fmr1* KO mice had larger testes thatn WT mice. Ser499Ala mice did not differ from WT mice. This experiment is still ongoing.

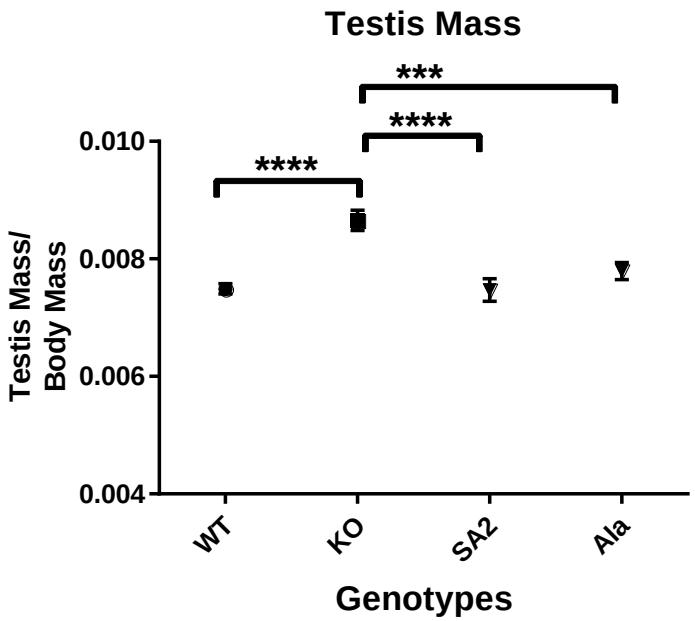

Figure 24. Testis Mass.
Testis mass was measured in adult male mice and normalized to body mass. Testes from *Fmr1* KO (n = 17) mice were larger than those from WT (n = 18) mice ($p < 0.0001$). SA2 (n = 11) and Ser499Ala (n = 13) mice were indistinguishable from WT mice. Error bars represent SEM. This experiment was performed by Tamika Malone.

Discussion

In this project, I attempted to target three different mutations to the *Fmr1* locus. In the two successful attempts I achieved a targeting efficiency of 0.84% and 0.28%. Given this low targeting efficiency, the lack of any correct Ser499Asp clones may be due to chance. However, it might indicate that this allele is lethal in ES cells. At the molecular level, we predict that the Ser499Asp allele constitutively represses translation of its protein targets. Since *Fmr1* is an X–linked gene and male ES cells are used in targeting, the Ser499Asp allele would be the only one present in correctly targeted cells. If any FMRP targets are an essential protein in ES cells then the constitutive repression by Ser499Asp-FMRP would be lethal to the cell. Other researchers in the Warren lab are

currently working to create a knockin mouse model that expresses the WT Ser499 residue but which, when exposed to Cre recombinase, can be switched to aspartic acid. We hope to use this system to examine the effects of the Ser499Asp allele at both the cellular and whole organism levels.

Previous work has shown that the phosphorylation status of Ser499 is a key regulator of FMRP's function. In particular, mutating the serine to alanine in fruit flies resulted in null phenotypes[30]. I successfully mutated Ser499 to alanine in a knockin mouse model. Unexpectedly, this mouse did not recapitulate the KO phenotype. It was indistinguishable from WT mice in terms of audiogenic seizures and macroorchidism. In contrast, the rate of new protein synthesis in Ser499Ala SNS did not show a consistent response to DHPG treatment. This is different from both the WT and KO behavior. I propose that, in vivo, the Ser499Ala allele is a hypormorph. At the molecular level it cannot fully respond to DHPG-induced signaling. However, it retains enough functionality that it does not have a KO phenotype. This reduced functionality is sufficient to result in WT phenotypes in the audiogenic seizure and macroorchidism assays.

I propose two possible mechanisms that could explain why previous work showed that the Ser499Ala allele is functionally a KO allele but in my mice the Ser499Ala allele is hypomorphic. First, Ser499Ala-FMRP may be regulated by the phosphorylation of alternate serines. Second, alternative isoforms of FMRP may be rescuing the null phenotype.

The original cell culture work on phospho-FMRP indicated that no other serines between residues 483 and 521 (in mouse) are phosphorylated in Ser499Ala FMRP [75].

This work was done by overexpressing the relevant proteins in L-M(TK-) cells, which do express endogenous WT FMRP. It is possible that Ser499Ala FMRP is phosphorylated differently in vivo than in this cell-based model. This could be examined by performing phosphoamino acid analysis on brain lysate from the relevant mouse models. Mass spectrometry-based analysis would allow mapping the location of any phosphorylated residues to narrow regions of FMRP [100].

Both the previous work in cell culture and fruit flies used cDNA of *Fmr1* isoform 1 [30, 75]. It is still possible that when Ser499 is mutated to alanine in isoform 1 in vivo, that isoform does in fact become nonfunctional. If isoform 1 is the only isoform of FMRP present, as it was in the previous research, the Ser499Ala mutation would result in a null phenotype. However, one or more of the alternative isoforms of FMRP present in my mice could be rescuing the null phenotype.

It may also be that none of the alternative WT isoforms can rescue the null phenotype. Instead, in revealing the two cryptic acceptor sites in exon 15, I may have created novel isoforms of FMRP that rescue the null phenotype. I have no data to disprove this possibility, but I believe it is unlikely for two reasons. First, the use of the first cryptic acceptor site results in a frameshift mutation and low levels of mRNA for all the isoforms using that acceptor site (isoforms 2, 5, 8, and 11). It seems unlikely that such low levels of a truncated protein would have any effect on the mouse's phenotype. Second, the use of the second cryptic acceptor site results in an in-frame deletion of three amino acids. I predict this deletion would either make those isoforms nonfunctional or have no effect on their function. However, it is formally possible that deletion of those residues converted a nonfunctional isoform to one capable of rescuing the null

phenotype. This seems unlikely, but if true would indicate that this small region of exon 15 is critical to the function of the protein.

Even if the alternative WT isoforms of FMRP rescue the null phenotype, I could not say which individual isoforms are responsible for this. In fact, certain isoforms may only contain a subset of FMRP's full functions. Investigating this issue would require studying each alternative isoform in isolation. The cDNA of isoform 1 of human FMRP rescues the null phenotype flies. Alternative isoforms of FMRP could be introduced into this model system, which would provide a way to determine if an individual isoform of FMRP rescues any of the null phenotype in flies. Alternatively, transgenic mice expressing individual isoforms of FMRP could be created and bred to *Fmr1* KO mice. This would allow the study of individual isoforms in a mammalian system.

Even in transgenic models, testing all 11 alternative isoforms of FMRP would be a substantial amount of work. I recommend first investigating the functions of isoform 7. Isoform 7 is expressed at higher levels than isoform 1, and is only missing a small region of the KH2 domain. It therefore seems likely that isoform 7 contains most or all WT functions of FMRP. If isoform 7 is a functional form of FMRP, it most likely is regulated by the phosphorylation status of Ser499. But it is possible that it is regulated by a different mechanism. To address this question, Ser499 could be mutated to alanine or aspartic acid specifically in the context of isoform 7.

There are also several reasons to prioritize studying FMRP isoforms in which Ser499 is skipped (isoforms 2, 3, 8, and 9). The fact that the removal of the two alternative splice acceptor sites in exon 15 resulted in the use of two cryptic splice acceptor sites suggests that isoforms which do not contain Ser499 play important

physiological roles.

This idea is supported by the distribution of various *Fmr1* isoforms in WT, SA2, and Ser499Ala mice. Ser499Ala mice expressed lower levels of mRNA of isoforms that do not contain residue 499 (i.e. isoforms 3 and 9). Although not statistically significant, Ser499Ala mice showed a trend of higher levels of mRNA of isoforms that contain residue 499 (i.e. isoforms 1 and 7). This is consistent with the idea that cells require a certain level of unphosphorylatable FMRP. In WT and SA2 mice isoforms 1 and 7 produce proteins that can be phosphorylated at Ser499. Therefore, these mice would require a certain level of the isoforms lacking residue 499. However, in Ser499Ala mice isoforms 1 and 7 produce proteins that cannot be phosphorylated at residue 499. Therefore, these mice can express higher levels of isoforms 1 and 7 and lower levels of the other isoforms and still produce the necessary amount of unphosphorylatable FMRP.

The distribution of isoforms raises another interesting point. Isoforms are expressed at different levels in SA2 mice as compared to Ser499Ala mice. However, the DNA sequence differences between these mice would not be expected to signal the spliceosome to produce different levels of isoforms. Therefore, there seems to be a mechanism for the cells to determine the levels of unphosphorylatable FMRP present and then signal to the spliceosome to produce different levels of various isoforms.

Finally, SNS from Ser499Ala mice do not recapitulate the *Fmr1* KO phenotype. However, the data raise the possibility that basal protein synthesis in Ser499Ala mice is slightly elevated as compared to WT mice. If true, this might mean that Ser499Ala mice synthesize a subset of FMRP targets at higher rates. If so, that would mean the phosphorylation status of Ser499 does control the function of FMRP, but only for a

fraction of the protein's targets. This would need to be investigated by, first, conducting an appropriately powered study to determine if protein synthesis levels in Ser499Ala mice are in fact elevated. If so, a proteomic approach could then be used to determine which proteins are elevated in *Fmr1* KO mice but not Ser499Ala mice. One method, BONCAT, allows the measurement of newly synthesized proteins in cell culture or SNS [101]. This makes it possible to identify individual proteins that are synthesized at different rates in mice with different genotypes.

Chapter 3
Polyribosome Profiles

In the FXS literature, polyribosome profiles are often used to study the effects of mutations in FMRP. However, there are many variations of the basic assay. It can be used on cultured cells expressing exogenous protein, cultured cells expressing endogenous protein, tissue lysate, and reconstructed in vitro systems. Also, the assay can be modified to examine different aspects of a given system. In this section, I'll give a brief overview of this assay, describe the different protocols I've used and the results I've seen, and make suggestions for how it can best be used in the future.

Background

In eukaryotic organisms, the 5’ and 3’ ends of an mRNA molecule associate with each other, causing the mRNA to form a loop. This allows the subunits of a ribosome that has finished translating and disassociated from the mRNA to quickly reassociate with the 5’ end of the mRNA and begin a new round of translation. Furthermore, multiple ribosomes can be translating on a single strand of mRNA at the same time. These complexes of looped mRNA and multiple ribosomes are referred to as polyribosomes. In general, higher numbers of ribosomes in a polyribosome imply higher rates of translation of that mRNA.

Polyribosome profiles are one method of measuring the translation activity in a

given system. In this assay, translation is stopped by the addition of cycloheximide (CHX), which prevents ribosomes from moving any farther along a strand of mRNA. Then, polyribosomes, monosomes, and ribosomal subunits are separated by density using a continuous sucrose gradient. The 80S monosomes migrate to heavier fractions than the 40S and 60S ribosomal subunits. Similarly, polyribosomes migrate to heavier fractions than monosomes, with polyribosomes containing more ribosomes migrating to heavier fractions. A profile can be generated by passing the gradient through a UV reader and measuring the amount of mRNA present at each point of the gradient.

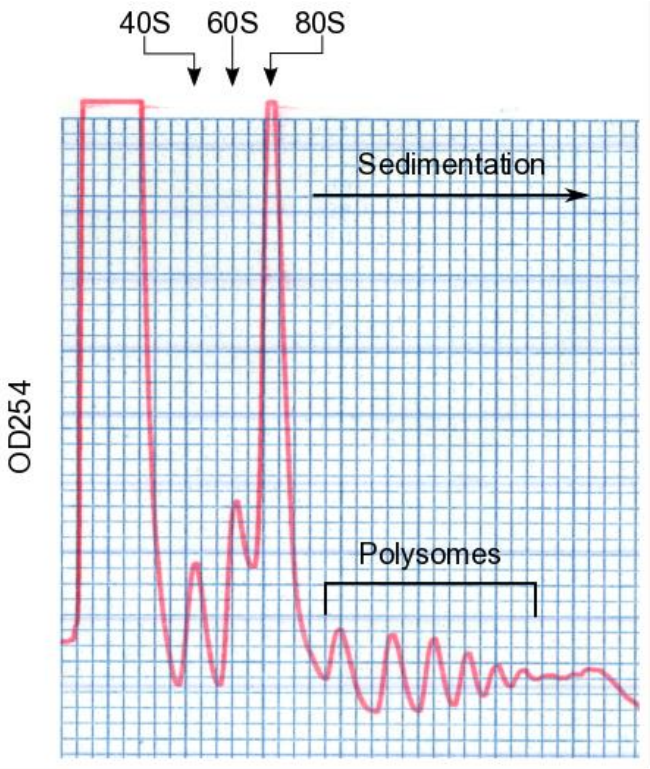

Figure 25. Representative polyribosome profile tracing.
Tracings of polyribosome profiles are generated by measuring the absorbance at OD254 as the gradient passes through the reader. Individual peaks for the 40S and 60S subunits and 80S monosomes are often visible, although they sometimes merge together. The different peaks for the polyribosomes represent polyribosomes with steadily increasing numbers of monosomes. The lightest fractions of the gradient are on the left of the graph, the heaviest fractions of the gradient are on the right of the graph.

Typically, mutations in FMRP do not cause any differences in the profiles themselves. However, the gradient can be divided into fractions. The amounts of particular proteins in each fraction can be measured by Western blot. Similarly, mRNA can be extracted from each fraction and the amounts of particular mRNAs measured by qPCR. This can be informative as different alleles of FMRP can themselves be distributed differently and can also change the distributions of target mRNAs. For instance, in polyribosome profiles on brain lysate from I304N mice, little to no FMRP is in fractions with polyribosomes [102]. This is consistent with the belief that the I304N mutation removes FMRP's ability to bind to mRNA. Investigators have also reported that the mRNAs of several FMRP targets are shifted to heavier fractions in neurons [73] and MEFs [103] lacking FMRP. This indicates that in the absence of FMRP these mRNAs associate with heavier polyribosomes and are therefore being more actively translated.

One limitation of this method is that some of the ribosomes on a strand of mRNA may be stalled and not actively translating protein. Therefore, the system at steady-state may not accurately reflect its level of translation. A refinement that addresses this problem is referred to as a run-off assay. In this version of the experiment, before being fractionated or exposed to cycloheximide, the sample is incubated with puromycin. Puromycin blocks initiation of new rounds of synthesis while allowing actively translating ribosomes to complete translation and disassociate from the mRNA (e.g. "run-off"). This has the effect of depleting the pool of actively translating ribosomes, leaving behind only ribosomes that were stalled. The tracings in a run-off assay show a characteristic loss of most polyribosomes.

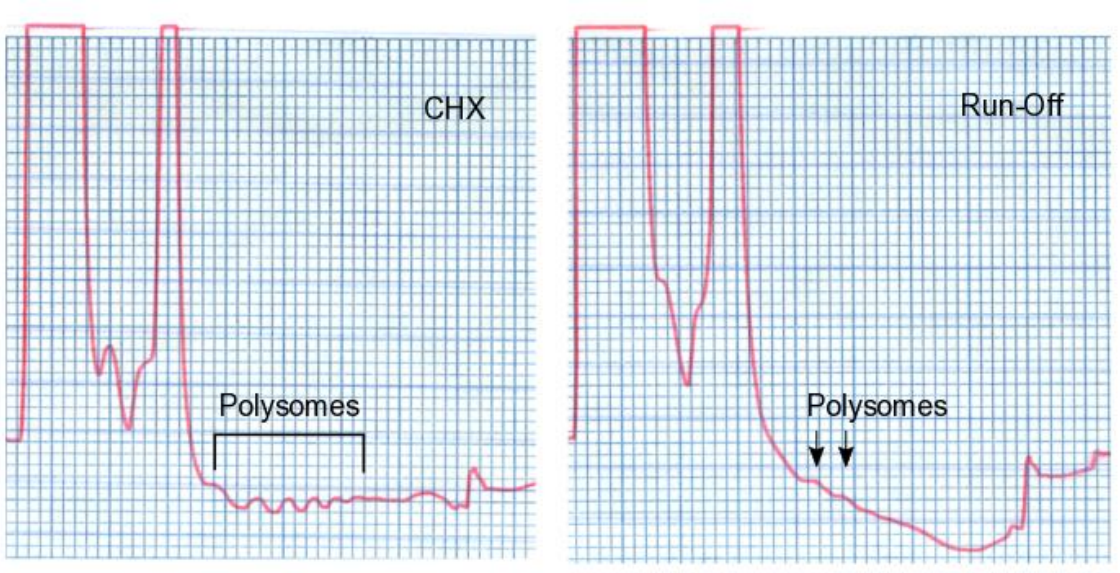

Figure 26. Polyribosome profile traces from a run-off experiment.
At steady-state, multiple distinct polyribosome peaks are visible (left panel). After run-off, only two small polyribosome peaks are visible (right panel). These represent polyribosomes with stalled ribosomes.

The difference between a system in steady-state and after run-off indicates how many polyribosomes were actively translating. Investigators have reported that in run-off assays certain mRNAs undergo larger shifts toward toward lighter fractions in the absence of FMRP [104]. This indicates that in the absence of FMRP these mRNAs are associated with a greater number of actively translating ribosomes.

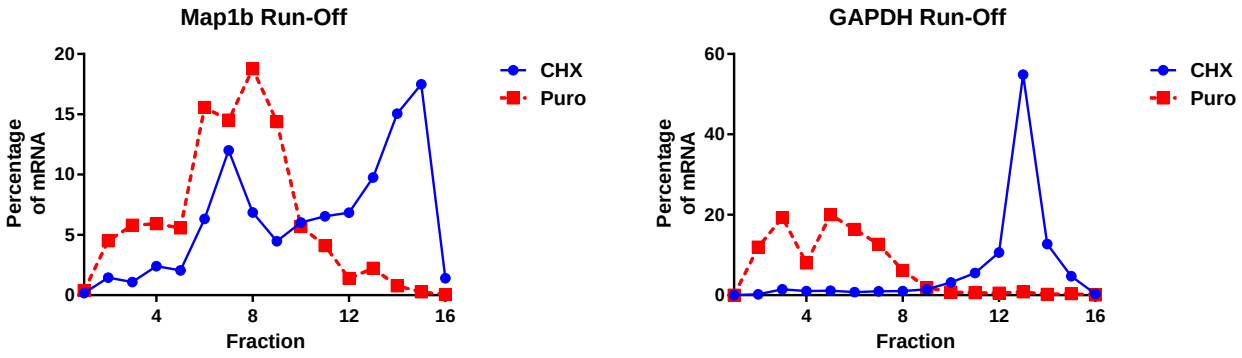

Figure 27. mRNA distributions from a run-off experiment.
The distributions of mRNA are typically shifted to lighter fractions in run-off experiments. The more actively translated an mRNA is, the bigger the shift in its distribution.

In previous work in L-M(TK-) cells, the distribution of exogenous FMRP was measured in run-off assays [75]. Ser499Ala FMRP showed a larger shift toward lighter fractions than did WT FMRP. This indicated that the mutant protein associated with more actively translating polyribosomes. In order to examine this phenotype in my knockin mice, I undertook polyribosome profile experiments. Since my goal was to examine the effects of my mutations in vivo, I could not simply repeat the experiments previously done in cell lines. I tried various version of the assay without ever satisfactorily answering how the Ser499Ala mutation affected translation in vivo.

Polyribosome Profiles on Brain Lysate

To start, I used a modified version of the protocol typically used in the Warren lab. The original version measures the steady-state distribution of FMRP in polyribosome profiles on cells transfected with various alleles of FMRP. I performed the experiment on polyribosomes in whole brain lysate from mice. This protocol produced clear separation of polyribosome peaks. As expected, the pattern of peaks showed no noticeable difference between WT and Ser499Ala mice. However, upon examining the distribution of FMRP, I discovered that the bulk of FMRP in both genotypes was located in the lighter fractions. Very little FMRP was present in the fractions that contained polyribosomes. This result agrees with previously published work that uses this protocol [105]. Given I was trying to investigate the association of FMRP with polyribosomes, I looked for a protocol that resulted in a better distribution of FMRP.

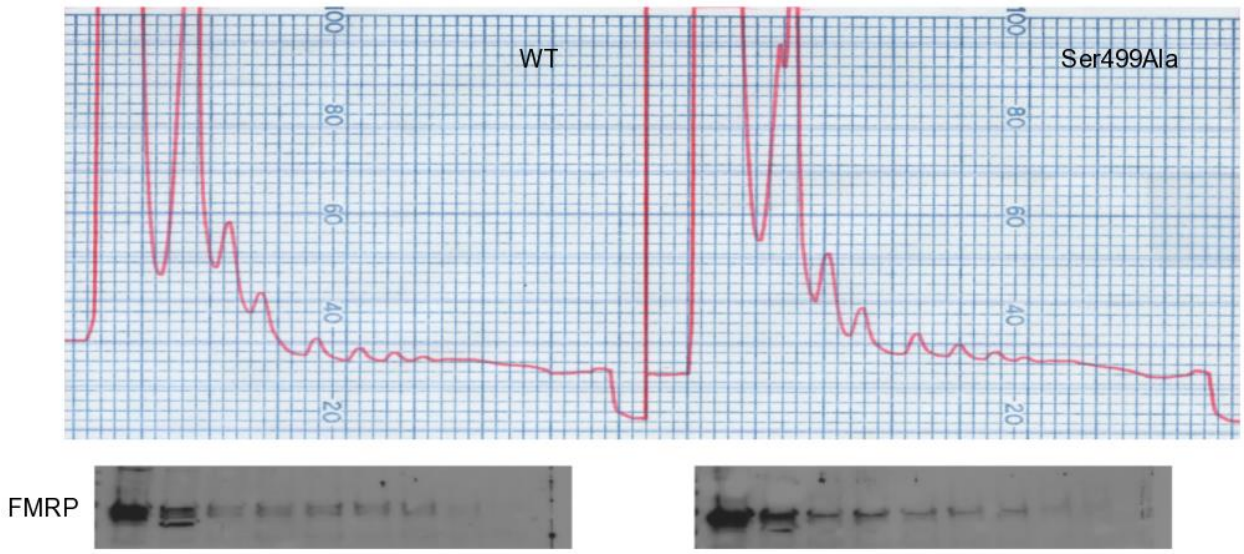

Figure 28. Polyribosome profiles on whole brain lysate.
Profiles do not show any gross differences in polyribosome distribution between WT and Ser499Ala mice (upper panel). Lower panel shows the distribution of FMRP in the fractions collected from each profile. In both cases, the majority of FMRP is located in the lighter fractions, with little FMRP located in the polyribosomal fractions. This makes it difficult to interpret results from experiments using this protocol.

The next protocol I tried has been used by the Darnell lab to examine the association of FMRP with polyribosomes [102]. This protocol modifies the lysis buffer and sucrose gradients to have a lower pH (7.3 instead of 7.5), different buffering agent (HEPES instead of Tris), and lower salt concentration (150 mM KCl instead of 200 mM). It also adds a gentler spin to pellet cellular debris before the addition of detergent. In Zang et al., the authors used this protocol to show that FMRP with the I304N mutation does not associate with polyribosomes [102]. Using this protocol on whole brain lysate from WT mice, I was again able to achieve clear separation of polyribosomes. Furthermore, FMRP was more evenly distributed throughout the gradient. Treatment with EDTA, which disrupts ribosomes, showed a shift of FMRP to the lighter fractions and a clear loss of monosomes and polyribosomes. However, as reported in the Zang et al. paper, using this protocol produced no difference in the distribution of FMRP target

mRNAs in KO mice [102].

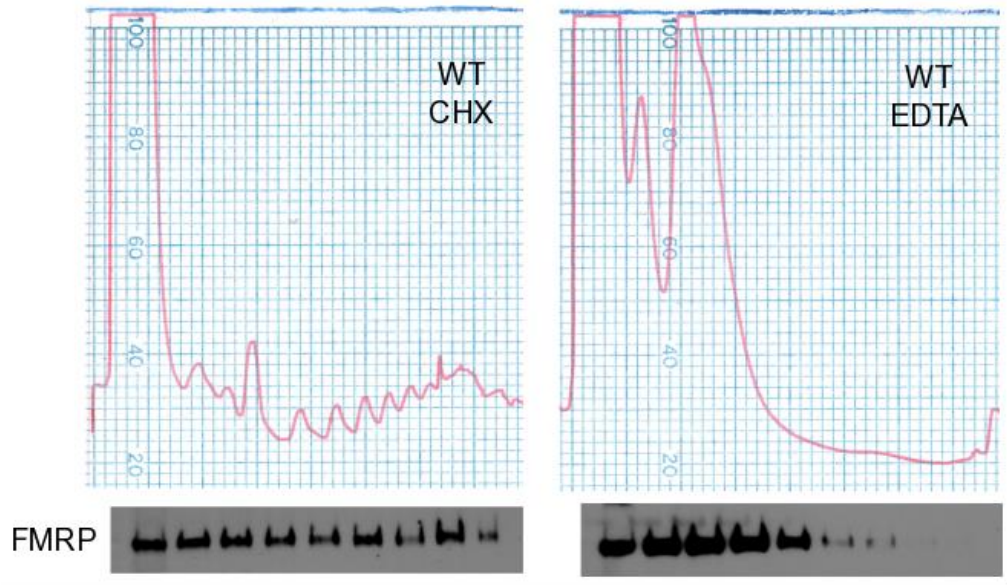

Figure 29. Traces of polyribosome profiles using Zang et al. protocol.
In traces with cycloheximide, FMRP is located in the fractions representing ribosomal subunits, monosomes, and polyribosomes (left panel). Upon disruption of the monosomes and polyribosomes with EDTA, FMRP substantially shifts towards the lighter fractions (right panel). This indicates that FMRP associates with polyribosomes. This is more consistent with the majority of published polyribosome profiles and seems to represent physiological conditions.

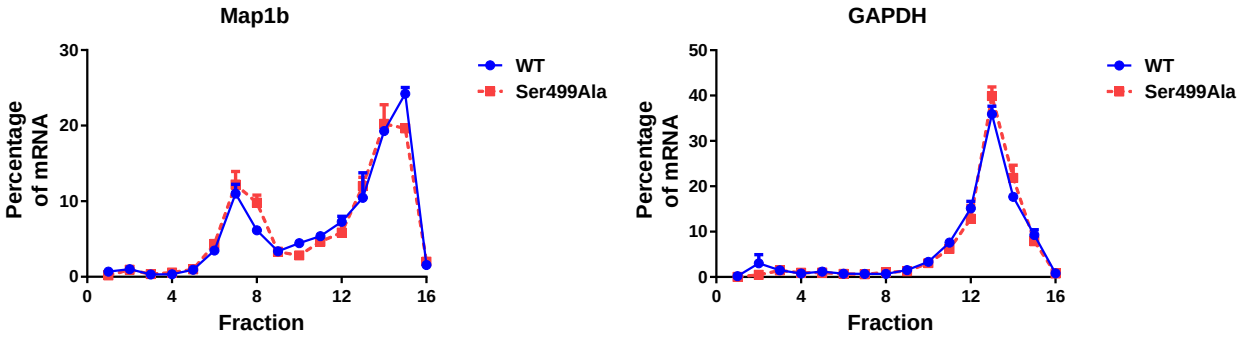

Figure 30. mRNA distribution in polyribosome profiles using Zang et al. protocol.
There is no difference in the distribution of *Map1b* mRNA in polyribosome profiles from WT and Ser499Ala mice. This is consistent with published data using this protocol that show no difference in the distribution of FMRP target mRNAs between WT and KO mice. As expected, there is also no difference in the distribution of GAPDH mRNA between WT and Ser499Ala mice.

Polyribosome Profiles in Cortical Neurons

Lu et al. performed polyribosome profiles on primary cortical neurons from *Fmr1* WT and KO mice [73]. The authors measured the distribution of the known FMRP target mRNA *Map1b*. They reported that at steady-state *Map1b* mRNA is found in heavier polyribosomes in KO neurons as compared to WT neurons. This would indicate that this mRNA is being translated at higher rates in KO neurons than in WT neurons, as would be expected for a target of FMRP. I repeated this assay, measuring both the distribution of *Map1b* and the FMRP target mRNA *Kif1a.* However, I was unable to show any consistent differences in the distributions of *Map1b* and *Kif1a* mRNA between WT and KO neurons. I measured the distribution of *GAPDH* mRNA as a control. *GAPDH* is not a target of FMRP and therefore its distribution should be the same in WT and KO samples.

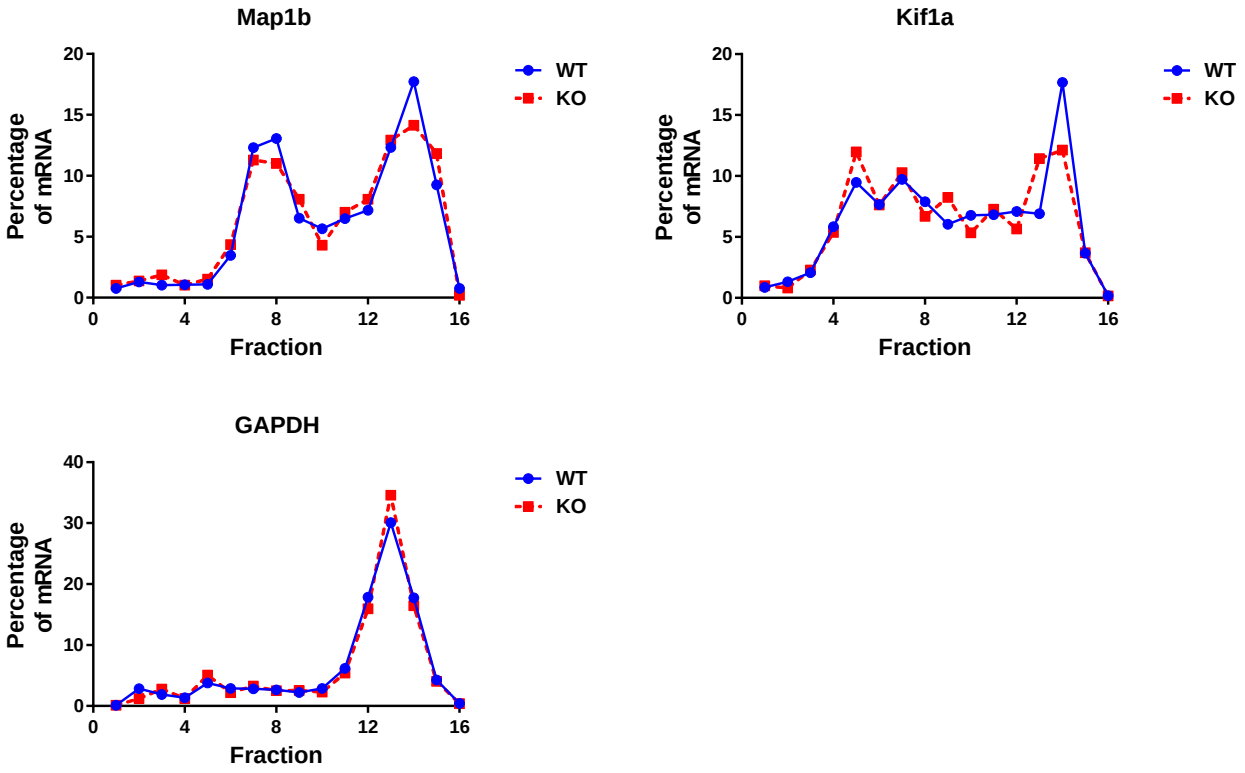

Figure 31. Polyribosome profiles from primary cortical neurons.
The distribution of *Map1b* and *Kif1a* mRNA showed no consistent differences between WT and KO neurons. The distribution of *GAPDH* mRNA was the same in WT and KO samples.

Polyribosome Profiles in MEFs

Nolze et al. performed polyribosome profiles on MEFs derived from *Fmr1* WT and KO mice [103]. They measured the distribution of three known targets of FMRP at steady-state. FMRP has been reported to suppress translation of the first two mRNAs, *p0071* and *Arc*. As expected, these mRNAs were shifted toward heavier polyribosomes in MEFs from KO mice. Unusually, FMRP has been reported to enhance translation of the third mRNA, *Sod1*. In KO MEFs *Sod1* was shown to be shifted toward lighter polyribosomes. However, when I repeated this protocol and examined the distribution of *Map1b* mRNA I was unable to detect any difference between WT and KO MEFs. The

distribution of *GAPDH*, which is not a target of FRMP, showed a small shift to lighter polyribosomes.

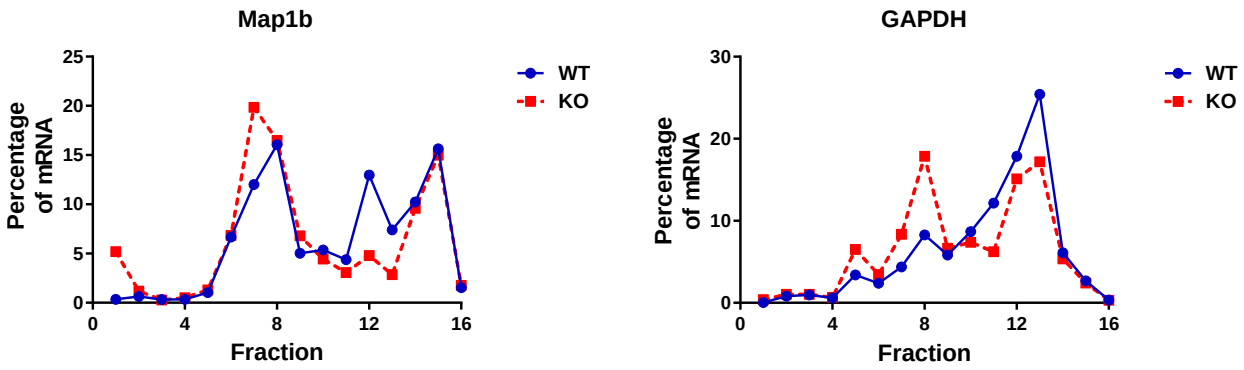

Figure 32. Polyribosome profiles in MEFs.
The distribution of *Map1b* mRNA showed no major differences between WT and KO MEFs. The non-FMRP target *GAPDH* did show minor differences between WT and KO MEFs.

In Vitro Run-Off Assays

Since none of the steady-state assays I tried were informative, I switched to a run-off assays. The Darnell lab published a protocol they named "in vitro translation system programmed with endogenous brain polyribosomes" (IVT_{EBP}) [104]. This protocol uses cortical lysate from mice combined with puromycin, rabbit reticulocyte lysate, ATP, and amino acids to run-off actively translating polyribosomes in the test tube. In published reports, this assay produces a small but distinct shift in the distribution of FMRP target mRNAs to lighter fractions in KO mice [104]. I was able to replicate the loss of polyribosomes in tracings of the profiles. However, I was unable to consistently replicate the shift in the distribution of mRNAs from KO mice.

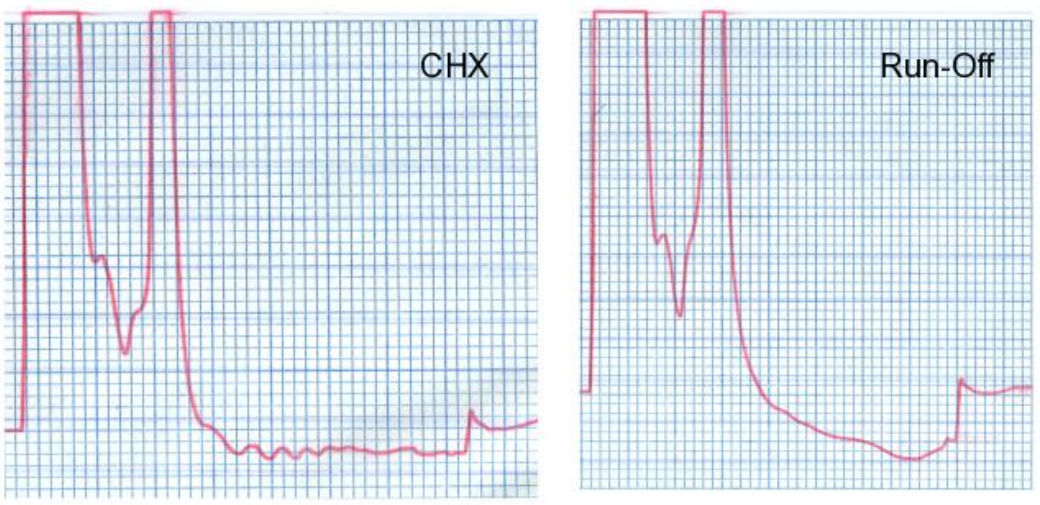

Figure 33. Traces for IVT-EBP profiles.
Traces from the IVT_{EBP} protocol treating lysate with cycloheximide show a good separation of polyribosomes (left panel). Treating the samples with puromycin in vitro causes the active polyribosomes to run-off (right panel).

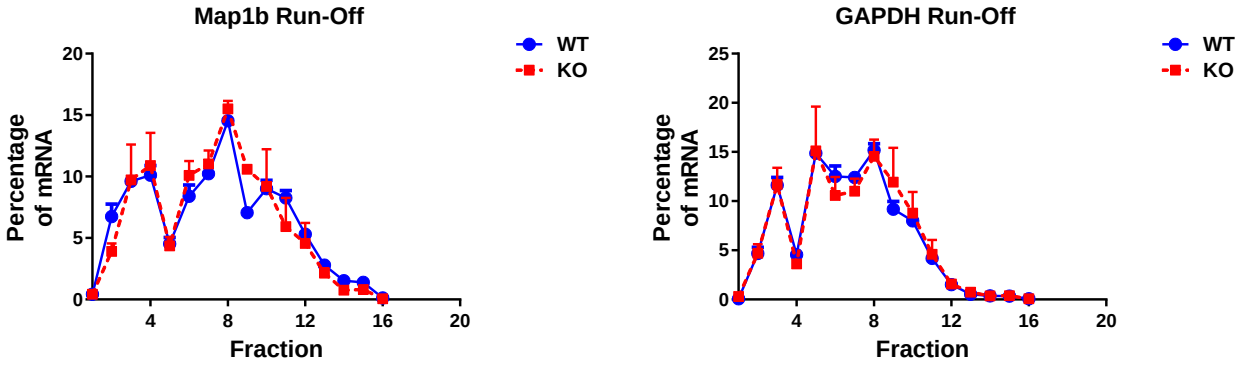

Figure 34. Polyribosome profiles using IVT-EBP protocol.
The distribution of *Map1b* mRNA in IVT_{EBP} samples from WT mice showed no consistent difference to that from KO mice.

Discussion

Polyribosome profiles have proven to be a useful technique to study many aspects of FMRP. The most straightforward use of polyribosome profiles is to determine if a given form of FMRP associates with polyribosomes at steady-state. This represents some of the earliest uses of this assay in the FXS literature and continues to be informative

concerning the effects of certain mutations. For instance, FMRP has been found to associate with polyribosomes in lymphoblastoid cell lysate, SNS from rat cortices, oligodendrocyte cells, brain lysate from mice, transfected cells, and lysate from an immortalized neuronal cell line. But different labs use different versions of the protocol and some of the differences are known to have large effects on the results. For example, the ionic detergent deoxycholate disrupts the association of FMRP with polyribosomes.

Although it is not widely appreciated, I believe other differences can also change the distribution of FMRP in sucrose gradients. When I fractionated whole brain lysate using a Tris-based protocol, only low levels of FMRP were present in polyribosomal fractions. In contrast, using a HEPES-based protocol I found FMRP more evenly distributed throughout the gradients. Both these protocols used the nonionic detergent IgePal.

I believe that the Tris-based protocol recently used in the Warren and Bassell labs disrupts the association of FMRP with polyribosomes. This protocol has been used in published research. In one report, cells expressing transfected FMRP had substantial amounts of the protein in polyribosomal fractions. Conversely, in neurons expressing physiologically typical levels of FMRP the majority of FMRP was present in lighter fractions. In this case, only low levels of FMRP were detected in polyribosomal fractions.

I cannot explain the reason for the differences seen in the Tris-based protocol I used compared to the HEPES-based protocol. Nor can I explain the differences seen in more recent uses of the Tris-based protocol as compared to older uses of a similar protocol. However, I can make several recommendations. First, anyone conducting polyribosome profiles should follow the HEPES-based protocols as closely as possible.

They have been used repeatedly and consistently produce the expected association of FMRP with polyribosomes. Second, anyone publishing data from polyribosome profiles should show the distribution of FMRP in the gradients. This is not consistently done in the literature, presumably because the results are so expected. But for the reason given above, I consider it an important control. Finally, the exact compositions of the buffers and gradients should be reported in Materials and Methods.

Polyribosome profiles can also be used to examine if a mutation in FMRP affects the translational state of a system. In mouse models this is more difficult in practice than the impression given in the literature. The simplest way to do this is to measure the distribution of FMRP target mRNAs at steady-sate. The results achieved this way are either uninformative or inconsistent. In brain lysate, the distribution of FMRP target mRNAs does not differ between WT and KO mice. There are reports in the literature of differences between WT and KO cells in culture. However, I could not replicate these results. I do not think the phenotypes seen in mRNA distributions at steady-state are robust and do not recommend relying on them to phenotype mutant mice.

Run-off assays are a more promising method of examing the level of translational activity in a system. The IVT_{EBP} protocol is well documented and was validated in three distinct loss-of-fuction systems (*Fmr1* KO, *Fmr1* I304N, and disruption of the FMRP-polyribosome association with kissing complex RNA). Unfortunately, I was unable to replicate these results in KO mice. Despite this, I am still optimistic concerning this protocol. I think it is most likely just a technically challenging protocol. I recommend that anyone wanting to use this assay receive training in the Darnell lab. If that is not practical, it would be necessary to invest time optimizing the protocol on WT and KO

samples before attempting to study the effects of a given mutation. Particular attention should be given to incubation times and drug concentrations. Also, using digital PCR rather than qPCR may result in more precise measurements, making it easier to detect small shifts.

One alternative to the IVT_{EBP} protocol is to perform run-off assays in neurons, MEFs, or SNS from mutant mice. I have not personally done this nor have I seen any reports of it in the literature. It should be straightforward to attempt this on samples from WT and KO mice. If successful, this may be an easier and more robust method than the IVT_{EBP} protocol.

One final alternative is to follow the polyribosome profiles conducted in the original Ser499Ala research. Ceman et al. examined the distribution of FMRP itself, rather than target mRNAs, in run-off assays. This seems to be the only example of this specific technique in the literature. Most likely this is because it cannot be used in KO mice, nor is it useful with the I304N and R138Q mutations. But for forms of FMRP that are well distributed at steady-state, it may be productive to examine the distribution of the protein in a run-off assay.

Chapter 4
Western Blots

One phenotype often measured in the FXS literature is the steady-state levels of FMRP target proteins. Several proteins have been reported to be elevated in knockout mice as compared to wild type mice in brain lysate, synaptoneurosomes, and cell culture. The primary method of measuring this is by Western blotting. I attempted to replicate some of these results, hoping to use the assays to phenotype my SA2 and Ser499Ala mice. However, I was unable to replicate the KO phenotypes reported in the literature and did not see any differences between WT and Ser499Ala mice. In this chapter I will discuss some of those attempts plus some of the technical limitations of Western blotting I have learned.

Loading Controls

Traditionally, housekeeping genes have been used as loading controls for Western blots. In qualitative Western blots, the loading controls verify that protein has been loaded into a given lane of a protein gel. In quantitative Western blots the loading controls are used to adjust for any differences in the amount of protein loaded into different lanes of the gel. Typically, the value for the protein of interest is divided by the value of the loading control in the same lane to produce normalized data. In this method it is critical that the values for the loading controls accurately reflect the amount of protein loaded into lanes.

The best way to assess the accuracy of loading controls is to perform a standard

curve. Ideally, this is done using the same sample preparation and blotting methods as will be used in a given experiment. In order to test this for myself, I undertook a series of experiments to see if the loading controls typically used in the Warren lab were in the linear range in my Western blot experiments. I harvested cortical lysate from mice, loaded protein samples ranging from 1 to 40 µg of total protein per lane of a gel, and probed the resulting blot for the levels of various housekeeping genes. Since I was doing this on film, I exposed the films for various times to see what effect that would have.

The standard Western blotting protocol that I follow calls for loading 20 to 40 µg of total protein into a given lane of the gel. None of the housekeeping genes I tested were acceptable in this range. Beta-actin was in the linear range up to 10 µg of total protein, but only at the shortest exposure times. eIF4e showed a linear response between 5 and 15 µg, but again only at the lightest exposures. At the 5 second exposure, beta-tubulin had a linear response over the entire range tested. However, in any of the other exposures the beta-tubulin signal was in the linear range only up to 10 µg of total protein. GAPDH showed a similar pattern, with a linear response over the whole range of protein levels at the lightest exposures but only up to 10 µg of total protein at longer exposures. All the housekeeping genes I tested were insensitive to the amount of protein loaded into a lane at any but the shortest exposure times.

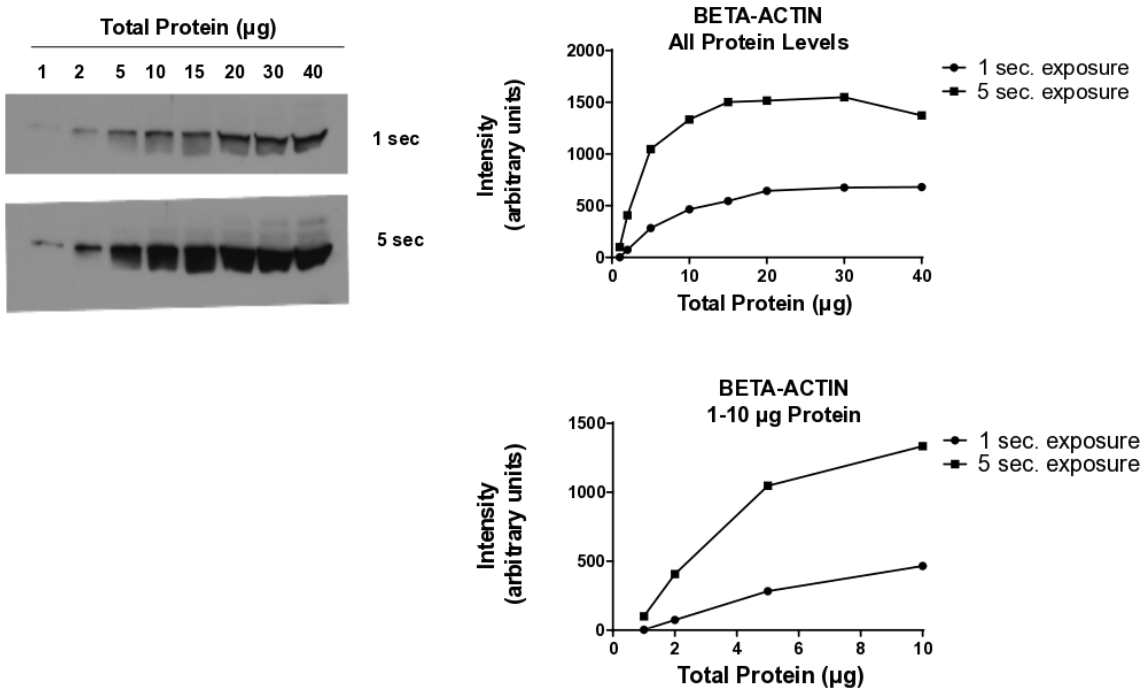

Figure 35. Standard curve for BETA-ACTIN.
The 1 second exposure of BETA-ACTIN was in the linear range up to 10 µg of total protein. The 5 second exposure of BETA-ACTIN was in the linear range up to 5 µg of total protein.

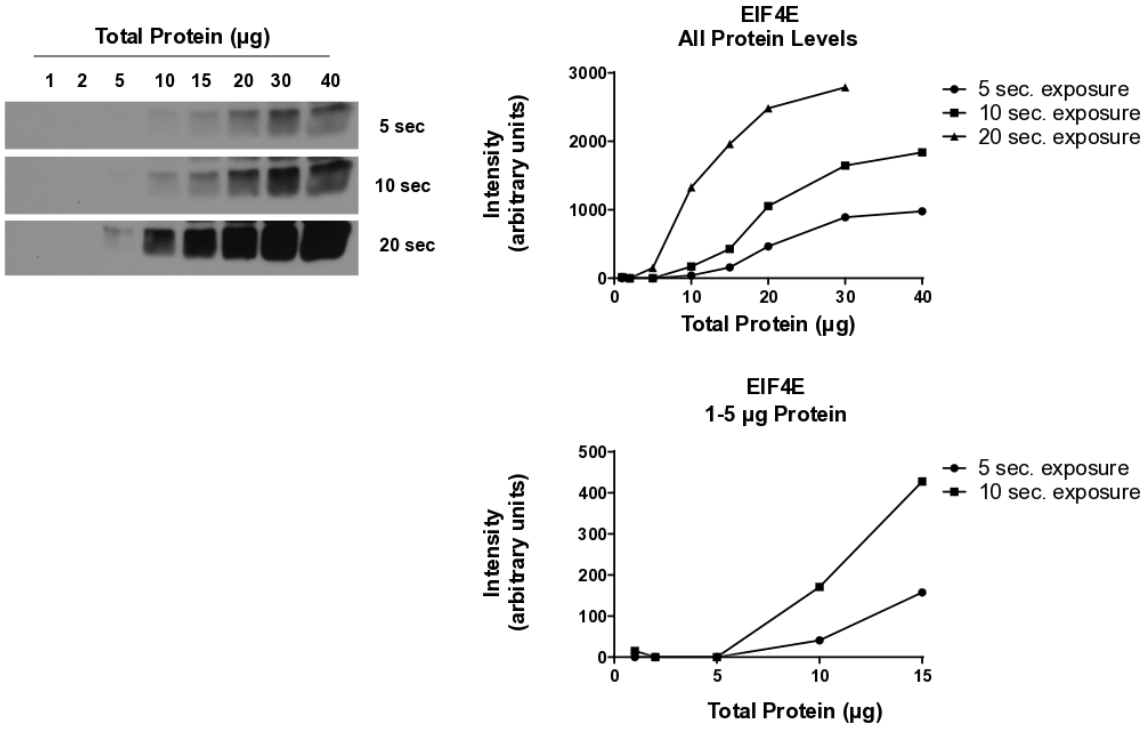

Figure 36. Standard curve for EIF4E.
The 5 and 10 second exposures of EIF4E showed a linear response between 5 and 15 µg of total protein. At those exposure times, amounts less than 5 µg were undetectable. The 20 second exposure was not in the linear range at any of the protein amounts tested.

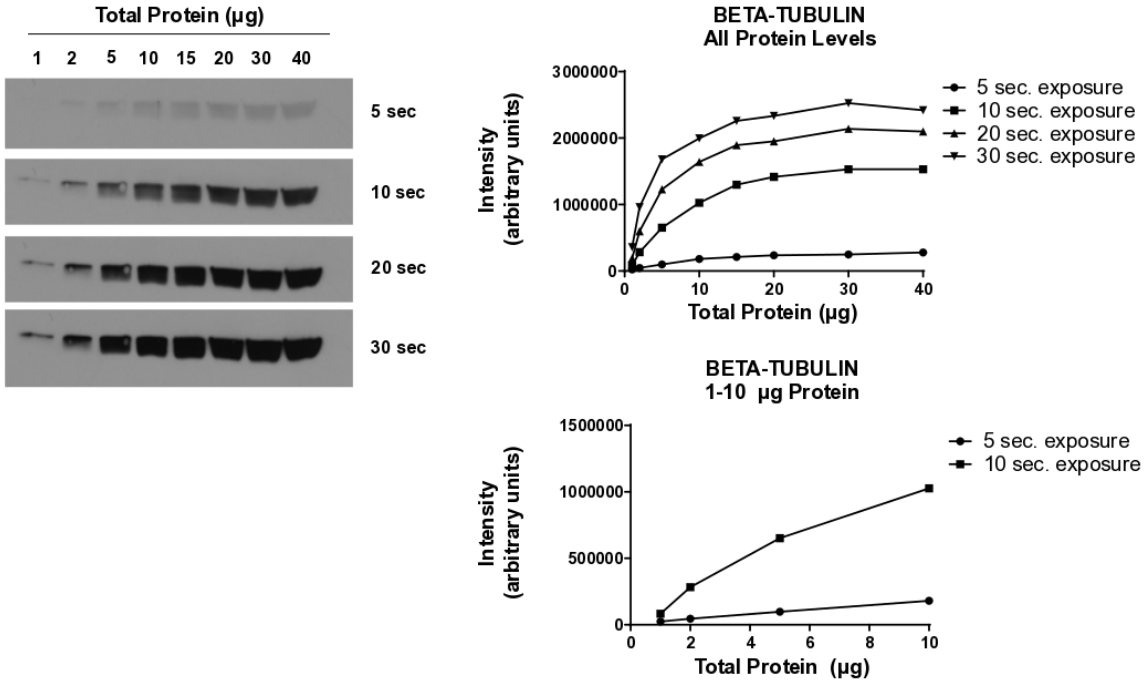

Figure 37. Standard curve for BETA-TUBULIN.
The 5 second exposure of BETA-TUBULIN was in the linear range up to 10 µg of total protein. The 10 second exposure was in the linear range up to 5 µg of total protein. The 20 and 30 second exposures were not in the linear range at any of the protein levels tested.

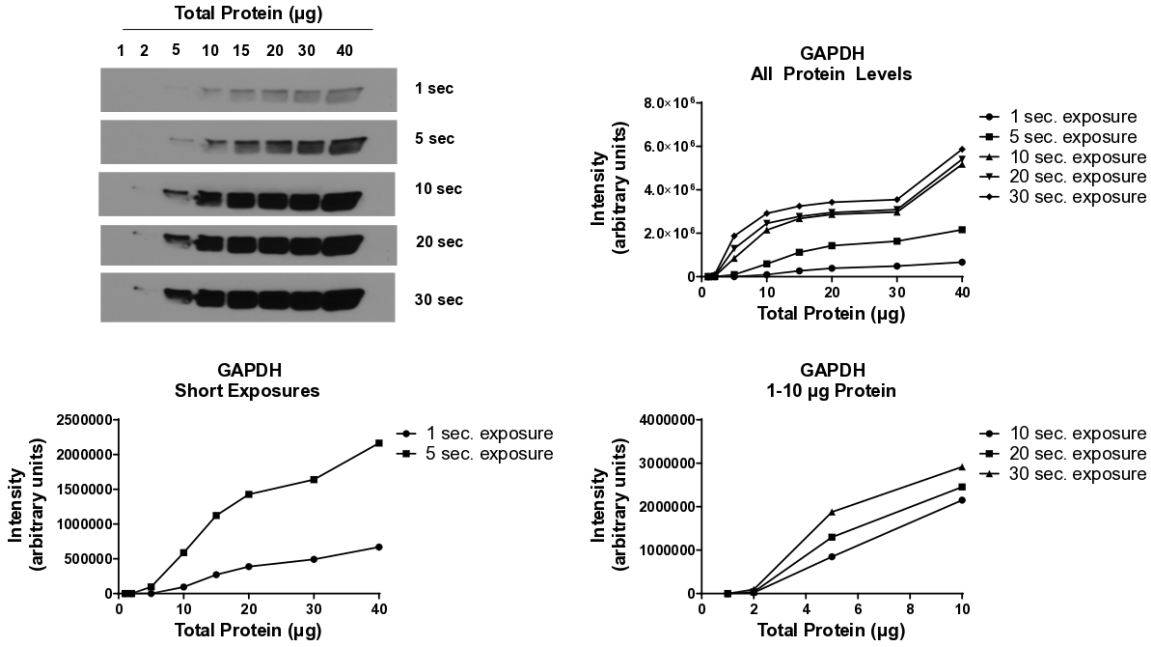

Figure 38. Standard curve for GAPDH.
The 1 second exposure of GAPDH was in the linear range for all amounts of total protein tested. The 5 second exposure was in the linear range up to 20 µg of total protein. The other exposures

were in the linear range up to 10 µg of total protein.

Fluorescent Westerns have been reported to have greater linear ranges than ECL-based ones. It is also easier to tell if a given signal is saturated when using fluorescent technologies than when using film. To examine these factors, I repeated the above test for GAPDH using fluorescent techniques. GAPDH had a linear response up to 20 µg of total protein. However, this limit is still lower than the total protein often loaded into a well of a protein gel.

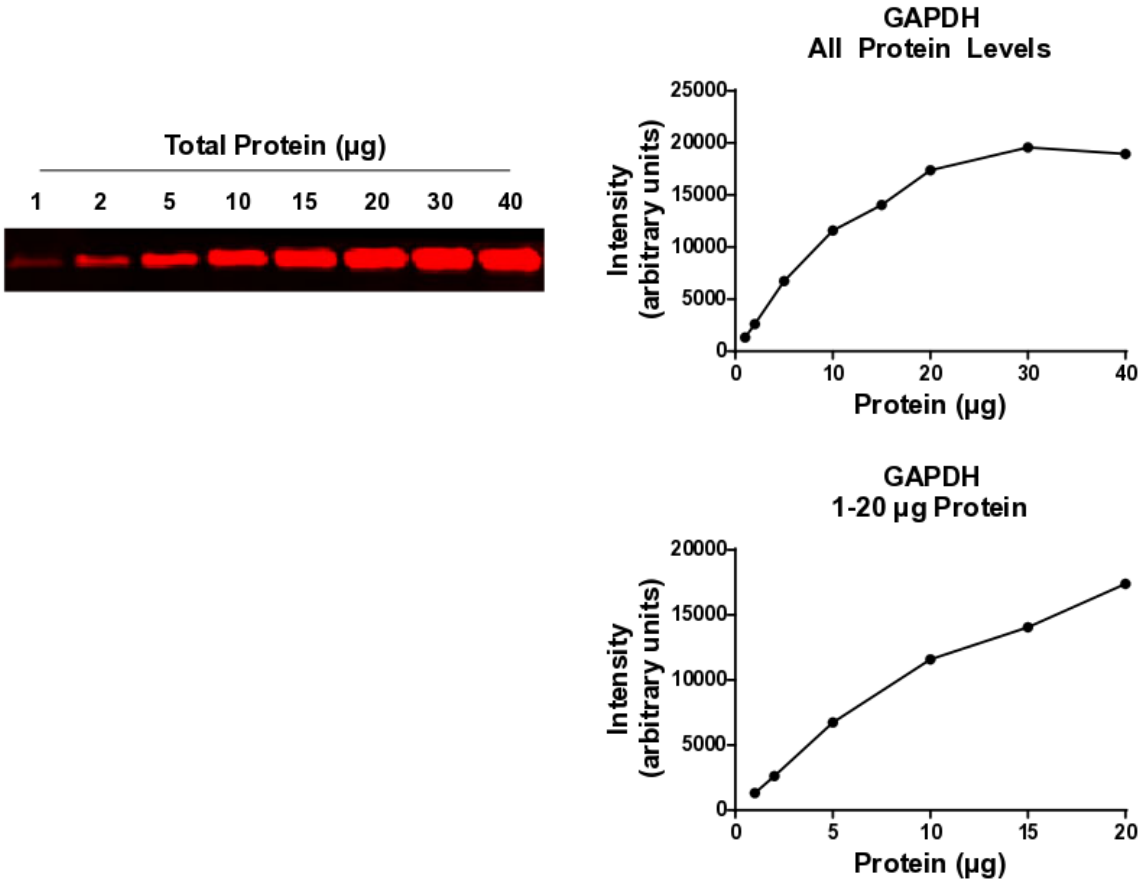

Figure 39. Standard curve for GAPDH using fluorescent Western technology. GAPDH was in the linear range up to 20 µg of total protein. Note that the software used can detect if the signal for a given band is saturated. The signals for 30 and 40 µg of total protein were not saturated.

I also performed standard curves for two FMRP target proteins often studied in

the Warren lab: MAP1B and PSD-95. In contrast to the housekeeping genes, these two genes were linear over the whole range examined. It is important to note that both these proteins were effectively undetectable in samples of less than 10 µg. Therefore, it is difficult to find an amount of total protein that is both in the linear range of the housekeeping genes and also produces a useful signal for the target proteins. And even then exposure times need to be tightly controlled to get a reliable signal for the housekeeping gene.

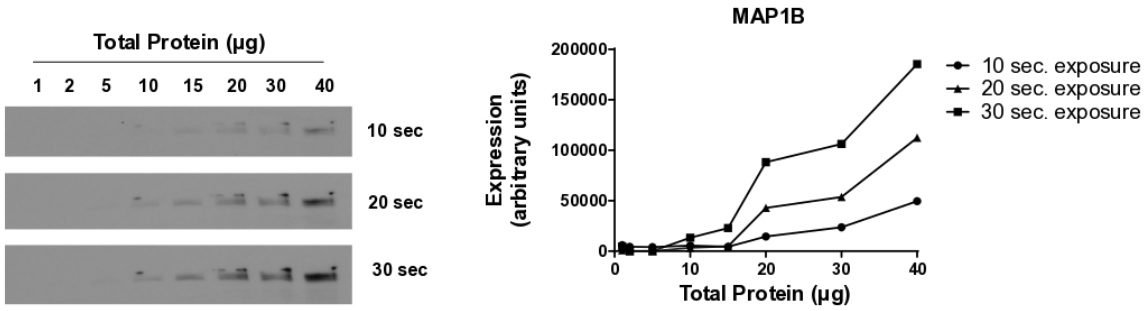

Figure 40. Standard curve for MAP1B.
At the exposure times used MAP1B was undetectable below 10 µg of total protein. All measurable signals were in the linear range across all protein levels tested.

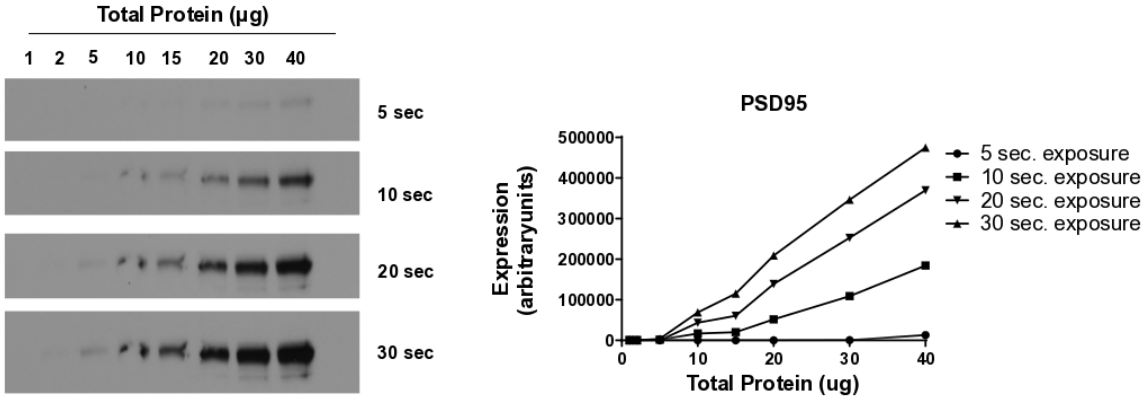

Figure 41. Standard curve for PSD-95.
At the exposure times used PSD-95 was undetectable below 5 µg of total protein. All measurable signals were in the linear range across all protein levels tested.

Several reports have discussed the use of total protein stains as loading controls.

Not only do total protein stains often have a wider linear range than housekeeping genes, total protein levels are rarely affected by drug treatments or other experimental manipulations To test this technique, I ran a series of four blots each with 1 to 40 µg of protein loaded in the lanes. I measured total protein levels on these blots using Ponceau S staining. The Ponceau stain was in the linear range for all amounts tested. After these results, I adopted total protein levels as my loading control in Western blots.

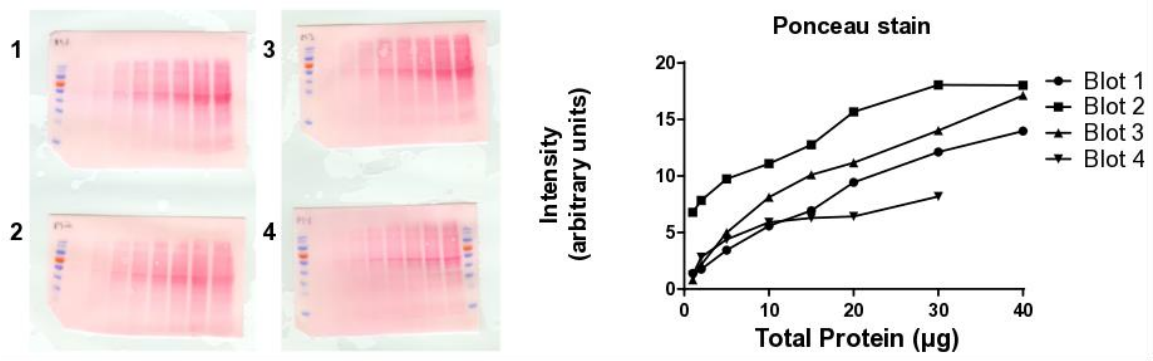

Figure 42. Standard curve for Ponceau S staining.
Ponceau staining was linear over all protein levels tested. Valid measurements could reliably be obtained down to 2 µg of total protein, and sometimes 1 µg of total protein.

The Warren lab now uses Bio-Rad stain-free technology to measure total protein levels in Western Blots. Bio-Rad claims this technology works over a wide range of protein levels. I tested this myself by again loading a standard curve of 1 to 40 µg of total protein in a gel, running the gel, and transferring the proteins to a PVDF membrane using Bio-Rad's Trans-Blot Turbo Transfer System. I used the stain-free technology to measure total protein levels in both the gel and on the membrane. In both cases, the measurements were in the linear range across all protein levels tested.

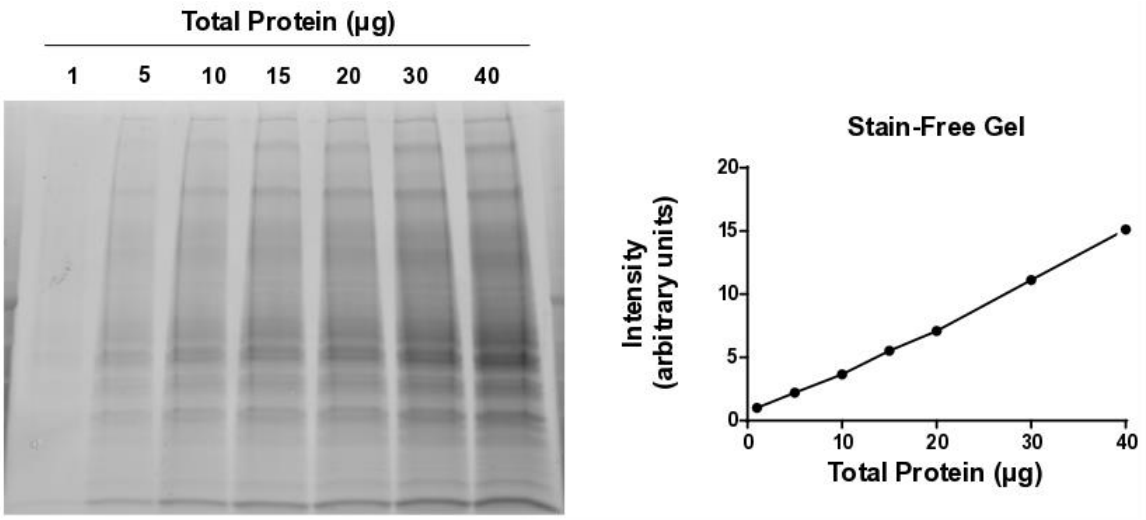

Figure 43. Standard curve for a stain-free polyacrylamide gel.
The stain-free technology was in the linear range over all protein levels tested in the gel.

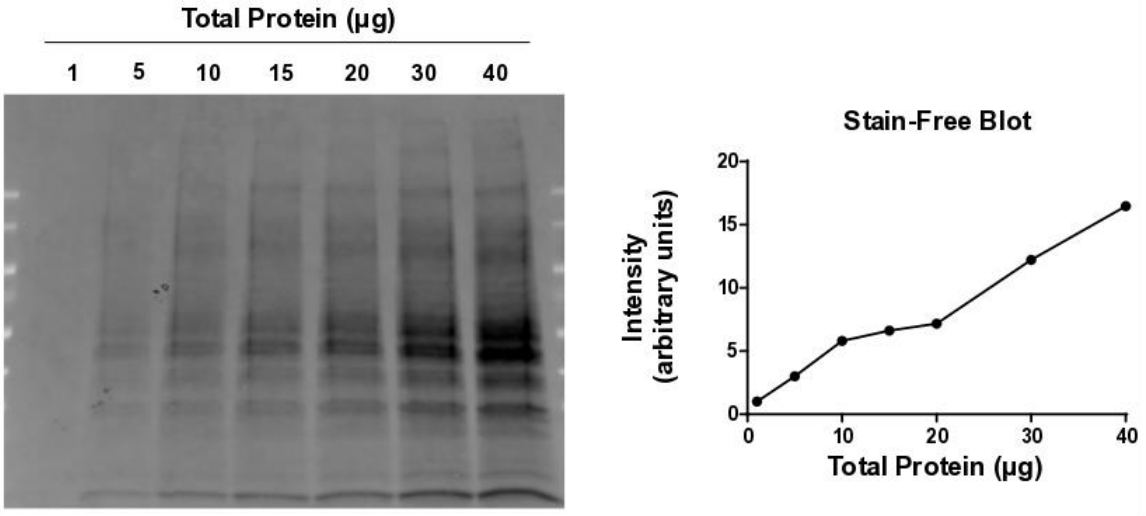

Figure 44. Standard curve for a stain-free membrane.
I transferred the proteins in figure 4-9 to a PVDF membrane. The stain-free technology was in the linear range over all protein levels tested on the membrane. The data points do not fit the line as well on the membrane as they do on the gel. It is unclear if this reflects different transfer efficiencies in different lanes or some limitation of measuring the signal on the membrane. My personal experience is that the imager consistently produces better images from gels than from membranes.

DARPP32 and SHANK1 Levels in Crude SNS

DARPP32 and SHANK1 have been reported to be elevated in crude SNS preparations in *Fmr1* KO mice as compared to WT mice[106]. I therefore undertook to measure the levels of these proteins in my Ser499Ala mice, while at the same time replicating the reports from the literature. But neither my Ser499Ala mice nor KO mice showed any differences compared to WT mice.

I harvested samples from WT/KO littermates and WT/Ser499Ala littermates. To control for blot-to-blot variation, before I began my experiments I collected a large volume of samples, pooled them, aliquoted them into separate tubes, and stored them at -80°C. For each blot, I thawed one of these control tubes and included it in the gel. Control samples were discarded after a single use.

I analyzed my data in two different ways. For the first method, I normalized every signal to the signal of the control sample on the same blot. Then, I averaged together all mice of a given genotype in a given litter. The results did not replicate the data in the literature. Levels of SHANK1 protein were the same in WT, KO, and Ser499Ala mice. Steady-state levels of DARPP32 did appear to be different in KO mice and WT mice, although too few litters were tested to draw any statistical conclusions. But the levels of DARPP32 were lower in KO mice, the opposite of what was reported in the literature. DARPP32 also appeared to be lower in Ser499Ala mice, but given the unexpected results for KO mice I was reluctant to consider this a reliable phenotype.

I also analyzed the data in a way that did not rely on the control samples. For each litter tested, I averaged all the WT values and all the mutant values. I then normalized the mutant average to the WT average. I was able to include an extra litter in this analysis, as

I had conducted one Western Blot without including control lysate. These results broadly matched my results above.

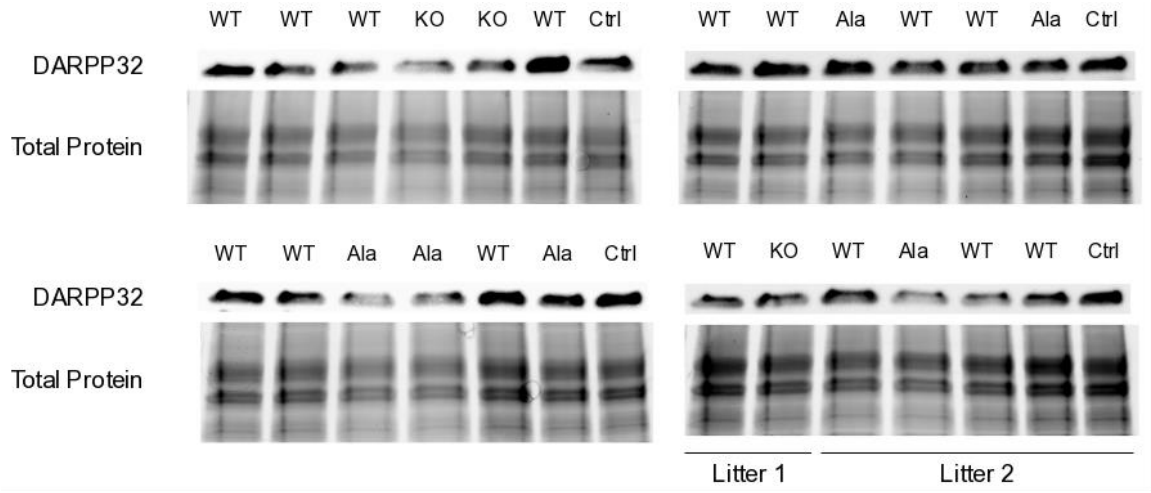

Figure 45. DARPP32 Western blots.
I tested two litters of WT/KO littermates and three litters of WT/Ala littermates. I included a lane of control lysate in each blot. Total protein levels were measured using stain-free technology One blot contained samples from two different litters (bottom right) All other blots contained samples from a single litter.

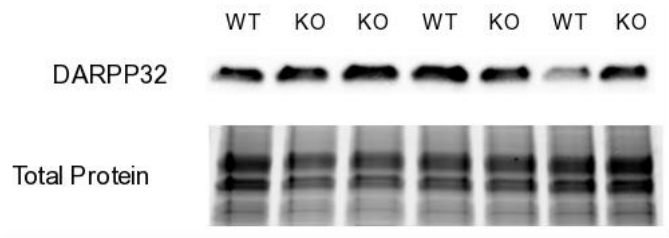

Figure 46. DARPP32 Western blot without control lysate.
This litter was included in the analysis which normalized to WT, but not in the analysis that normalized to control lysate.

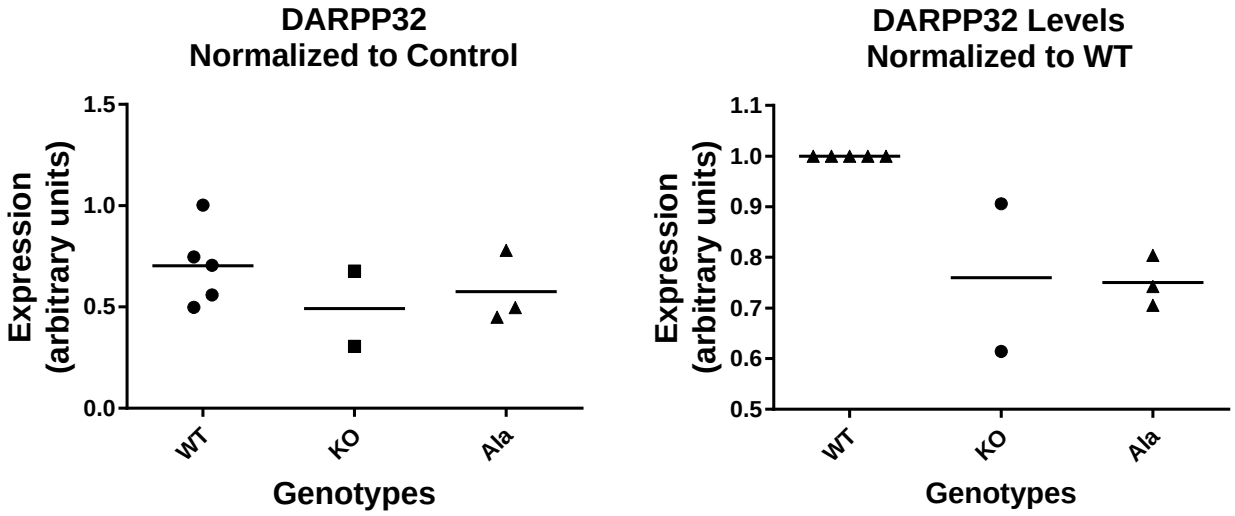

Figure 47. DARPP32 levels in cortical lysate.
I analyzed samples both by normalizing to control lysate and normalizing to WT littermates. Each point represents the average signal from all mice of a given genotype from a single litter. Using either method of analysis, DARPP32 levels in both KO and Ser499Ala mice were lower than levels in WT mice. The levels measured in Ser499Ala mice seemed lower when analyzed the second way.

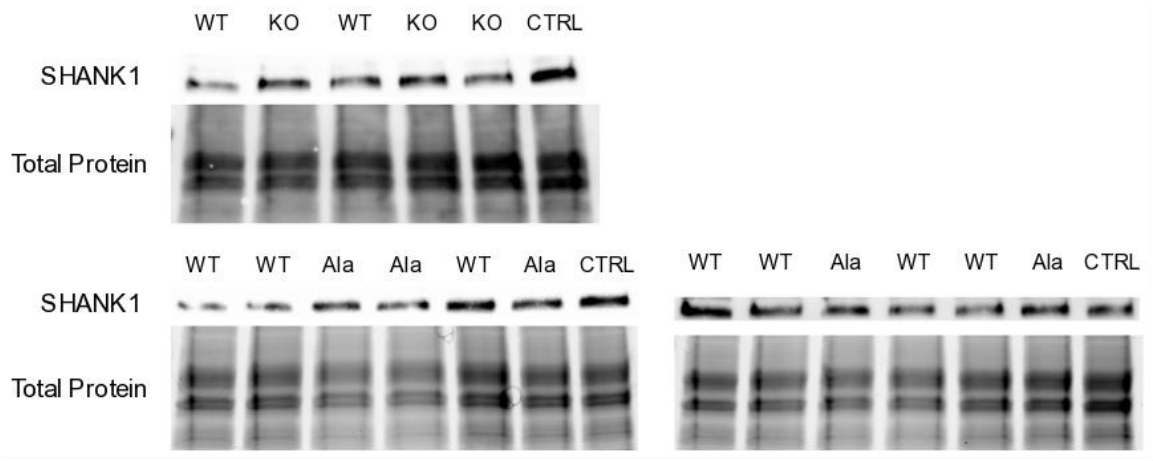

Figure 48. SHANK1 Western blots.
I tested one litter of WT/KO littermates and two litters of WT/Ala littermates. I included a lane of control lysate in each blot. Total protein levels were measured using stain-free technology. All blots contained samples from a single litter.

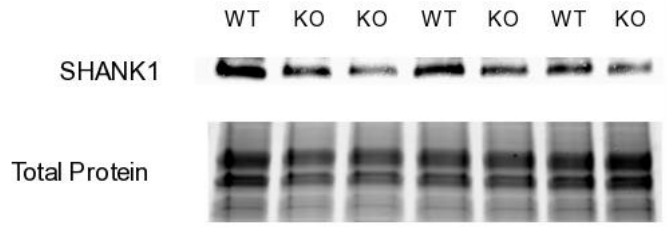

Figure 49. SHANK1 Western blot without control lysate.
This litter was included in the analysis which normalized to WT, but not in the analysis that normalized to control lysate.

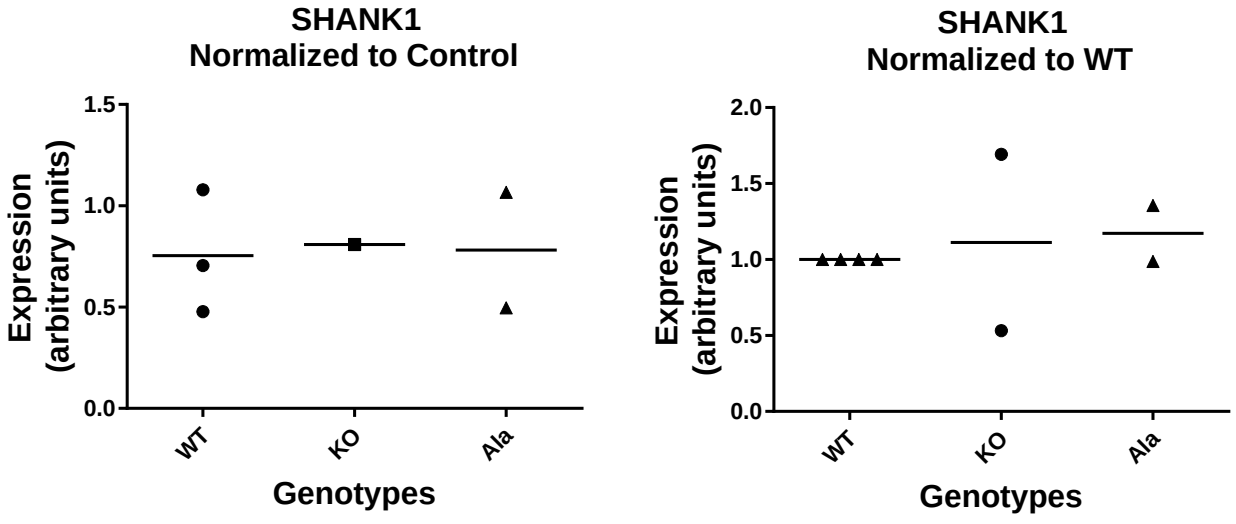

Figure 50. SHANK1 levels in cortical lysate.

I analyzed samples both by normalizing to control lysate and normalizing to WT littermates. Each point represents the average signal from all mice of a given genotype from a single litter. The results were broadly the same using either method of analysis.

MAP1B Levels in Hippocampi

MAP1B has been reported to be elevated in the hippocampi of juvenile mice, particularly at P10[73]. I measured MAP1B levels in the hippocampi of a single pair of WT/KO littermates and also in a larger litter of WT/Ala mice. Steady-state MAP1B levels were not different in either genotype as compared to WT.

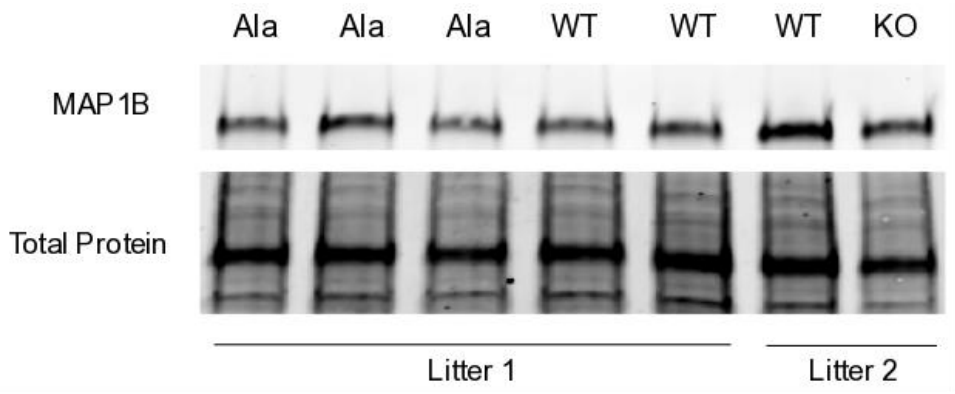

Figure 51. MAP1B Western blots.
I tested a litter of WT/Ala littermates and a single WT/KO littermate pair. This blot was analyzed using fluorescent blotting techniques. Total protein levels were measured using SYPRO Ruby stain.

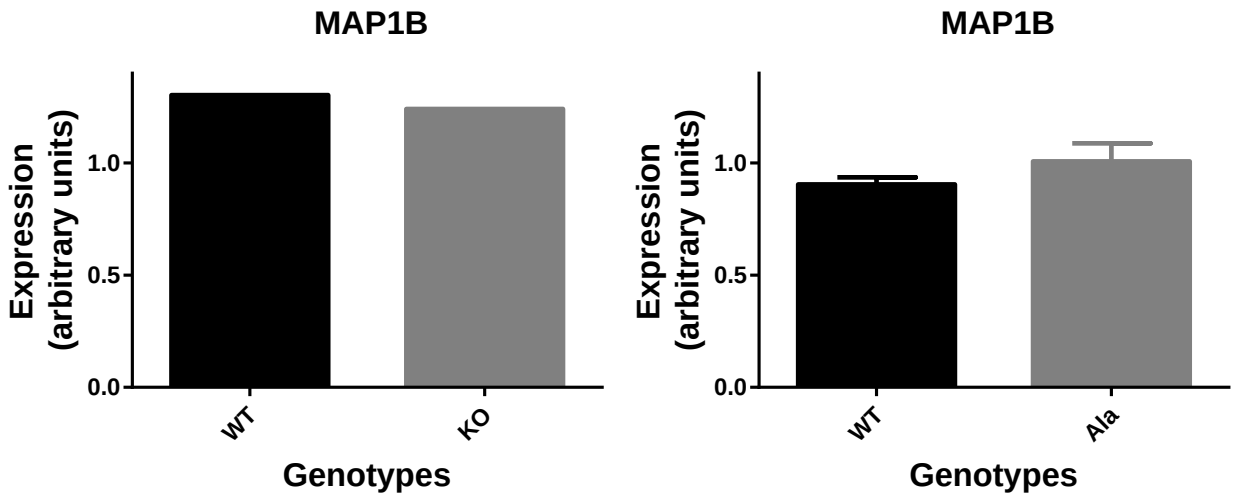

Figure 52. MAP1B levels in hippocampi.
MAP1B levels in KO and Ser499Ala mice were comparable to levels in WT mice.

Discussion

After examining the FXS literature, I chose three phenotypes to examine in my knockin mice: DARPP32 levels in crude SNS fractions, SHANK1 levels in crude SNS levels, and MAP1B levels in hippocampal lysate from juvenile mice. I found no evidence that steady-state levels of these proteins were elevated in my Ser499Ala mice. Furthermore, I was unable to reliably replicate the original results in Fmr1 KO mice. I believe there are multiple possible causes for this.

First, quantitative Western Blots are hard. Although they are commonly used for measuring differences in protein expression, getting reliable data from Western Blots is harder than is commonly appreciated. These issues have been discussed elsewhere[107-110], and I have described my personal experiences concerning loading controls and exposure times. For these reasons, I recommend the use of ELISAs for any assays that measure steady-state protein levels. Although developing assays for all the proteins

commonly studied in the FXS field would be time-consuming, once developed and validated ELISAs are faster, cheaper, and more reliable than Western Blots for the purposes of measuring differences in protein expression.

Second, there seem to be inherent limitations in using steady-state protein levels as a phenotype. Changes in the rates of protein synthesis do not necessarily result in commensurate changes in protein levels. And protein levels seem to be inherently noisy. In my crude SNS experiments I saw large variation in the levels of protein even in mice of the same genotype from the same litter. Examples of this can be seen in the Shank1 levels in WT mice normalized to control lysate and Shank1 levels in KO mice normalized to WT littermates (see figure 4-16). Yue Feng saw similar mouse-to-mouse variation in the original MAP1B experiment (personal communication). I don't believe these variations are technical artifiacts – I think they reflect large variations in the underlying biology.

I think measuring rates of new protein synthesis for individual FMRP target proteins would provide more reliable data. Total protein synthesis in SNS is a robust assay that consistently shows elevated rates of protein synthesis in SNS from KO mice. Until recently, this assay had to be done using radioactively labeled amino acids. This made it difficult to measure synthesis levels for specific proteins. But the introduction of AHA-labeling of newly synthesized proteins combined with IP now makes this easier[111]. I recommend using this assay to examine the rates of synthesis for specific proteins as opposed to their steady-state levels.

Chapter 5
Perspectives

Since the cloning of the *FMR1* gene, the fragile X field has learned a great deal about the function of FMRP. To date, research has mostly relied on *Fmr1* KO models developed in mice, cell culture, and fruit flies. Although productive, this limits opportunities to study the effects of other mutations on the gene. Very few patients have been identified with missense mutations in *FMR1*. This is reflected in the fact that few models of other mutations have been developed. One of the few missense mouse models, the I304N mouse, is functionally a null allele[102]. Therefore, there's been little progress in identifying which molecular functions of FMRP are responsible for specific phenotypes.

This is slowly changing. Recent cell culture work on the R138Q mutation has identified some specific functions of FMRP disrupted by that mutation[42]. The Warren lab is developing BAC transgenic mice with truncated alleles of *FMR1* to study the functions of the N-terminus of the protein. I believe my my thesis work suggests two ways to further disentangle the many functions of FMRP. First, the functions of alternative isoforms of FMRP should be examined. Second, the effects of my Ser499Ala mutation can be examined further. These goals will require new assays and the refinement of others.

Measuring FXS Phenotypes

The *Fmr1* KO mouse model was created in 1995. Since then, many research

groups have used it to investigate a large number of phenotypes in the mice. However, there has been little incentive for other groups to replicate established phenotypes. Because of this, it is not immediately obvious which assays are robust. If new mutation models are to be created in mice or the functions of isoforms are to be investigated, I believe that researchers need a reliable set of assays to determine if a given mutation recapitulates the FXS phenotypes.

Several molecular assays have been shown to be robust. In particular, AMPAR internalization and protein synthesis are not only reliable but can be performed in cell culture without having to create a whole new mouse model. Electrophysiology assays consistently show phenotypes in FXS mice. I think a reliable form of polyribosome profiles is necessary, but for reasons discussed in chapter 3 I'm not able to recommend a specific version of this assay. In mice, audiogenic seizures, macroorchidism, and dendritic spine maturation assays seem to be robust. Furthermore, several behavioral assays, including marble burying and the open field assays, have been successfully repeated by multiple research groups. This set of molecular and behavioral assays represent a reliable method to assess FXS phenotypes in different mouse models.

Alternative Isoforms of *FMR1*

This suite of tests could be used to identify specific FXS phenotypes rescued by individual isoforms of FMRP. Although 12 alternative isoforms of *FMR1* were identified twenty years ago, very little research into the functions of these isoforms has been published. Isoform 1, which is the full-length isoform, has been used almost exclusively in research involving cDNA. More recently, it has been reported that isoform 7 mRNA is

expressed at higher steady-state levels than isoform 1 mRNA[38], suggesting isoform 7 may be playing an important physiological role. I believe my research adds weight to the idea that many of the other isoforms should be studied more closely.

This conclusion follows from the fact that my mice do not recapitulate the phenotypes predicted from research using isoform 1. It may be that alternative isoforms of FMRP are able to rescue most null phenotypes. It is important to note that the original work which established Ser499 as the key residue in regulation of FMRP did not examine the phosphorylation status of any isoform other than isoform 1. These other isoforms may therefore be regulated by the phosphorylation of different residues.

The most straightforward way to test the function of the alternative isoforms is to use cDNA to express these other isoforms in *Fmr1* KO cells. New protein synthesis can be measured in MEF cells and AMPAR internalization can be measured in primary neurons. These assays could provide a quick readout of the ability of alternative isoforms to rescue the major FXS phenotypes. Later, certain isoforms could be tested in fly or mouse transgenic models.

Further Uses of Ser499Ala Mice

I think the Ser499Ala phenotype in the protein synthesis assay suggests that there might be multiple pools of FMRP involved in local protein synthesis. In this model, the Ser499Ala mutation has inactivated a subset of FMRP but allowed a different subset to function normally. Measuring total levels of protein synthesis only allows us to see the combined effects from these two subsets of protein.

Specifically, I favor the idea that these two distinct pools of FMRP are regulating

distinct sets of target mRNAs. This would mean that one subset of mRNAs is dysregulated in my Ser499Ala mice, but another subset is being regulated normally. Until recently, this would be difficult to investigate. But using the BONCAT method it is now possible to measure rates of protein synthesis for individual proteins at a proteomic level[101]. This would allow a researcher to identify specific proteins that are being synthesized at higher rates in *Fmr1* KO cells. Furthermore, it would be possible to test if a subset of these proteins are being overexpressed in the Ser499Ala mice. Since the signaling pathways that control the phosphorylation and dephosphorylation of FMRP at Ser499 have been identified, this would indicate which specific mRNA targets are downstream of those pathways.

The Ser499Ala mice may also be useful in studying how FMRP regulates its target mRNAs. At least three different mechanisms have been proposed for this function, although the mechanisms are not necessarily mutually exclusive. Again, it's possible there are distinct pools of FMRP, with the proteins in different pools using different mechanisms to regulate translation of target mRNAs. If the FMRP in only one of these pools is regulated by the phosphorylation of Ser499, then it may be possible to identify the specific mechanism that is disrupted in Ser499Ala mice.

Conclusions

To date, most of the focus in the FXS literature has been on determining the many functions of FMRP. I think the time has come to focus on mapping known functions of FMRP to specific domains of the protein and to specific phenotypes seen in patients and

mice. Much of this work can begin with existing reagents, such as my Ser499Ala mice. Other reagents, such as plasmids expressing cDNA of alternative isoforms of *Fmr1*, can be easily created.

Chapter 6
Materials and Methods

Mouse Husbandry

All mice were housed in the Warren lab mouse colony at Emory University. Knockin mice were backcrossed to C57BL/6J strain mice for more than 10 generations before being used in assays. All mice used in experiments were male unless otherwise stated. All mouse work followed accepted standards for the ethical treatment of mice. Protocol 2003350 was approved by Emory University IACUC.

Cloning *Fmr1* Gene

BAC RP23-397L15 was obtained from the BACPAC Resources Center at the Children's Hospital Oakland Research Institute and used as the source of DNA for cloning of the *Fmr1* sequence. This BAC is from a library generated using kidney and brain DNA from a 3.5 week old female C57BL/6J mouse. It is 195kb long and contains the entire murine *Fmr1* gene.

DNA was cloned from BAC RP23-397L15 using red-recombination, as described previously [96]. Bacterial cells containing the BAC were made electrocompetent by growing in 5 mL of SOB media at 37°C for 5 hours. The cells were transferred to a 15 mL conical tube and centrifuged at 2000 x g for five minutes at 4°C. Cells were resuspended in 1 mL ice cold 10% glycerol by pipetting, transferred to an Eppendorf tube, centrifuged at 8000 x g for 10 seconds at 4°C, and the supernatant removed. Cells

were then washed one more time with 1 mL ice cold 10% glycerol, centrifuged at 8000 x g for 10 seconds at 4°C, and the pellet resuspended in 100 µL ice cold 10% glycerol.

1 µL of 10 ng/µL of plasmid pKD46 was added to 50 µL of cells in a 0.1 cm cuvette and electroporated using a Bio-Rad Gene Pulser Xcell set to 1.8 kV, 25 µF, and 200 ohms. After electroporation, 300 µL of SOC media was added to the cells and the cells were plated on an LB plate containing 100 µg/mL ampicillin and 20 µg/mL chloramphenicol. The plate was incubated at 30°C for 24 to 30 hours. A colony was picked from the plate and used to inoculate a 5 mL starter culture in SOB media supplemented with 100 µg/mL ampicillin and 20 µg/mL chloramphenicol. The starter culture was incubated at 30°C with shaking overnight. The starter culture was used to inoculate a 250 mL culture of SOB media to an OD 600 reading of 0.1 to 0.2.

L–arabinose was added to a final concentration of 0.1% and the culture was incubated at 30°C with shaking until it achieved an OD 600 reading of 0.3 (3 hours). Additional L-arabinose was added to a final concentration of 0.2% and the culture was incubated at 37°C with shaking for an additional hour. The culture was then transferred to 50 ml conical tubes and placed on ice for 10 minutes, swirling occasionally. The culture was centrifuged at 2000 x g for 15 minutes at 4°C, the supernatant removed, and the pellet was resuspended in 50 mL of ice cold 10% glycerol. The cells were washed two more times with 25 mL of ice cold 10% glycerol, centrifuged at 2000 x g for 15 minutes at 4°C after each wash, and resuspended in 100 µL ice cold 10% glycerol.

Fresh PCR product from the amplification of pStart-K was produced as described below and 10 µL of 146 ng/µL PCR product was electroporated into 50 µL of the above cells using the settings above. After electroporation, 1 mL of SOB media was added to

the cells. Cells were transferred to an Eppendorf tube, incubated at 37°C for one hour, plated on LB plates containing 50 µg/mL kanamycin, and incubated at 37°C overnight.

PCR of pStart-K

The required regions of pStart-K were amplified by PCR (125 µL reaction; 1X Invitrogen Buffer A, 100 µM dNTPs, 400 nM primer pStart_Fmr1_5', 400 nM primer pStart_Fmr1_3', 250 ng plasmid pStart-K, 5 units Invitrogen Platinum Taq polymerase; thermocycler program: 2 minutes at 94°C, 32 x [30 seconds at 94°C, 2 minutes at 68°C], 7 minutes at 68°C). PCR products were purified using the Qiagen PCR Purification Kit and eluted with 100 µL of water. 2 µL of 20 units/µL of DpnI and 25 µL of 10X NEB Buffer 4 were added to the eluate. The digestion mix was incubated at 37°C for two hours, purified using the Qiagen PCR Purification Kit, and eluted with 30 µL of water. Concentration of the final product was measured on a Nanodrop ND-1000 spectrophotometer.

Site Directed Mutagenesis

Site directed mutagenesis was carried out using the Stratagene QuikChange XL Kit. The following primers were used:

- Removing splice acceptor site 1: SA1_S, SA1_AS
- Removing splice acceptor site 2: SA2_S, SA2_AS
- Ser499Ala mutation: S499A_S, S499A_AS
- Ser499Asp mutation: S499D_S, S499D_AS

For each mutation, the PCR reaction was carried out following the manufacturer's directions, with 10 ng of plasmid and 125 ng each of the sense and antisense primers. The thermocycler program was 1 minute at 95°C, 18 x [50 seconds at 95°C, 50 seconds at 60°C, 10:30 at 68°C], and 7 minutes at 60°C. 1 µL of 10 units/µL DpnI enzyme was added to the PCR product and the mixture was incubated at 37°C for 1 hour. One tube of XL10–Gold ultra competent cells were thawed on ice, 45 µL of cells were aliquoted into a 14 mL BD Falcon tube, and 2 µL of beta-mercaptoethanol was added to the tube. The mixture was incubated on ice for 10 minutes, being swirled by hand every two minutes. 2 µL of the DpnI-treated PCR product was added to the tube. The mixture was incubated on ice for 30 minutes, heat pulsed for 30 seconds in a 42°C water bath, and incubated on ice for 2 minutes. 500 µL of pre-warmed NYZ+ media was added to the tube and the mixture was incubated at 37°C with shaking for 1 hour. This culture was plated on LB plates with 100 µg/mL ampicillin, 20 µg/mL X–gal, and 20 mM IPTG and incubated overnight at 37°C. The resulting colonies were grown in LB media containing 100 µg/mL ampicillin and DNA was extracted using the Qiagen MIDI Prep Kit.

Mutated DNA was sequenced by Sanger sequencing using the Int14_S and Int15_AS primers to verify the correct mutation was introduced. Key sequences (exons, vector/insert junctions, region chosen for insertion of neomycin cassette) in candidate plasmids were verified by Sanger sequencing using the following primers: 5'_Junc_AS, 3'_Junc_S, Fmr1_Neo_S, Fmr1_Neo_AS, Int12_S, Int13_AS, Int13_S, Int14_AS, Int14_S, Int15_AS, Int15_S, Int16_AS, ws275, and ws276. Plasmids were further verified by digesting with NheI (1X NEB Buffer 2, 100 µg/mL BSA, 1 µg plasmid, 20 units NheI), AseI (1X NEB Buffer 3, 1 µg plasmid, 20 units AseI), HincII (1X NEB

Buffer 3, 100 µg/mL BSA, 1 µg plasmid, 20 units HincII), and SacI (1X NEB Buffer 1, 100 µg/mL BSA, 1 µg plasmid, 20 units SacI). All four digests were incubated at 37°C overnight and the results were visualized in a 1X TBE, 0.7% agarose gel stained with 400 ng/mL ethidium bromide.

Insertion of Neomycin Resistance Cassette

The neomycin selection cassette was inserted with in vitro recombination using the "Choo-Choo cloning" Kit. The vector was linearized by digestion with MfeI (50 µL reaction; 1X NEB Buffer 4, 10 µg plasmid, 20 units MfeI) at 37°C for 3 hours, and the enzyme was heat inactivated by incubating at 65°C for 20 minutes. The neomycin cassette was amplified by PCR (5 x 50 µL reactions; each reaction: 1X Invitrogen Pfx Buffer, 1X Invitrogen Enhancer Solution, 300 µM dNTPs, 1 mM magnesium sulfate, 400 nM primer FnF11_Fmr1_choo1, 400 nM primerFnF11_Fmr1_choo2, 10 ng plasmid FnF11, 2.5 units Invitrogen Platinum Pfx DNA polymerase). PCR products were combined, purified using the Qiagen PCR Purification Kit, and eluted with 30 µL of water. Concentration of the final product was measured on a Nanodrop ND-1000 spectrophotometer.

The recombination reaction was carried out following manufacturer's directions using a 5:1 molar ratio of vector:insert. The reaction was incubated on ice for 45 minutes and then added to a tube of Choo-Choo Golden competent cells thawed on ice. The mixture was incubated on ice for 15 minutes, heat shocked for 45 seconds in a 42°C water bath, and incubated on ice for an additional 2 minutes. 300 µL of room temperature SOC media was added and the mixture was incubated at 37°C for 1 hour with shaking.

The culture was spread on LB plates containing 50 µg/mL kanamycin and incubated at 37°C overnight.

The resulting colonies were screened by PCR (20 µL reaction; 1X Invitrogen Buffer C, 125 µM dNTPs, 500 nM primer FnF11_5721_S, 500 nM primer Fmr1_Neo_S, 500 nM primer Fmr1_Mfe_AS, 5 units Invitrogen Platinum Taq polymerase; thermocycler program: 5 minutes at 95°C, 30 x [1 minute at 95°C, 1 minute at 60°C, 1 minute at 68°C], 5 minutes at 68°C). This PCR produces a 312 base pair band if the neomycin cassette has inserted in the desired orientation. The vector/insert junctions in candidate plasmids were sequenced by Sanger sequencing using the following primers: Fmr1_Mfe_S, Fmr1_Mfe_AS, FnF11_1453_AS, and FnF11_5721_S. The plasmids were also sequenced using the same primers listed in the site directed mutagenesis section and were digested with AseI and SacI as described in the site directed mutagenesis section.

Creation of Probes for Southerns

Probes for Southern blotting were created by PCR using BAC RP23-397L15 as a template (25 µL reaction; 1X Invitrogen Buffer C, 100 µM dNTPs, 400 nM forward primer, 400 nM reverse primer, 5 units Invitrogen Platinum Taq polymerase, 72 ng BAC DNA; thermocycler program: 2 minutes at 94°C, 30 X [30 seconds at 94°C, 30 seconds at 55°C, 1 minute at 68°C], 10 minutes at 68°C). Primers used for probe M2 were 5'_478_F and 5'_478_R; primers used for probe M5 were 3'_971_F and 3'_971_R. 2 µL of each PCR product was visualized in a 1% agarose gel stained with 400 ng/mL ethidium bromide to verify the correct sizes of the PCR products. The remaining PCR products were purified with the Qiagen PCR Purification Kit and cloned into vector pCR2.1-

TOPO-TA using Invitrogen's TOPO TA Cloning Kit. Potential recombinants were spread on LB plates containing 100 µg/mL ampicillin and 20 µg/mL X-gal. For each probe five white colonies were picked from the plate, each colony was used to inoculate a 5 mL LB plus 100 µg/mL ampicillin culture, and the cultures were incubated at 37°C with shaking overnight. Plasmid DNA was prepared from the cultures using the Qiagen Plasmid Miniprep Kit.

Plasmids containing putative M2 clones were digested by HindIII (25 µl reaction; 1X NEB Buffer 2, 40 units HindIII, 4 µL plasmid); plasmids containing putative M5 clones were digested by PciI (25 µl reaction; 1X NEB Buffer 3, 10 units PciI, 4 µL plasmid). All digests were incubated at 37°C for 3 hours and the results were visualized in a 1X TBE, 1% agarose gel stained with 400 ng/mL ethidium bromide. For each probe, one plasmid with the correct digestion pattern was chosen and 200 µL of that plasmid's starter culture was used to inoculate a 100 mL LB culture containing 100 µg/mL ampicillin. These cultures were incubated at 37°C with shaking overnight, and plasmid DNA was prepared using the Qiagen Maxiprep Kit. The inserts were verified by Sanger sequencing the plasmids with primers M13_F and M13_R.

Probe template DNA was produced by digesting the plasmids with EcoRI (50 µL reaction; 1X NEB Buffer 3, 40 units EcoRI, 25 to 40 µg plasmid) at 37°C for 4 hours, running the product in an agarose gel, excising the bands corresponding to the appropriate insert, and extracting the DNA using the Qiagen Gel Extraction Kit. Template DNA was stored at 4°C.

Digestion of ES Cell DNA for Southern Blots

Embryonic stem cell DNA was received from the Emory Mouse Transgenic and Gene Targeting Core in 95% ethanol in 96-well format. The ethanol was poured off and the plate was allowed to dry at room temperature for 30 to 90 minutes. DNA was digested with enzymes from New England Biolabs (25 units ScaI, 15 units BglI, 1X NEB Buffer 3, 100 µg/mL BSA, 1 mM spermidine) or Fast Digest enzymes from Life Technologies (1X Fast Digest Buffer, 1.5 µL FD–ScaI, 1.5 µL FD–BglI). 30 µL of digest mix was added to each well, the plate was wrapped in plastic wrap with two damp paper towels and incubated at 37°C overnight in a hybridization oven.

Digestion of Tail-Snip DNA for Southern Blots

5-10 µg of tail-snip DNA was digested with Fast Digest enzymes from Life technologies (40 µl reaction, 1X Fast Digest Buffer, 1.75 µl FD-ScaI, 1.75 µl FD-BglI) at 37°C overnight.

DNA Gel for Southerns

Digested DNA was run in a 0.8% agarose, 1X TBE gel at 40 V for 20 to 24 hours. The gels were stained with 400 ng/mL ethidium bromide, visualized, rinsed with dH2O three times, rocked in 0.25 N HCL on an orbit shaker for 15 minutes, rinsed with dH2O three times, and rocked in 0.4 N NaOH on an orbit shaker for 30 minutes. DNA was transferred to a positively charged nylon membrane overnight using the downward capillary method, with 0.4 N NaOH as the transfer buffer. The membrane was rinsed in

2X SSC, dried at room temperature for 30 minutes, and cross-linked with ultraviolet light in a Stratagene UV Stratalinker 1800 set to "auto cross-link".

Probe Labeling by Nick Translation

2 µL of DNase I (10 units/µL) was diluted in 200 µL of activation mix (10 mM Tris-HCl pH 7.5, 5 mM MgCl2, 1 mg/mL BSA) and incubated on ice for 20 minutes. 1 µL of diluted DNase was combined with 250 ng of template DNA, 5 µL of 5X NT Buffer (0.1 M Tris–HCl pH 7.5, 50 mM MgCl2, 250 µg/ml BSA, 0.625% beta-mercaptoethanol), 5 µL of dGAT mix (11 µm dGTP, 11 µm dATP, 11 µm dTTP), and 7 µL of α32P-dCTP. The mixture was adjusted to 23 µL with dH2O and incubated at room temperature for 2 minutes. 1.5 µL of DNA polymerase I (1000 units/0.22 mL) was added and the mixture was incubated at 15°C for 30 minutes. The reaction was stopped by adding 5 µL of stop buffer (0.25 M EDTA, 0.05% SDS, 10 µg /mL tRNA, 0.0008% phenol red), the mixture was incubated at 65°C for 10 minutes, placed on ice, and purified by pipetting the probe onto a Sephadex column and centrifuging the column at 355 x g for 2 minutes at room temperature.

Southern Blot

Pre-hybridization buffer was made by boiling 1 mL of 10 mg/mL sheared salmon sperm DNA at 95°C for 10 minutes and adding 600 µL of the boiled DNA to 14 mL of prewarmed hybridization buffer (7% SDS, 1.5 X SSC, 10% PEG 8000, .025% heparin). The membrane was placed in a hybridization tube, the pre-hybridization buffer was

added, and the tube was rotated at 65°C for 4 hours. The labeled probe was added to 400 µL of sheared salmon sperm DNA and boiled at 95°C for 10 minutes. The 14 mL of pre-hybridization buffer was poured out of the hybridization tube, 10 mL of prewarmed hybridization buffer was added to the tube, and the boiled probe/sperm DNA was added. The membrane was hybridized at 65°C with rotation overnight. The next day, the hybridization buffer/probe mixture was poured out of the tube, the membrane was rinsed twice with room temperature Wash Buffer I (0.1% SDS, 2X SSC), washed with Buffer I at 65°C with rotation for 15 minutes, and washed twice with Buffer II (0.5% SDS, 0.1 X SSC) at 65°C with rotation for 30 minutes. The membrane was removed from the hybridization tube, rinsed in 2X SSC, wrapped in plastic wrap, and placed on a phosphor storage screen overnight. The screen was imaged on a GE Healthcare Typhoon 9400 scanner.

Mouse Genotyping by PCR/Digest of Exon 15

Genomic DNA was amplified by PCR (5×50 µL reactions; each reaction: 1X Invitrogen AccuPrime Buffer A, 2 mM magnesium sulfate, 2 units Invitrogen AccuPrime GC-rich DNA polymerase, 200 nM primer Int14_S, 200 nM primer Int15_AS, 2 µL genomic DNA; thermocycler program: 3 minutes at 95°C, 30 x [30 seconds at 95°C, 30 seconds at 55°C, 90 seconds at 72°C], 10 minutes at 72°C). The 5 reactions for a given template were combined and purified using the Qiagen PCR Purification Kit.

For each reaction, 400 ng of PCR product was digested by AlwNI (25 µL reaction, 1X NEB CutSmart Buffer, 10 units AlwNI), NlaIV (25 µl reaction, 1X NEB CutSmart Buffer, 2 units NlaIV), and BbvI (25 µL reaction, 1X NEB Buffer 2, 4 units

BbvI). The reactions were incubated at 37°C overnight and the results were visualized in a 1X SB, 1.5% agarose gel stained with 400 ng/mL ethidium bromide.

Genotyping Phosphomutant Mice by PCR

Genomic DNA was amplified by PCR (25 µL reaction; 1X Invitrogen PCR Buffer, 1.25 mM MgCl2, 100 µM dNTPs, 40 nM primer Int15_528_S, 40 nM primer Int15_762_AS, 2.5 units Invitrogen Platinum Taq Polymerase, 1 µL genomic DNA; thermocycler program: 5 minutes at 95°C, 30 x [1 minute at 95°C, 1 minute at 55°C, 30 seconds at 68°C], 5 minutes at 68°C). The results were visualized in a 1X SB, 2% agarose gel stained with 400 ng/ml ethidium bromide.

Western Blot of pFMRP/FMRP

12 to 13 week old mice were euthanized by cervical dislocation, their brains dissected, and both cortices removed. Each pair of cortices was homogenized in 500 µL of lysis buffer (50 mM Tris, 300 mM NaCl, 30 mM EDTA, 0.5% Triton X-100, pH 7.6) supplemented with protease inhibitors (Roche Complete Ultra Mini EDTA-free tablets) in an Eppendorf tube on ice with a sterile pestle for 90 seconds. Samples were centrifuged at 20000 x g for 5 minutes at 4°C. The supernatant was transferred to a new Eppendorf tube and total protein concentration was measured by Bradford assay.

For each sample, 50 µg protein was incubated in a dephosphorylation reaction (50 µL reaction, 1X NEB Buffer for PMP, 1 mM manganese chloride, 300 units lambda phosphatase) and a mock reaction (same as dephosphorylation reaction except without

phosphatase). Samples were incubated at 30°C for 30 minutes, 12.5 µL of 5X Laemmli buffer was added, and samples were boiled at 95°C for 5 minutes. 40 µL of each sample was run in a 4-15% polyacrylamide gel in 1X running buffer (192 mM glycine, 25 mM Tris, 3.5 mM SDS) at 200 V for 35 minutes. Proteins were transferred to a PVDF membrane in 1X transfer buffer (192 mM glycine, 25 mM Tris, 20% methanol) at 90 V for 1 hour at 4°C. The membrane was blocked with PBS StartingBlock buffer for 15 minutes at room temperature and then incubated with anti-pFMRP antibody (Abcam, ab48127) diluted 1:200 in PBS StartingBlock buffer at 4°C with rocking overnight. The membrane was washed 3×10 minutes with wash buffer (1X PBS, 1% nonfat dry milk, 0.2% Tween-20), incubated with anti-rabbit HRP-conjugated secondary antibody (Cell Signaling, 7074) diluted 1:2000 in dilution buffer (1:1 Wash Buffer:RIPA) at room temperature for 45 minutes, washed 3×10 minutes with wash buffer, incubated in HyGlo ECL substrate at room temperature for 5 minutes, and imaged on film.

The membrane was then washed in 1X PBS for 5 minutes at room temperature, incubated in Thermo Scientific Stripping Buffer at room temperature for 15 minutes, washed in 1X PBS for 5 minutes at room temperature, and blocked in PBS StartingBlock buffer for 15 minutes at room temperature. The membrane was incubated in anti-FMRP antibody (EMD Millipore, clone 1C3, MAB2160) diluted 1:1000 in PBS StartingBlock buffer at 4°C with rocking overnight. The membrane was washed 3×10 minutes with wash buffer, incubated with anti-mouse HRP-conjugated secondary antibody diluted 1:10000 in dilution buffer at room temperature for 45 minutes, washed 3×10 minutes with wash buffer, incubated in ECL substrate at room temperature for 5 minutes, and imaged on film.

Reverse Transcription of *Fmr1* mRNA

7 to 8 week old male mice were enthanized by cervical dislocation, their brains dissected, and cortices removed. Cortices were homogenized in 3 mL of Trizol in a dounce homogenizor with 12 to 14 strokes. Samples were split into 3×1 mL aliquots in Eppendorf tubes and RNA was extracted according to the manufacturer's instructions. RNA in each tube was resuspended in 33 µL of RNase-free water and the 3 aliquots for a given sample were recombined. The concentration of RNA was measured on a Nanodrop ND-1000 spectrophotometer and samples were adjusted to 1 µg/µl with RNase-free water.

RNA was reverse transcribed to cDNA using the Invitrogen Superscript III First-Strand Supermix Kit. For each sample, 3 reactions were performed:

1. Sample: 5 µL water, 1 µL of 2 µM primer Fmr1_RT, 1 µL of Invitrogen Annealing Buffer, 1 µL of 1 µg/µl RNA
2. No Template Control (NTC): 6 µL water, 1 µL of 2 µM primer Fmr1_RT, 1 µL of Invitrogen Annealing Buffer
3. No Reverse Transcriptase (NRT): 5 µL water, 1 µL of 2 µM primer Fmr1_RT, 1 µL of Invitrogen Annealing Buffer, 1 µL of 1 µg/µl RNA

The mixtures were incubated at 65°C for 5 minutes and then put on ice for 1 minute. The following was added to each mixture:

1. Sample: 10 µL of 2X Invitrogen First-Strand Reaction Mix, 2 µL of Invitrogen SuperScriptIII/RNase OUT Enzyme Mix
2. NTC: 10 µL of 2X Invitrogen First-Strand Reaction Mix, 2 µL of

Invitrogen SuperScriptIII/RNase OUT Enzyme Mix

3. NRT: 10 µL of 2X Invitrogen First-Strand Reaction Mix, 2 µL water

The mixtures were incubated at 50°C for 50 minutes, 85°C for 5 minutes, and the cDNA was stored at -20°C.

PCR of *Fmr1* cDNA

Fmr1 cDNA was amplified by PCR (50 µl reaction; 1X Invitrogen Taq DNA Polymerase PCR Buffer, 2.5 mM MgCl2, 100 µM dNTPs, 400 nM primer Ex13_39_S, 400 nM primer Ex15_108_AS, 5 units Invitrogen Platinum Taq polymerase, 2 µl cDNA; thermocycler program: 5 minutes at 95°C, 30 x [30 seconds at 95°C, 30 seconds at 61°C, 45 seconds at 68°C], 5 minutes at 68°C). PCR products were visualized in a 1X SB, 3% agarose gel stained with 400 ng/mL Ethidium Bromide.

qPCR of *Fmr1* Isoforms

RNA was extracted from 7-8 week old male mice and cDNA prepared as described above. MuP0 cDNA was transcribed in a similar fashion, using the primer MuP0_RT. For each isoform, qPCR samples were run in triplicate, as well as NTC and NRT controls using the same primer combinations. For each sample, all 12 isoforms were processed on a single plate, and a MuP0 loading control was run on the same plate. The samples were run in 10 µl reactions, with 1X Bio-Rad SYBR Green mix, 1 µl 10x forward/reverse primer combination, and 1 µl cDNA product. The reaction was run on a Bio-Rad CFX 96 Real-Time System, and Cq values were calculated using Bio-Rad CFX

Manager 2.1 software. The raw value for each replicate was calculated as 2^(40-Cq). Each replicate was normalized to the raw value of MuP0 on the same plate, and the three normalized values for a given isoform were averaged for a single data point. Each group of three genotypes was analyzed by one-way ANOVA, with post tests comparing each mean to the other two means in the group.

Audiogenic Seizures

The audiogenic seizure testing chamber consisted of a standard mouse cage containing a RadioShack personal alarm modified to run-off of 120 V AC power. The alarm was mounted inside the cage in the center of one of the cage' s shorter walls. P21 male mice were placed in the chamber, the lid was replaced, and the alarm was turned on. The alarm was turned off after one minute or if the mouse displayed a seizure. Mice displaying a seizure were immediately euthanized. Any wild running behavior was noted but was not considered by itself to be a seizure. All experiments were performed between 3:00 and 6:00 PM. P-values for each wild type/mutant comparison were calculated using a contingency table.

SNS Protein Synthesis

Cortical SNS were prepared as described previously [64] and treated with solvent for 5 min at 37°C, followed by DHPG (100 μM) for 15 min at 37°C. Metabolic labeling was performed with 100 μCi Pro-Mix, L-(35S) in vitro cell labeling mix (GE Healthcare) for 5 min. Triplicate samples from time point 0 and 5 min were washed once in

homogenization buffer, followed by lysis (100 mM Tris-HCl, pH 7.4, 150 mm NaCl, 0.5% deoxycholate, and 1% Triton X-100, supplemented with protease inhibitors) and TCA precipitation. 35S-incorporation levels were estimated by scintillation counting. Data was analyzed by two-way ANOVA, matching treated and untreated samples.

Marble Burying

Small cages (approx 26 x 20 x 14 cm) were filled with approximately twice the normal amout of standard mouse bedding (~5 cm deep) and 20 marbles were equally distributed on top of the bedding. A single adult male mouse (8-10 weeks old) was placed in each chage. The mice were left and videotaped for 30 minutes. An observer blind to the genotype counted the number of marbles more than 50% visible at the 10 minute, 20 minute, and 30 minute time points. Marbles were cleaned with water, cleaned with 70% ethanol, and dried completely between experiments.

Nestlet Shredding

3.0g of standard nesting material was placed in a cage. A single adult male mouse (8-10 weeks) was placed in the cage for 30 minutes. After 30 minutes, the mouse was removed from the cage. The amount of nesting material not shredded was weighed. Data was recorded as the percentage of nestlet material shredded.

Testis Mass

Adult male mice (8-10 weeks old) were euthanized by cervical dislocation. The mouse was weighed before any other procedure was performed. Both testes were dissected out and weighed. Testis mass was normalized to body weight for each individual mouse.

Statistics

All statistical tests were performed in GraphPad Prism version 6.05. Individual tests are described in the relevant Materials and Methods sections.

Polyribosome Profiles with Tris

15% - 45% continuous sucrose gradients were made by layering 6ml of 15% sucrose (50mM Tris-HCl pH 7.5, 200mM KCl, 5mM MgCl2, 100 µg/ml cycloheximide, 20 units/ml SuperAse) on top of 5.4 ml of 45% sucrose (50mM Tris-HCl pH 7.5, 200mM KCl, 5mM MgCl2, 100 µg/ml cycloheximide, 20 units/ml SuperAse) in Beckman Coulter 9/16" x 3.5" centrifuge tubes. The gradients were formed in a Biocomp Gradient Master 108 gradient former, using the built in "Long Sucrose 15-45% ww" program. The gradients were stored at 4°C until they were used.

2 to 3 week old male mice were euthanized by cervical dislocation, their brains were removed, and their cortices dissected out. The tissue was homogenized in 1 ml of lysis buffer (50mM Tris-HCl pH 7.5, 200mM KCl, 5mM MgCl2, 1% IgePal, 100 µg/ml cycloheximide, 100 units/ml SuperAse) supplemented with protease inhibitors (Roche

Complete Ultra Mini EDTA-free tablets) in a dounce homogenizer with 12 strokes on ice. Samples were transferred to Eppendorf tubes and centrifuged at 20000 x g for 30 minutes at 4°C. The supernatant was removed and transferred to a new Eppendorf tube. Samples for EDTA runs were adjusted to 30mM EDTA. RNA concentration was measured with a Nanodrop ND-1000 spectrophotometer, and samples were adjusted to equal concentrations with lysis buffer.

700 µl of each sample was loaded on to a 15% - 45% continuous sucrose gradient. The gradients were placed in a SW41 Ti bucket rotor and centrifuged at 38000 x g for 2 hours at 4°C in a Beckman Coulter Optima XPN-100 ultracentrifuge.

The gradients were placed in a Teledyne Isco Tube Piercer and displaced from below with 60% sucrose. Tracings were recorded by sending the gradients through a UA-6 Absorbance Detector which measured absorbance at 254 nm. The gradients were fractionated into 10 x 1.1ml fractions using a Teledyne Isco Foxy R1 fractionator. Fractions were stored at -80°C until ready for further processing.

Polyribosome Profiles with HEPES

15% - 45% sucrose gradients were formed as above, except with the following composition: 10mM HEPES pH 7.3, 150mM KCl, 5mM MgCl2, 100 µg/ml cycloheximide, 20 units/ml SuperAse.

2 to 3 week old male mice were euthanized by cervical dislocation, their brains were removed, and their cortices and cerebellum dissected out. The tissue was homogenized in 1 ml of lysis buffer (10mM HEPES pH 7.3, 150mM KCl, 5mM MgCl2, 100 µg/ml cycloheximide, 100 units/ml SuperAse) supplemented with protease inhibitors

(Roche Complete Ultra Mini EDTA-free tablets) in a dounce homogenizer with 12 strokes on ice. Samples were transferred to Eppendorf tubes and centrifuged at 2000 x g for 10 minutes at 4°C. The supernatant was removed and transferred to a new Eppendorf tube. IgePal was added to a final concentration of 1%, then samples were mixed by inversion and incubated on ice for 5 minutes. Samples were centrifuged at 20000 x g for 10 minutes at 4°C. The supernatant was removed and transferred to a new Eppendorf tube. RNA concentration was measured with a Nanodrop ND-1000 spectrophotometer, and samples were adjusted to equal concentrations with lysis buffer.

700 µl of each sample was loaded on to a 15% - 45% continuous sucrose gradient. Gradients were centrifuged, processed, and fractionated as above, with the exception that the gradient was fractionated into 16 x 750 µl fractions. For each fraction, 295 µl of sample was combined with 5 µl of 10 pg/µl of luciferase RNA and 900 µl of Trizol-LS, mixed by inversion, and stored at -80°C. The remaining samples were also stored at -80°C.

Polyribosome Profiles Using IVT_{EBP} Method

15% - 45% sucrose gradients were formed as above, except with the following composition: 10mM HEPES pH 7.3, 150mM NaCl, 5mM MgCl2, 100 µg/ml cycloheximide, 20 units/ml SuperAse.

2 to 3 week old male mice were euthanized by cervical dislocation, their brains were removed, and their cortices and cerebellum dissected out. The tissue was homogenized in 500 µl of lysis buffer (10mM HEPES pH 7.3, 150mM NaCl, 5mM MgCl2, 100 units/ml SuperAse) supplemented with protease inhibitors (Roche Complete

Ultra Mini EDTA-free tablets) in a dounce homogenizer with 12 strokes on ice. Samples were transferred to Eppendorf tubes and centrifuged at 2000 x g for 10 minutes at 4°C. 300 µl of supernatant was removed and transferred to a new Eppendorf tube. The following was added to each sample: 9.6 µl 100mM ATP, 15 µl of –Met amino acid mixture from the Promega RRL Kit (catalog number L4960), 15 µl of –Leu amino acid mixture from the Promega RRL Kit, and 150 µl nuclease-treated rabbit reticulocyte lysate from the Promega RRL Kit. Samples were split into 2 x 220 µl samples. 2.2 µl of 10 mg/ml of cycloheximide was added to the first sample; 2.2 µl of 720 µg/ml puromycin was added to the second sample. Samples were incubated at 30°C for 20 minutes. The reactions were stopped by adding 1 ml of stop buffer (lysis buffer with 100 µg/ml cycloheximide, 1% IgePal) and mixed by inverting the tube 8 times. Samples were incubated on ice for 10 minutes and centrifuged at 20000 x g at 4°C.

1 ml of the supernatant from each sample was loaded on to a 15% - 45% continuous sucrose gradient. Gradients were centrifuged, processed, and fractionated as described in the "Polyribosome Profiles with HEPES" section.

Polyribosome Profiles on MEFs

15% - 45% sucrose gradients were formed as above, except with the following composition: 20mM Tris-HCl pH 8.0, 100mM KCl, 5mM MgCl2, 100 µg/ml cycloheximide, 20 units/ml SuperAse.

MEF cells were incubated with either 100 µg/mL cycloheximide for 15 minutes or 1 mM puromycin for 30 minutes. Cells were washed with cold PBS and detached by incubating with 0.25% Trypsin-EDTA for 5 minutes at room temperature. Cold media

was added, cells were resuspended by pipetting, and cells were centrifuged at 375 x g for 5 minutes at 4°C. The supernatant was removed, the cells were washed with cold PBS, and cells were centrifuged at 375 x g for 5 minutes at 4°C. Cells were resuspended in 900 µl of lysis buffer (20mM Tris-HCl pH 8.0, 100mM KCl, 5mM MgCl2, 0.3% IgePal, 100 µg/ml cycloheximide, 100 units/ml SuperAse), transferred to an Eppendorf tube, and incubated on ice for 10 minutes. Samples were centrifuged at 13000 x g for 10 minutes at 4°C. The supernatant was removed and transferred to a new Eppendorf tube. Samples for EDTA runs were adjusted to 30mM EDTA. RNA concentration was measured with a Nanodrop ND-1000 spectrophotometer, and samples were adjusted to equal concentrations with lysis buffer.

700 µl of the supernatant from each sample was loaded on to a 15% - 45% continuous sucrose gradient. Gradients were centrifuged, processed, and fractionated as described in the “Polyribosome Profiles with HEPES” section.

Polyribosome Profiles on Neurons

Embryonic cortical neurons were plated at high density (1×10^7 cells per 10 cm plate). Neurons were fed at days in vitro (DIV) 5 and 10 by replacing half the media with fresh media.

15% - 45% sucrose gradients were formed as above, except with the following composition: 20mM Tris-HCl pH 8.0, 100mM KCl, 5mM MgCl2, 100 µg/ml cycloheximide, 20 units/ml SuperAse.

At DIV 14, 1 mL of lysis buffer (20mM Tris-HCl pH 8.0, 100mM KCl, 5mM MgCl2, 0.3% IgePal, 100 µg/ml cycloheximide, 100 units/ml SuperAse) was added to

each 10 cm plate, the plates were scraped with a cell scraper, and the plates were rocked for 5 minutes at 4°C. Lysate was removed from each plate, transferred to an Eppendorf tube, and incubated on ice for 10 minutes. Samples were centrifuged at 13,000 x g for 10 minutes at 4°C. The supernatant was removed and transferred to a new Eppendorf tube. Samples for EDTA runs were adjusted to 30mM EDTA. RNA concentration was measured with a Nanodrop ND-1000 spectrophotometer, and samples were adjusted to equal concentrations with lysis buffer.

700 µl of the supernatant from each sample was loaded on to a 15% - 45% continuous sucrose gradient. Gradients were centrifuged, processed, and fractionated as described in the "Polyribosome Profiles with HEPES" section.

Western Blot of Sucrose Fractions

Sucrose fractions were thawed on ice and 500ml of each fraction was aliquoted into an Amicon Ultra 0.5 ml 30K filter. Samples were concentrated by centrifuging filters at 14000 x g for 10 minutes, placing filters upside down in a new Eppendorf tube, and centrifuging them at 1000 x g for 2 minutes. 48 µl of each concentrated sample was combined with 12 µl of 5X Laemmli buffer, boiled at 95°C for 5 minutes, and loaded into a 4% – 15% polyacrylamide gel. The gel was run at 200V for 37 minutes and transferred to a nitrocellulose membrane. The membrane was incubated with anti-FMRP antibody (EMD Millipore, clone 1C3, MAB2160) at 1:2000 dilution and anti-S6 antibody (Cell Signaling 2317) at 1:1000 dilution overnight at 4°C. HRP-conjugated anti-mouse secondary antibody was used at a 1:50000 dilution and the membrane was incubated in SuperSignal West Femto ECL substrate for 4 minutes. The results were visualized on

photographic film.

cDNA Synthesis from Polyribosome Profile Fractions

RNA samples were thawed at room temperature and RNA was extracted following manufacturer's directions, with the exception that 2 µl of glycoBlue was added to each sample immediately before isopropanol precipitation. Samples were resuspended in 8 µl of RNase-free water and incubated at 55°C for 20 minutes.

cDNA was synthesized using the Thermo Scientific SuperScript III Supermix. For each fraction, 6 µl of RNA was combined with 1 µl of oligo(dT) primers and 1 µl of Annealing Buffer in a well of a 96-well plate. NTC, NRT, and H2O controls were run for each set of fractions. The plate was incubated at 65°C for 5 minutes and placed on ice for 1 minute. 10 µl of 2X First-Strand Mix and 2 µl of SuperScript III Enzyme Mix were added to each sample. The plate was incubated at 50°C for 50 minutes plus 85°C for 5 minutes to stop the reaction. cDNA samples were stored at -20°C.

qPCR of Polyribosome Profile Fractions

For each gradient, all fractions were processed on a single plate. *Map1b*, *Kif1a*, *GAPDH*, and *luciferase* reactions were run for each fraction (primer combinations are listed in attached spreadsheet). The samples were run in 10 µl reactions, with 1X Bio-Rad SYBR Green mix, 1 µl 10x forward/reverse primer combination, and 1 µl cDNA product. The reaction was run on a Bio-Rad CFX 96 Real-Time System, and Cq values were calculated using Bio-Rad CFX Manager 2.1 software. Each data point was

normalized to the amount of luciferase RNA in that fraction using the Pfaffl method [112].

Standard Curves on Film

A single adult male mouse was euthanized by cervical dislocation, the brain removed, and both cortices dissected out. Cortices were homogenized in 1 ml of lysis buffer (50 mM Tris pH 7.6, 30 mM EDTA, 0.5% Triton X-100) supplemented with protease inhibitors (Roche Complete Ultra Mini tablets) in a dounce homogenizer with 8-12 strokes on ice. Samples were centrifuged at 20000 x g for 5 minutes at 4°C. The supernatant was transferred to a new Eppendorf tube and total protein concentration was measured by Bradford assay. The sample was boiled in 1X Laemmli buffer for 5 minutes at 95°C. Serial dilutions of the sample were made in 1X Laemmli buffer such that 40 µL of sample contained the specified amount of total protein.

40 µL of each dilution was run in a 4-15% polyacrylamide gel in 1X running buffer (192 mM glycine, 25 mM Tris, 3.5 mM SDS) at 200 V for 35 minutes. Proteins were transferred to a PVDF membrane in 1X transfer buffer (192 mM glycine, 25 mM Tris, 20% methanol) at 90 V for 1 hour at 4°C. The membrane was blocked with PBS StartingBlock buffer for 15 minutes at room temperature and then incubated with appropriate antibodies diluted in PBS StartingBlock buffer (dilutions listed below) at 4°C with rocking overnight. The membrane was washed 3×10 minutes with wash buffer (1X PBS, 1% nonfat dry milk, 0.2% Tween), incubated with anti-mouse or anti-rabbit HRP-conjugated secondary antibody diluted 1:10000 in dilution buffer (1:1 Wash Buffer:RIPA) at room temperature for 45 minutes, washed 3×10 minutes with wash

buffer, incubated in HyGlo ECL substrate at room temperature for 5 minutes, and imaged on film. The films were scanned on an Epson office scanner and the intensity of bands were measured in ImageJ version 1.47.

Antibody	**Host**	**Vendor**	**Catalog #**	**Dilution**
Anti-BETA-ACTIN	Mouse	Abcam	Ab125248	1:4000
Anti-EIF4E	Mouse	BD Transduction Laboratories	610270	1:2000
Anti-GAPDH	Rabbit	Cell Signaling	5174	1:4000
Anti-MAP1B	Mouse	BD Transduction Laboratories	612678	1:200000
Anti-PSD95	Mouse	Millipore	MAB1596	1:400
Anti-BETA-TUBULIN	Rabbit	Cell Signaling	5666	1:32000

Total Protein Stain Using Ponceau S

Membranes were stained for total protein levels by incubating in Ponceau S stain (0.1% Ponceaus S in 5% acetic acid) for 10 minutes. Background stain was removed by incubating membranes in H2O for 2 minutes followed by multiple 2 minute incubations in destain buffer (25% methanol and 7% acetic acid). The incubations in destain buffer were repeated until suitable amount of background stain was removed. The stained membranes were scanned on an Epson office scanner. Signal intensities were measured in ImageJ version 1.47.

Standard Curve Using Fluorescent Westerns

A single adult male mouse was euthanized by cervical dislocation and the sample

was processed as in the “Standard Curves on Film” section.

40 µL of each dilution was run in a 4-15% polyacrylamide gel in 1X running buffer (192 mM glycine, 25 mM Tris, 3.5 mM SDS) at 200 V for 35 minutes. Proteins were transferred to a PVDF-LF membrane in 1X transfer buffer (192 mM glycine, 25 mM Tris, 20% methanol) at 25 V for 2.5 hours at 4°C. The membrane was incubated in blocking buffer (2% Amersham ECL Prime blocking agent in 1X PBS with 0.1% Tween) for 1 hour at room temperature and washed 2 x 5 minutes in wash buffer (1X PBS with 0.1% Tween) at room temperature. The membrane was incubated with anti-GAPDH antibody (described above) diluted 1:4000 in blocking buffer at 4°C overnight.

The membrane was washed 2 x 5 minutes with wash buffer at room temperature and incubated with secondary antibody (anti-rabbit conjugated to Cy5) diluted 1:2500 in wash buffer for 1 hour at room temperature. The membrane was washed 4 x 5 minutes in wash buffer at room temperature, rinsed 3 times in 1X PBS, and incubated at 37°C for 1 hour to dry. During the incubation with secondary antibody and all subsequent steps the membrane was protected from light. The fluorescent signal was measured on a GE Healthcare Typhoon laser scanner. Signal intensities were calculated in GE Healthcare ImageQuant TL version 7.0.

Western Blots of Crude SNS

P15-17 male mice were euthanized by cervical dislocation, brains removed, and cortices dissected out. Cortices were homogenized in 2 ml of homogenization buffer (320 mM sucrose, 4 mM HEPES) supplemented with protease inhibitors (Roche Complete Ultra Mini tablets) in a dounce homogenizer with 8 strokes on ice. Lysate was transferred

to a 15 ml conical tube and centrifuged at 700 x g for 15 minutes at 4°C. The supernatant was transferred to an Eppendorf tube and centrifuged at 10000 x g for 15 minutes at 4°C. The supernatant was removed and the pellet was resuspended in 400 µl of homogenization buffer by pipetting. The sample was sonicated on ice at power = 2.0 for 15 seconds. Protein concentration was measured by BCA assay. 40 µg of sample was boiled in 1X Laemmli buffer for 5 minutes.

40 µg of each sample was run in a 4-15% polyacrylamide gel in 1X running buffer (192 mM glycine, 25 mM Tris, 3.5 mM SDS) at 200 V for 35 minutes. Proteins were transferred to a PVDF membrane in a Bio-Rad Trans-Blot Turbo Transfer System using the built in "HMW" program. The membrane was blocked with PBS StartingBlock buffer for 15 minutes at room temperature and then incubated with appropriate antibodies diluted in PBS StartingBlock buffer (dilutions listed below) at 4°C with rocking overnight. The membrane was washed 3×10 minutes with wash buffer (1X PBS, 1% nonfat dry milk, 0.2% Tween), incubated with anti-mouse or anti-rabbit HRP-conjugated secondary antibody diluted 1:10000 in dilution buffer (1:1 Wash Buffer:RIPA) at room temperature for 45 minutes, washed 3×10 minutes with wash buffer, incubated in Bio-Rad Clarity ECL substrate at room temperature for 5 minutes, and imaged on a Bio-Rad ChemiDoc Touch CCD camera. Signal intensities were measured using Bio-Rad Image Lab version 5.2.1.

Antibody	Host	Vendor	Catalog #	Dilution
Anti-DARPP32	Rabbit	Cell Signaling	2302	1:1000
Anti-SHANK1	Rabbit	Abcam	ab154224	1:1000

Western Blots of MAP1B in Hippocampi

P10 male mice were euthanuized by cervical dislocation, brains removed, and hippocampi dissected out. Hippocampi were minced with a clean scalpel and placed in 200 µl of 1X Laemmli buffer supplemented with 8M urea. Samples were sonicated with a probe sonicator at power = 2.0 for 15 seconds. Total protein levels were measured by Bradford assay.

4 µg of each sample was run in a 4-15% polyacrylamide gel in 1X running buffer (192 mM glycine, 25 mM Tris, 3.5 mM SDS) at 200 V for 35 minutes. Proteins were transferred to a PVDF-LF membrane in 1X transfer buffer (192 mM glycine, 25 mM Tris, 20% methanol) at 25 V for 2.5 hours at 4°C. The membrane was incubated in blocking buffer (2% Amersham ECL Prime blocking agent in 1X PBS with 0.1% Tween) for 1 hour at room temperature and washed 2 x 5 minutes in wash buffer (1X PBS with 0.1% Tween) at room temperature. The membrane was incubated with anti-MAP1B antibody (BD Transduction Laboratories, #612678) diluted 1:100000 in blocking buffer at 4°C overnight.

The membrane was washed 2 x 5 minutes with wash buffer at room temperature and incubated with secondary antibody (anti-mouse conjugated to Cy3) diluted 1:2500 in wash buffer for 1 hour at room temperature. The membrane was washed 4 x 5 minutes in wash buffer at room temperature, rinsed 3 times in 1X PBS, and incubated at 37°C for 1 hour to dry. During the incubation with secondary antibody and all subsequent steps the membrane was protected from light. The fluorescent signal was measured on a GE Healthcare Typhoon laser scanner. Signal intensities were calculated in GE Healthcare ImageQuant TL version 7.0.

References

1. Coffee, B., et al., *Incidence of fragile x syndrome by newborn screening for methylated FMR1 DNA.* Am J Hum Genet, 2009. **85**(4): p. 503-14.
2. Lubs, H.A., *A marker X chromosome.* Am J Hum Genet, 1969. **21**(3): p. 231-44.
3. Sutherland, G.R., *Fragile sites on human chromosomes: demonstration of their dependence on the type of tissue culture medium.* Science, 1977. **197**(4300): p. 265-6.
4. Hecht, F. and G.R. Sutherland, *Detection of fragile sites on human chromosomes.* Clin Genet, 1985. **28**(1): p. 95-6.
5. Garber, K.B., J. Visootsak, and S.T. Warren, *Fragile X syndrome.* Eur J Hum Genet, 2008. **16**(6): p. 666-672.
6. Sherman, S.L., et al., *Further segregation analysis of the fragile X syndrome with special reference to transmitting males.* Hum Genet, 1985. **69**(4): p. 289-99.
7. Sherman, S.L., et al., *The marker (X) syndrome: a cytogenetic and genetic analysis.* Ann Hum Genet, 1984. **48**(Pt 1): p. 21-37.
8. Verkerk, A.J.M.H., et al., *Identification of a gene (FMR-1) containing a CGG repeat coincident with a breakpoint cluster region exhibiting length variation in fragile X syndrome.* Cell, 1991. **65**(5): p. 905-914.
9. Krawczun, M.S., E.C. Jenkins, and W.T. Brown, *Analysis of the fragile-X chromosome: localization and detection of the fragile site in high resolution preparations.* Hum Genet, 1985. **69**(3): p. 209-11.
10. Fu, Y.-H., et al., *Variation of the CGG repeat at the fragile X site results in genetic instability: Resolution of the Sherman paradox.* Cell, 1991. **67**(6): p. 1047-1058.
11. Pieretti, M., et al., *Absence of expression of the FMR-1 gene in fragile X syndrome.* Cell, 1991. **66**(4): p. 817-822.
12. Verheij, C., et al., *Characterization and localization of the FMR-1 gene product associated with fragile X syndrome.* Nature, 1993. **363**(6431): p. 722-724.
13. Coffee, B., et al., *Acetylated histones are associated with FMR1 in normal but not fragile X-syndrome cells.* Nat Genet, 1999. **22**(1): p. 98-101.
14. Coffee, B., et al., *Histone Modifications Depict an Aberrantly Heterochromatinized FMR1 Gene in Fragile X Syndrome.* The American Journal of Human Genetics, 2002. **71**(4): p. 923-932.
15. Rauch, A., et al., *Diagnostic yield of various genetic approaches in patients with unexplained developmental delay or mental retardation.* American Journal of Medical Genetics Part A, 2006. **140A**(19): p. 2063-2074.
16. Coffee, B., et al., *Mosaic FMR1 deletion causes fragile X syndrome and can lead to molecular misdiagnosis: a case report and review of the literature.* Am J Med Genet A, 2008. **146A**(10): p. 1358-67.
17. Collins, S.C., et al., *Identification of novel FMR1 variants by massively parallel sequencing in developmentally delayed males.* Am J Med Genet A, 2010. **152A**(10): p. 2512-20.

18. De Boulle, K., et al., *A point mutation in the FMR-1 gene associated with fragile X mental retardation.* Nat Genet, 1993. **3**(1): p. 31-5.
19. Myrick, L.K., et al., *Fragile X syndrome due to a missense mutation.* Eur J Hum Genet, 2014. **22**(10): p. 1185-9.
20. Ashley, C.T., et al., *Human and murine FMR-1: alternative splicing and translational initiation downstream of the CGG-repeat.* Nat Genet, 1993. **4**(3): p. 244-51.
21. Brouwer, J.R., et al., *Elevated Fmr1 mRNA levels and reduced protein expression in a mouse model with an unmethylated Fragile X full mutation.* Exp Cell Res, 2007. **313**(2): p. 244-53.
22. Dutch-Belgian Fragile X Consortium, *Fmr1 knockout mice: a model to study fragile X mental retardation. .* Cell, 1994. **78**(1): p. 23-33.
23. Grossman, A.W., et al., *Local protein synthesis and spine morphogenesis: Fragile X syndrome and beyond.* J Neurosci, 2006. **26**(27): p. 7151-5.
24. Mientjes, E.J., et al., *The generation of a conditional Fmr1 knock out mouse model to study Fmrp function in vivo.* Neurobiol Dis, 2006. **21**(3): p. 549-55.
25. Pan, L., et al., *The Drosophila fragile X gene negatively regulates neuronal elaboration and synaptic differentiation.* Curr Biol, 2004. **14**(20): p. 1863-70.
26. Zhang, Y.Q., et al., *Drosophila fragile X-related gene regulates the MAP1B homolog Futsch to control synaptic structure and function.* Cell, 2001. **107**(5): p. 591-603.
27. Morales, J., et al., *Drosophila fragile X protein, DFXR, regulates neuronal morphology and function in the brain.* Neuron, 2002. **34**(6): p. 961-72.
28. Bolduc, F.V., et al., *Excess protein synthesis in Drosophila fragile X mutants impairs long-term memory.* Nat Neurosci, 2008. **11**(10): p. 1143-5.
29. Dockendorff, T.C., et al., *Drosophila Lacking dfmr1 Activity Show Defects in Circadian Output and Fail to Maintain Courtship Interest.* Neuron, 2002. **34**(6): p. 973-984.
30. Coffee, R.L., Jr., et al., *In vivo neuronal function of the fragile X mental retardation protein is regulated by phosphorylation.* Hum Mol Genet, 2012. **21**(4): p. 900-15.
31. Devys, D., et al., *The FMR-1 protein is cytoplasmic, most abundant in neurons and appears normal in carriers of a fragile X premutation.* Nat Genet, 1993. **4**(4): p. 335-40.
32. Hinds, H.L., et al., *Tissue specific expression of FMR-1 provides evidence for a functional role in fragile X syndrome.* Nat Genet, 1993. **3**(1): p. 36-43.
33. Feng, Y., et al., *Fragile X Mental Retardation Protein: Nucleocytoplasmic Shuttling and Association with Somatodendritic Ribosomes.* The Journal of Neuroscience, 1997. **17**(5): p. 1539-1547.
34. Weiler, I.J., et al., *Fragile X mental retardation protein is translated near synapses in response to neurotransmitter activation.* Proc Natl Acad Sci U S A, 1997. **94**(10): p. 5395-400.
35. Verkerk, A.J.M.H., et al., *Alternative splicing in the fragile X gene FMR1.* Human Molecular Genetics, 1993. **2**(4): p. 399-404.

36. Banerjee, P., et al., *Short- and Long-Term Memory Are Modulated by Multiple Isoforms of the Fragile X Mental Retardation Protein.* The Journal of Neuroscience, 2010. **30**(19): p. 6782-6792.
37. Dictenberg, J.B., et al., *A Direct Role for FMRP in Activity-Dependent Dendritic mRNA Transport Links Filopodial-Spine Morphogenesis to Fragile X Syndrome.* Developmental Cell, 2008. **14**(6): p. 926-939.
38. Brackett, D.M., et al., *Fmr1 Transcript Isoforms: Association with Polyribosomes; Regional and Developmental Expression in Mouse Brain.* PLoS ONE, 2013. **8**(3): p. e58296.
39. Myrick, L.K., et al., *Human FMRP contains an integral tandem Agenet (Tudor) and KH motif in the amino terminal domain.* Hum Mol Genet, 2015. **24**(6): p. 1733-40.
40. Blackwell, E., X. Zhang, and S. Ceman, *Arginines of the RGG box regulate FMRP association with polyribosomes and mRNA.* Human Molecular Genetics, 2010. **19**(7): p. 1314-1323.
41. Eberhart, D.E., et al., *The Fragile X Mental Retardation Protein is a Ribonucleoprotein Containing Both Nuclear Localization and Nuclear Export Signals.* Human Molecular Genetics, 1996. **5**(8): p. 1083-1091.
42. Myrick, L.K., et al., *Independent role for presynaptic FMRP revealed by an FMR1 missense mutation associated with intellectual disability and seizures.* Proc Natl Acad Sci U S A, 2015. **112**(4): p. 949-56.
43. Maurer-Stroh, S., et al., *The Tudor domain 'Royal Family': Tudor, plant Agenet, Chromo, PWWP and MBT domains.* Trends in Biochemical Sciences, 2003. **28**(2): p. 69-74.
44. Adams-Cioaba, M.A., et al., *Structural Studies of the Tandem Tudor Domains of Fragile X Mental Retardation Related Proteins FXR1 and FXR2.* PLoS ONE, 2010. **5**(11): p. e13559.
45. Ashley, C.T., et al., *FMR1 protein: conserved RNP family domains and selective RNA binding.* Science, 1993. **262**(5133): p. 563-566.
46. Brown, V., et al., *Microarray Identification of FMRP-Associated Brain mRNAs and Altered mRNA Translational Profiles in Fragile X Syndrome.* Cell, 2001. **107**(4): p. 477-487.
47. Miyashiro, K.Y., et al., *RNA cargoes associating with FMRP reveal deficits in cellular functioning in Fmr1 null mice.* Neuron, 2003. **37**(3): p. 417-31.
48. Zou, K., et al., *Identification of FMRP-associated mRNAs using yeast three-hybrid system.* Am J Med Genet B Neuropsychiatr Genet, 2008. **147B**(6): p. 769-77.
49. Dolzhanskaya, N., et al., *The fragile X mental retardation protein interacts with U-rich RNAs in a yeast three-hybrid system.* Biochemical and Biophysical Research Communications, 2003. **305**(2): p. 434-441.
50. Joachimi, A., A. Benz, and J.S. Hartig, *A comparison of DNA and RNA quadruplex structures and stabilities.* Bioorganic & Medicinal Chemistry, 2009. **17**(19): p. 6811-6815.
51. Darnell, J.C., et al., *Fragile X Mental Retardation Protein Targets G Quartet mRNAs Important for Neuronal Function.* Cell, 2001. **107**(4): p. 489-499.

52. Schaeffer, C., et al., *The fragile X mental retardation protein binds specifically to its mRNA via a purine quartet motif.* Embo J, 2001. **20**(17): p. 4803-13.
53. Menon, L., S.A. Mader, and M.R. Mihailescu, *Fragile X mental retardation protein interactions with the microtubule associated protein 1B RNA.* Rna, 2008. **14**(8): p. 1644-55.
54. Menon, L. and M.R. Mihailescu, *Interactions of the G quartet forming semaphorin 3F RNA with the RGG box domain of the fragile X protein family.* Nucleic Acids Res, 2007. **35**(16): p. 5379-92.
55. Chen, L., et al., *The fragile X mental retardation protein binds and regulates a novel class of mRNAs containing U rich target sequences.* Neuroscience, 2003. **120**(4): p. 1005-17.
56. Fahling, M., et al., *Translational regulation of the human achaete-scute homologue-1 by fragile X mental retardation protein.* J Biol Chem, 2009. **284**(7): p. 4255-66.
57. Darnell, J.C., et al., *Kissing complex RNAs mediate interaction between the Fragile-X mental retardation protein KH2 domain and brain polyribosomes.* Genes & Development, 2005. **19**(8): p. 903-918.
58. Bechara, E.G., et al., *A novel function for fragile X mental retardation protein in translational activation.* PLoS Biol, 2009. **7**(1): p. e16.
59. Kindler, S., et al., *Distinct spatiotemporal expression of SAPAP transcripts in the developing rat brain: a novel dendritically localized mRNA.* Molecular Brain Research, 2004. **126**(1): p. 14-21.
60. Huang, F., J.K. Chotiner, and O. Steward, *The mRNA for Elongation Factor 1α Is Localized in Dendrites and Translated in Response to Treatments That Induce Long-Term Depression.* The Journal of Neuroscience, 2005. **25**(31): p. 7199-7209.
61. Antar, L.N., et al., *Localization of FMRP-associated mRNA granules and requirement of microtubules for activity-dependent trafficking in hippocampal neurons.* Genes, Brain and Behavior, 2005. **4**(6): p. 350-359.
62. Zalfa, F., et al., *The Fragile X Syndrome Protein FMRP Associates with BC1 RNA and Regulates the Translation of Specific mRNAs at Synapses.* Cell, 2003. **112**(3): p. 317-327.
63. Bramham, C.R. and D.G. Wells, *Dendritic mRNA: transport, translation and function.* Nat Rev Neurosci, 2007. **8**(10): p. 776-789.
64. Muddashetty, R.S., et al., *Dysregulated metabotropic glutamate receptor-dependent translation of AMPA receptor and postsynaptic density-95 mRNAs at synapses in a mouse model of fragile X syndrome.* J Neurosci, 2007. **27**(20): p. 5338-48.
65. Zalfa, F., et al., *A new function for the fragile X mental retardation protein in regulation of PSD-95 mRNA stability.* Nat Neurosci, 2007. **10**(5): p. 578-87.
66. Feng, Y., et al., *FMRP Associates with Polyribosomes as an mRNP, and the I304N Mutation of Severe Fragile X Syndrome Abolishes This Association.* Molecular Cell, 1997. **1**(1): p. 109-118.
67. Khandjian, E.W., et al., *Biochemical evidence for the association of fragile X mental retardation protein with brain polyribosomal ribonucleoparticles.* Proc Natl Acad Sci U S A, 2004. **101**(36): p. 13357-62.

68. Stefani, G., et al., *Fragile X Mental Retardation Protein Is Associated with Translating Polyribosomes in Neuronal Cells.* The Journal of Neuroscience, 2004. **24**(33): p. 7272-7276.
69. Didiot, M.C., et al., *Cells lacking the fragile X mental retardation protein (FMRP) have normal RISC activity but exhibit altered stress granule assembly.* Mol Biol Cell, 2009. **20**(1): p. 428-37.
70. Laggerbauer, B., et al., *Evidence that fragile X mental retardation protein is a negative regulator of translation.* Hum. Mol. Genet., 2001. **10**(4): p. 329-338.
71. Mazroui, R., et al., *Trapping of messenger RNA by Fragile X Mental Retardation protein into cytoplasmic granules induces translation repression.* Hum Mol Genet, 2002. **11**(24): p. 3007-17.
72. Li, Z., et al., *The fragile X mental retardation protein inhibits translation via interacting with mRNA.* Nucl. Acids Res., 2001. **29**(11): p. 2276-2283.
73. Lu, R., et al., *The fragile X protein controls microtubule-associated protein 1B translation and microtubule stability in brain neuron development.* Proc Natl Acad Sci U S A, 2004. **101**(42): p. 15201-6.
74. Napoli, I., et al., *The Fragile X Syndrome Protein Represses Activity-Dependent Translation through CYFIP1, a New 4E-BP.* Cell, 2008. **134**(6): p. 1042-1054.
75. Ceman, S., et al., *Phosphorylation influences the translation state of FMRP-associated polyribosomes.* Hum. Mol. Genet., 2003. **12**(24): p. 3295-3305.
76. Buchan, J.R. and I. Stansfield, *Halting a cellular production line: responses to ribosomal pausing during translation.* Biol Cell, 2007. **99**(9): p. 475-87.
77. Caudy, A.A., et al., *Fragile X-related protein and VIG associate with the RNA interference machinery.* Genes & Development, 2002. **16**(19): p. 2491-2496.
78. Ishizuka, A., M.C. Siomi, and H. Siomi, *A Drosophila fragile X protein interacts with components of RNAi and ribosomal proteins.* Genes & Development, 2002. **16**(19): p. 2497-2508.
79. Plante, I., et al., *Dicer-derived microRNAs are utilized by the fragile X mental retardation protein for assembly on target RNAs.* J Biomed Biotechnol, 2006. **2006**(4): p. 64347.
80. Jin, P., et al., *Biochemical and genetic interaction between the fragile X mental retardation protein and the microRNA pathway.* Nat Neurosci, 2004. **7**(2): p. 113-7.
81. Edbauer, D., et al., *Regulation of Synaptic Structure and Function by FMRP-Associated MicroRNAs miR-125b and miR-132.* Neuron, 2010. **65**(3): p. 373-384.
82. Pillai, R.S., S.N. Bhattacharyya, and W. Filipowicz, *Repression of protein synthesis by miRNAs: how many mechanisms?* Trends in Cell Biology, 2007. **17**(3): p. 118-126.
83. Bear, M.F., K.M. Huber, and S.T. Warren, *The mGluR theory of fragile X mental retardation.* Trends Neurosci, 2004. **27**(7): p. 370-7.
84. Huber, K.M., et al., *Altered synaptic plasticity in a mouse model of fragile X mental retardation.* Proc Natl Acad Sci U S A, 2002. **99**(11): p. 7746-50.
85. Nosyreva, E.D. and K.M. Huber, *Metabotropic receptor-dependent long-term depression persists in the absence of protein synthesis in the mouse model of fragile X syndrome.* J Neurophysiol, 2006. **95**(5): p. 3291-5.

86. McBride, S.M., et al., *Pharmacological rescue of synaptic plasticity, courtship behavior, and mushroom body defects in a Drosophila model of fragile X syndrome.* Neuron, 2005. **45**(5): p. 753-64.
87. Tucker, B., R.I. Richards, and M. Lardelli, *Contribution of mGluR and Fmr1 functional pathways to neurite morphogenesis, craniofacial development and fragile X syndrome.* Hum Mol Genet, 2006. **15**(23): p. 3446-58.
88. Yan, Q.J., et al., *Suppression of two major Fragile X Syndrome mouse model phenotypes by the mGluR5 antagonist MPEP.* Neuropharmacology, 2005. **49**(7): p. 1053-66.
89. de Vrij, F.M., et al., *Rescue of behavioral phenotype and neuronal protrusion morphology in Fmr1 KO mice.* Neurobiol Dis, 2008. **31**(1): p. 127-32.
90. Nakamoto, M., et al., *Fragile X mental retardation protein deficiency leads to excessive mGluR5-dependent internalization of AMPA receptors.* Proc Natl Acad Sci U S A, 2007. **104**(39): p. 15537-42.
91. Dölen, G., et al., *Correction of Fragile X Syndrome in Mice.* Neuron, 2007. **56**(6): p. 955-962.
92. Bassell, G.J. and C. Gross, *Reducing glutamate signaling pays off in fragile X.* Nat Med, 2008. **14**(3): p. 249-250.
93. Narayanan, U., et al., *FMRP Phosphorylation Reveals an Immediate-Early Signaling Pathway Triggered by Group I mGluR and Mediated by PP2A.* J. Neurosci., 2007. **27**(52): p. 14349-14357.
94. Muddashetty, R.S., et al., *Reversible inhibition of PSD-95 mRNA translation by miR-125a, FMRP phosphorylation and mGluR signaling.* Molecular Cell, 2011. **In Press**.
95. Cheever, A. and S. Ceman, *Phosphorylation of FMRP inhibits association with Dicer.* Rna, 2009. **15**(3): p. 362-6.
96. Wu, S., et al., *A protocol for constructing gene targeting vectors: generating knockout mice for the cadherin family and beyond.* Nat Protoc, 2008. **3**(6): p. 1056-76.
97. Gross, C., et al., *Increased expression of the PI3K enhancer PIKE mediates deficits in synaptic plasticity and behavior in fragile X syndrome.* Cell Rep, 2015. **11**(5): p. 727-36.
98. Peier, A.M., et al., *(Over)correction of FMR1 deficiency with YAC transgenics: behavioral and physical features.* Hum Mol Genet, 2000. **9**(8): p. 1145-59.
99. Turner, G., A. Daniel, and M. Frost, *X-linked mental retardation, macro-orchidism, and the Xq27 fragile site.* J Pediatr, 1980. **96**(5): p. 837-41.
100. Dephoure, N., et al., *Mapping and analysis of phosphorylation sites: a quick guide for cell biologists.* Mol Biol Cell, 2013. **24**(5): p. 535-42.
101. Dieterich, D.C., et al., *Labeling, detection and identification of newly synthesized proteomes with bioorthogonal non-canonical amino-acid tagging.* Nat Protoc, 2007. **2**(3): p. 532-40.
102. Zang, J.B., et al., *A mouse model of the human Fragile X syndrome I304N mutation.* PLoS Genet, 2009. **5**(12): p. e1000758.
103. Nolze, A., et al., *FMRP regulates actin filament organization via the armadillo protein p0071.* Rna, 2013. **19**(11): p. 1483-96.

104. Darnell, J.C., et al., *FMRP stalls ribosomal translocation on mRNAs linked to synaptic function and autism.* Cell, 2011. **146**(2): p. 247-61.
105. Gross, C., et al., *Excess phosphoinositide 3-kinase subunit synthesis and activity as a novel therapeutic target in fragile X syndrome.* J Neurosci. **30**(32): p. 10624-38.
106. Tang, B., et al., *Fmr1 deficiency promotes age-dependent alterations in the cortical synaptic proteome.* Proc Natl Acad Sci U S A, 2015. **112**(34): p. E4697-706.
107. Taylor, S.C. and A. Posch, *The design of a quantitative western blot experiment.* Biomed Res Int, 2014. **2014**: p. 361590.
108. Gassmann, M., et al., *Quantifying Western blots: pitfalls of densitometry.* Electrophoresis, 2009. **30**(11): p. 1845-55.
109. Aldridge, G.M., et al., *The use of total protein stains as loading controls: an alternative to high-abundance single-protein controls in semi-quantitative immunoblotting.* J Neurosci Methods, 2008. **172**(2): p. 250-4.
110. Romero-Calvo, I., et al., *Reversible Ponceau staining as a loading control alternative to actin in Western blots.* Anal Biochem, 2010. **401**(2): p. 318-20.
111. Briz, V., et al., *Activity-dependent rapid local RhoA synthesis is required for hippocampal synaptic plasticity.* J Neurosci, 2015. **35**(5): p. 2269-82.
112. Pfaffl, M.W., *A new mathematical model for relative quantification in real-time RT–PCR.* Nucleic Acids Research, 2001. **29**(9): p. e45-e45.